Design calculations and model measurements for the EUTERPE accelerating cavity

Rubingh, M.J.A.

Award date:
1993

Design Calculations and Model Measurements for the EUTERPE Accelerating Cavity

M.J.A. Rubingh

VDF/NK 93-20

Eindhoven University of Technology
Department of Technical Physics
Accelerator Physics Group

Report on a graduate study
June 1992 - June 1993
Guidance: Dr. Ir. W.J.G.M. Kleeven
Dr. Ir. J.A. van der Heide

Abstract

At the accelerator laboratory of the TUE a 400 MeV electron storage ring EUTERPE is under construction. As a part of the EUTERPE project, a 45 MHz quarter wave cavity, operating at a gap voltage of 50 kV was designed to accelerate the electrons. Due to space limitations in the circumference of the ring, the cavity length should not exceed 0.5 meter. Therefore, we looked for special geometries, which have an effective length several times the physical length. Three solutions were found; the first employing radial transmission line folding, the second longitudinal transmission line folding and the third employing capacitive loading at the open end of the transmission line.

Transmission line theory was used to predict important cavity parameters like resonance frequency, quality factor and shunt impedance. These analytical calculations show good agreement with numerical calculations done with the computer codes SUPERFISH and URMEL-T. We found that a cavity which employs longitudinal transmission line folding is superior to a cavity which employs radial transmission line folding, because it is simpler of construction and because it has a better shunt impedance. An important alternative, however, is the capacitive loading design because this would result in the far simplest construction while the rf parameters like shunt impedance and quality factor are still rather good.

Two different ways of coupling rf power into the cavity are considered.

An LC equivalent circuit is used to model the impedance matching with respect to the rf generator. From this, the conditions for perfect matching are derived.

In order to verify the analytical and numerical models used, a cold scale 1:1 experimental model was built of a 2-layer cavity that employs longitudinal transmission line folding. For convenience this cavity was designed operating at 43 MHz, because at this frequency measuring equipment was available from the ILEC project.

Furthermore, a part of this report deals with the modeling of the Eimac tetrode which will be used as a power source for the EUTERPE cavity.

Contents

Chapter 1

Introduction

1.1 Scope of the study

This report presents the results of a graduate study, performed in the Accelerator Laboratory of the Eindhoven University of Technology (EUT). This study is a part of the EUTERPE project (Eindhoven University of TEchnology Ring for Protons and Electrons). One of the devices that will be accommodated in the ring is an rf accelerating cavity. The cavity will operate according to the principles of a ¼λ-resonator.

The aim of the study is to find a design for the cavity that meets with the requirements of the storage ring. This means resonant at a rf frequency of 45 MHz, but with a physical length that is shorter than 50 centimetres. The accelerating frequency is the sixth harmonic of the revolution frequency of 7.5 MHz. At present, an experimental model cavity has been built, on which the numerical and analytical model calculations were tested.

In this chapter an overview of the EUTERPE project will be given. Furthermore the basic principles of a ¼λ rf accelerating structure are reviewed.
In chapter 2 the basic parameters of an accelerating structure will be discussed, including the transit time factor, the shunt impedance and the quality factor. Also a representation of a cavity by a lumped element circuit will be described.
In chapter 3 transmission line matrix theory is used to model the length, quality factor and the shunt impedance of a cavity. Furthermore numerical calculations with the computer code URMEL-T are done to study the effect of slight changes in geometry on the important cavity properties.
In chapter 4 the problem of coupling power into the cavity is discussed. Two different methods are considered, namely direct coupling and inductive coupling.
In chapter 5 the design and construction of a scale 1:1 cold measuring model is presented, together with results of numerical calculations done on this cavity. For the model a resonance frequency of 43 MHz was chosen because it is the operating frequency of the ILEC project, which is also accommodated in the accelerator laboratory. From this project specific knowledge and measuring equipment could be used.
Results of measurements on the model cavity are discussed in chapter 6.
Chapter 7 gives an alternative design of a cavity which has the advantage that it is much simpler to construct. This cavity design will only be treated briefly because the underlying principle of capacitive loading was proposed at the end of this graduate study.
Finally, in chapter 8 the planned power source, a tetrode, will be described, together with calculations on its current characteristics and determination of an operating line.

1.2 The EUTERPE project

In the Cyclotron Laboratory of the Eindhoven University of Technology research is done on accelerator technology. At present the 400 MeV electron storage ring EUTERPE is being constructed. It is a university project set up for studies of charged particle beam dynamics and applications of synchrotron radiation. EUTERPE is a low energy ring, and it is being built by the EUT technical workshop. In this section a brief description will be given of the main characteristics of EUTERPE.

The lattice of EUTERPE consists of four superperiods. The magnetic structure of one superperiod consists of three 30° dipole magnets and eight quadrupoles for beam focusing. Moreover, sextupoles and closed orbit distortion correction magnets are added. Fig. 1.1 shows the proposed layout of the storage ring.

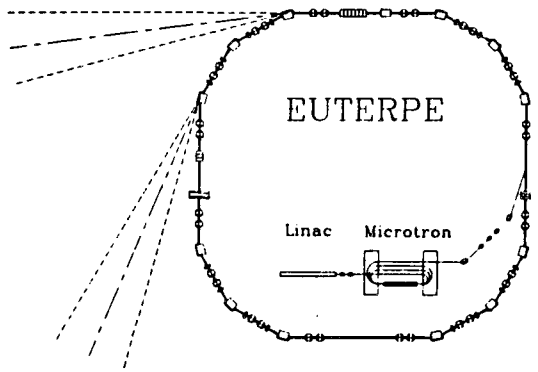

Figure 1.1: Layout of the storage ring EUTERPE. For clarity, the synchrotron radiation is only shown on some of the bending magnets.

The ring has a circumference of 40 meters, and has 2 meter long dispersion free straight sections to be used for insertion devices. The injector of EUTERPE is a 75 MeV racetrack microtron. This machine is injected from a 10 MeV (medical) linac. In table 1.1 some main parameters of the linac and the microtron are given. The pre-accelerators and the storage ring will be connected with two transfer lines. Transfer line 1 connects the linac and the microtron, and transfer line 2 connects the microtron and the storage ring. In table 1.2 main parameters of EUTERPE are given.

	Linac	Microtron
Injection Energy		10 MeV
Extraction Energy	10 MeV	75 MeV
Average Pulse Current	30 mA	6 mA
Energy Spread	10%	0.15%
Pulse Duration	2.2μs	2.2μs
rf frequency	3000 MHz	3000 MHz

Table 1.1: Main parameters of the linac and microtron.

Circumference	40 m
Electron energy	400 MeV
Injection energy	75 MeV
Beam current	200 mA
Lifetime	2 h
No. of superperiods	4
rf frequency	45 MHz
Harmonic number	6
rf voltage	50 kV
Dipoles:	
length	0.48 m
gap height	2.5 cm
max. field	1.4 T
Quadrupoles:	
length	0.25 m
aperture radius	2.5 cm
max. poletip field	0.3 T
Min. emittance	5.4 nm
Min. hor. beam size	0.07 mm
Bunch length	3.0 cm
Energy spread $\Delta E/E$	3.5×10^{-4}
Energy loss/turn	2.3 keV

Table 1.2: Main parameters of EUTERPE.

As can be seen from table 1.2 the injection energy is 75 MeV. In order to accelerate the electrons to an energy of 400 MeV, an accelerating structure must be designed. This accelerating structure also has to compensate the energy loss due to synchrotron radiation. This loss is about 2.3 keV per turn. The accelerating structure will be placed in one of the four dispersion free straight sections. There will also be other insertion devices placed in these sections so there is little space left for this accelerating structure.
The accelerating station will be a cavity operating according to the principles of a $\frac{1}{4}\lambda$-resonator. Because of space limitations it is desired that the maximum length should not exceed 50 cm. This means that the physical length of the cavity must be essentially shorter than the electrical length, which is 1.67 meter.

1.3 Transmission line theory of a $\frac{1}{4}\lambda$ cavity.

The basic shape of a coaxial $\frac{1}{4}\lambda$ cavity is given in Fig. 1.2. It consists of a beam pipe with a gap in it (the accelerating gap) and an outer conductor connected with the beam pipe by a shorting plate. In the cavity a standing wave electromagnetic field is generated such that the voltage is maximum across the accelerating gap.

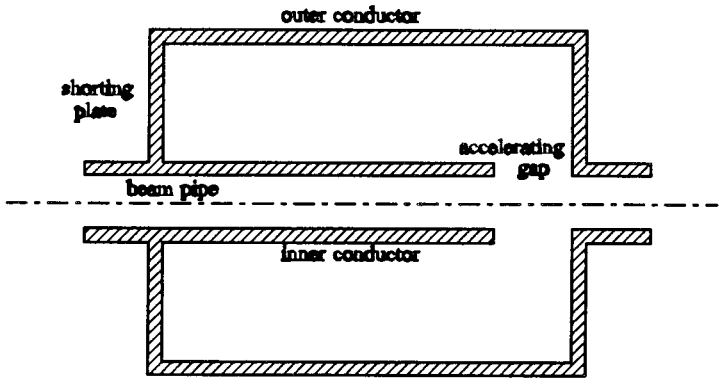

Figure 1.2: Basic design of a ¼λ coaxial transmission line cavity.

The electrical features of the cavity can be described with transmission line theory. A general transmission line can be represented as two parallel conductors, see Fig. 1.3.

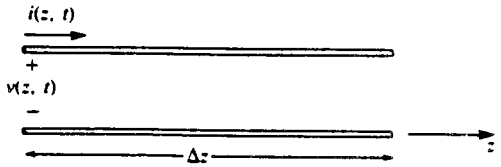

Figure 1.3: Voltage and current definitions of a transmission line.

The short piece of line of length Δz of Fig. 1.3 can be modelled as a lumped-element circuit, shown in Fig. 1.4, where R,L,G and C are per-unit-length quantities defined as follows:

R=resistance due to the finite conductivity of the two conductors.
L=total self-inductance of the two conductors.
G=shunt conductance due to dielectric loss in the material between the conductors.
C=shunt capacitance due to the close proximity of the two conductors

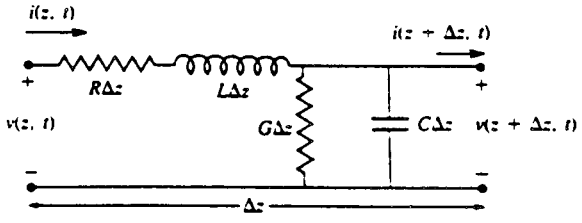

Figure 1.4: Lumped-element equivalent circuit of a short section of a transmission line.

A finite length of transmission line can be viewed as a cascade of sections of the form of Fig. 1.4. Using the symbols as defined in Fig. 1.4 the following equations can be derived by application of Kirchhoff's voltage law

$$v(z+\Delta z,t)-v(z,t)\equiv\Delta v(z,t)=-R\Delta z i(z,t)-L\Delta z\frac{\partial i(z,t)}{\partial t}, \tag{1.1}$$

and with Kirchhoff's current law

$$i(z+\Delta z,t)-i(z,t)\equiv\Delta i(z,t)=-G\Delta z v(z+\Delta z,t)-C\Delta z\frac{\partial v(z+\Delta z,t)}{\partial t}. \tag{1.2}$$

Dividing Eqs. (1.1) and (1.2) by Δz and then letting Δz approach to zero leads to the partial differential equations:

$$\frac{\partial v(z,t)}{\partial z}=-Ri(z,t)-L\frac{\partial i(z,t)}{\partial t}, \tag{1.3}$$

$$\frac{\partial i(z,t)}{\partial z}=-Gv(z,t)-C\frac{\partial v(z,t)}{\partial t}. \tag{1.4}$$

These equations are the time-domain form of the transmission line equations.
For the sinusoidal steady-state condition, for which we use the complex representation

$$v(z,t)\rightarrow V(z)e^{j\omega t}$$

$$i(z,t)\rightarrow I(z)e^{j\omega t}$$

Eqs. (1.3) and (1.4) simplify to

$$\frac{dV(z)}{dz}=-(R+j\omega L)I(z), \tag{1.5}$$

$$\frac{dI(z)}{dz}=-(G+j\omega C)V(z). \tag{1.6}$$

The Eqs. (1.5) and (1.6) can be solved simultaneously to give wave equations:

$$\frac{d^2V(z)}{dz^2}-\gamma^2V(z)=0, \tag{1.7}$$

$$\frac{d^2I(z)}{dz^2}-\gamma^2I(z)=0, \tag{1.8}$$

where

$$\gamma=\alpha+j\beta=\sqrt{(R+j\omega L)(G+j\omega C)}\ , \tag{1.9}$$

is the complex propagation constant. Travelling wave solutions can be found as

$$V(z)=V_0^{+}e^{-\gamma z}+V_0^{-}e^{\gamma z}, \tag{1.10}$$

$$I(z)=I_0^{+}e^{-\gamma z}+I_0^{-}e^{\gamma z}. \tag{1.11}$$

The voltage and the current on the line are related as

$$\frac{V_0^{+}}{I_0^{+}}=Z_0=\frac{-V_0^{-}}{I_0^{-}}, \tag{1.12}$$

where the characteristic impedance Z_0 is defined as

$$Z_0=\sqrt{\frac{R+j\omega L}{G+j\omega C}}\ . \tag{1.13}$$

The solution above is for a general transmission line. In many practical cases the loss of the line is so small, that it can be neglected. So by setting R=G=0 Eq. (1.9) gives

$$\beta=\omega\sqrt{LC}=k, \tag{1.14}$$

$$\alpha=0. \tag{1.15}$$

So $\gamma=jk$ with k the wave factor. The characteristic impedance reduces to

$$Z_0=\sqrt{\frac{L}{C}}\ . \tag{1.16}$$

For a ¼λ-resonator we get a standing wave solution if we short the line at z=0 (V(z=0)=0) and terminate the line at z=¼λ (I(z=λ/4)=0) as an open circuit

$$v(z,t)=U_0\sin(kz)\sin(\omega t)\ , \tag{1.17}$$

$$i(z,t)=I_0\cos(kz)\cos(\omega t)\ , \tag{1.18}$$

with

$$U_0=2V_0^+ \quad , \quad I_0=2I_0^+ ,$$

and

$$U_0=Z_0I_0 \ . \tag{1.19}$$

Here U_0 is the gap voltage, I_0 the current on the shorting plate and Z_0 the characteristic impedance.

Chapter 2

Basic Parameters of an Accelerating structure

2.1 Introduction

In this chapter some fundamental properties of an accelerating structure will be explained. The following paragraphs will treat successively the transit time factor, shunt impedance and quality factor. Furthermore the general features of a cavity will be explained by representing it as a lumped element circuit.

2.2 Transit time factor

The transit time factor takes into account the reduction in energy gain when crossing an accelerating gap due to the finite velocity of the particle. For simplicity we first assume that the electrical field is independent of the longitudinal coordinate z in the accelerating gap of a cavity. This is illustrated in Fig. 2.1.

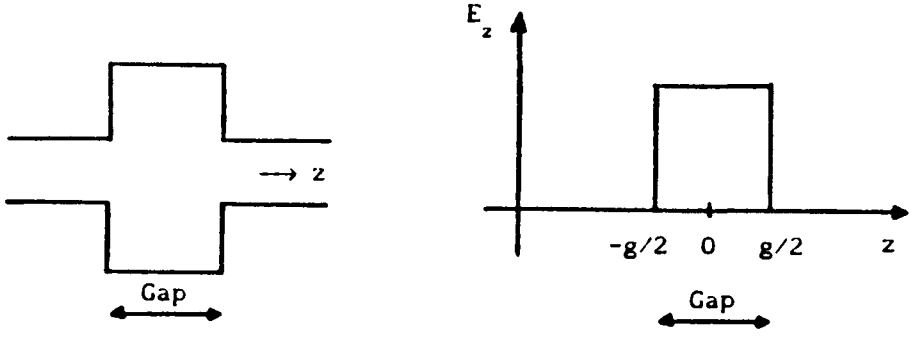

Figure 2.1: The accelerating gap and its approximate field pattern.

Suppose the voltage over the gap is V_g, then the accelerating field is given by

$$E_z = \frac{V_g}{g}\cos(\omega t) \ , \tag{2.1}$$

for -g/2<z<g/2, where g is the width of the gap and ω the angular rf frequency. When the particle needs a finite transit time to cross the gap its energy gain will be smaller than eV_g. If we assume that its velocity v is constant then the longitudinal coordinate is

$$z = vt \ . \tag{2.2}$$

The total energy gain ΔE of the electron passing the gap will be

$$\Delta E=\int_{-g/2}^{g/2}\frac{eV_g}{g}\cos(\frac{\omega z}{v})dz=eV_g\frac{\sin(\theta/2)}{\theta/2}=eV_gT\ , \tag{2.3}$$

where $\theta=\omega g/v$ is called the transit angle and T the transit time factor.
In reality the shape of the accelerating field will depend on the z coordinate as illustrated in Fig. 2.2

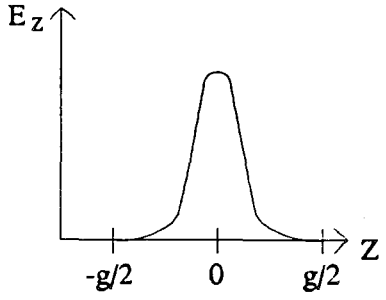

Figure 2.2: An inhomogeneous accelerating field.

The transit time factor for a inhomogeneous accelerating field is given by

$$T=\frac{|\int E_z(z)e^{j\omega t}dz|}{|\int E_z(z)dz|}\ . \tag{2.4}$$

2.3 Shunt impedance

When power is coupled into the cavity in order to generate an accelerating voltage over the gap, power will be dissipated in the cavity walls. This power will be proportional to the gap voltage squared. Mathematically this can be written as:

$$Z=\frac{V_g^2}{P_{dis}}\ . \tag{2.5}$$

In this formula Z is a cavity parameter called the shunt impedance, which is a measure for the necessary power to achieve a certain gap voltage. The higher the shunt impedance the less power is needed. One can also define a corrected shunt impedance R_{sh} which relates the actual energy gain of the particle to the dissipated power. This corrected shunt impedance is related to the uncorrected shunt impedance by the equation

$$R_{sh}=ZT^2\ , \tag{2.6}$$

where T is the transit time factor.

2.4 Quality factor

Every cavity has a certain quality, expressed in the cavity parameter called the quality factor. The quality factor of a cavity isolated from the surroundings (i.e. the unloaded quality factor) is given by

$$Q_0=\omega\frac{W_{st}}{P_{dis}}\ , \tag{2.7}$$

where W_{st} is the stored energy, P_{dis} the power dissipated in the cavity walls and $\omega=2\pi/T_{rf}$ the angular rf frequency. In order to couple power into a cavity it must be connected to a rf generator. When so, some of the stored energy may flow out of the cavity to the generator. In this case a loaded quality factor is defined as

$$Q_L=\omega\frac{W_{st}}{P_{dis}+P_{rad}}\ , \tag{2.8}$$

where P_{rad} is the power which flows out of the cavity. The loaded quality factor is related with the unloaded quality factor by the equation

$$Q_L=\frac{Q_0}{1+\beta}\ , \tag{2.9}$$

with $\beta=P_{rad}/P_{dis}$ a coupling constant expressing the amount of coupling between the generator and the cavity.

2.5 Representation of a cavity by a lumped element circuit.

A cavity can be represented by a parallel RLC-circuit as is shown in Fig. 2.3.

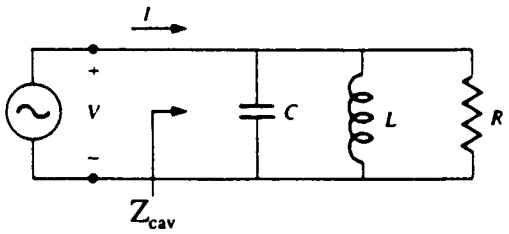

Figure 2.3: The parallel RLC circuit.

This circuit has a resonance spectrum from which the bandwidth can be determined. From this bandwidth the quality factor can be calculated.

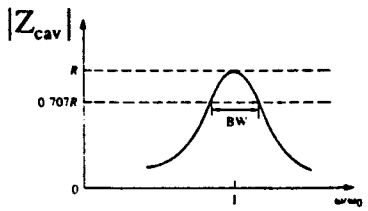

Figure 2.4: Resonance curve, the cavity impedance magnitude versus frequency.

In the RLC-circuit the capacitance is related to the total capacitance between the inner and outer conductor of the cavity. The power dissipation in the cavity walls is represented by the ohmic losses due to the resistance R. The inductance L relates the currents on the surface of the cavity with the induced magnetic fields in the cavity.
The cavity impedance is

$$Z_{cav}=\left(\frac{1}{R}+\frac{1}{j\omega L}+j\omega C\right)^{-1}, \tag{2.10}$$

The power dissipated by the resistor, R, is

$$P_{dis}=\frac{1}{2}\frac{|V|^2}{R}. \tag{2.11}$$

The average electric energy stored in the capacitor C and the average magnetic energy stored in the inductor L are given by

$$W_e=\frac{1}{4}|V|^2C, \tag{2.12}$$

$$W_m=\frac{1}{4}|I_L|^2L=\frac{1}{4}|V|^2\frac{1}{\omega^2L}, \tag{2.13}$$

where I_L is the current through the inductance L. Resonance occurs when $W_m=W_e$. Then the cavity impedance is $Z_{cav}=R$, which is a purely real impedance. From Eqs. (2.13) and (2.14), $W_m=W_e$ implies that the resonance frequency, ω_0, should be defined as

$$\omega_0=\frac{1}{\sqrt{LC}}. \tag{2.14}$$

Assuming that the cavity is on resonance, the quality factor Q_0 defined in equation (2.7) can (with $W_{st}=W_e+W_m$) be written as

$$Q_0=\omega_0\frac{2W_m}{P_{dis}}=\frac{R}{\omega_0L}=\omega_0RC=R\sqrt{\frac{C}{L}}. \tag{2.15}$$

Near resonance, letting $\omega=\omega_0+\Delta\omega$ where $\Delta\omega$ is very small, the cavity impedance can be simplified to [POZ 90]

$$Z_{cav}\approx\frac{R}{1+2jQ_0\delta}, \qquad \delta=\frac{\Delta\omega}{\omega_0}. \tag{2.16}$$

The half-power bandwidth edges occur at frequencies

$$\frac{\Delta\omega}{\omega_0}=\frac{BW}{2}\ , \tag{2.17}$$

where $\Delta\omega$ is determined by

$$|Z_{cav}|^2=\frac{R^2}{2}\ ,$$

which, from Eq. (2.17), implies that

$$BW=\frac{1}{Q_0}\ . \tag{2.18}$$

We can define a detuning angle ψ which is defined as

$$\tan\psi=-2Q_0\delta\ , \tag{2.19}$$

so that Z_{cav} can be written as

$$Z_{cav}=R\cos\psi e^{j\psi}\ . \tag{2.20}$$

In fig. 2.5 Z_{cav} is drawn in the complex plane as a function of ψ.

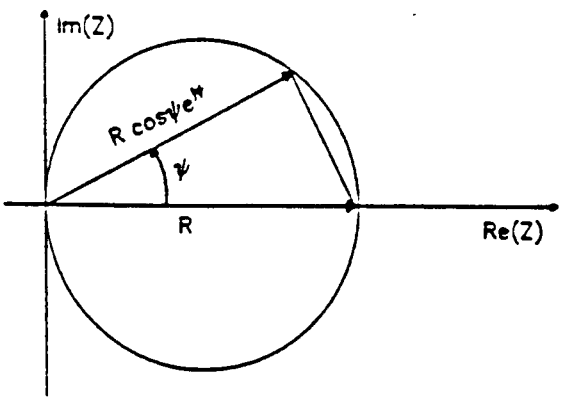

Figure 2.5: The complex cavity impedance as a function of the detuning angle.

When the cavity is on resonance then $\delta=0$, which gives $\psi=0$, and a purely real cavity impedance.

Chapter 3

The EUTERPE Cavity

3.1 Radial transmission line folding.

Due to space limitations in the storage ring, the physical length of a cavity must be much smaller than its electrical length. The first design of an accelerating cavity for the EUTERPE storage ring was based on the principles of radial transmission line folding. A study was done in order to describe the cavity parameters, such as the resonance frequency, the quality factor and the shunt impedance, and to find a optimum design. Also the problem of coupling power into the cavity was analyzed. This work is described in appendix A, since this cavity will not actually be built. We only give here the final results. Fig. 3.1 gives a layout for the cavity and in table 3.1 the main parameters are given. The geometrical dimensions of this design are given in table A.1 of appendix A.2

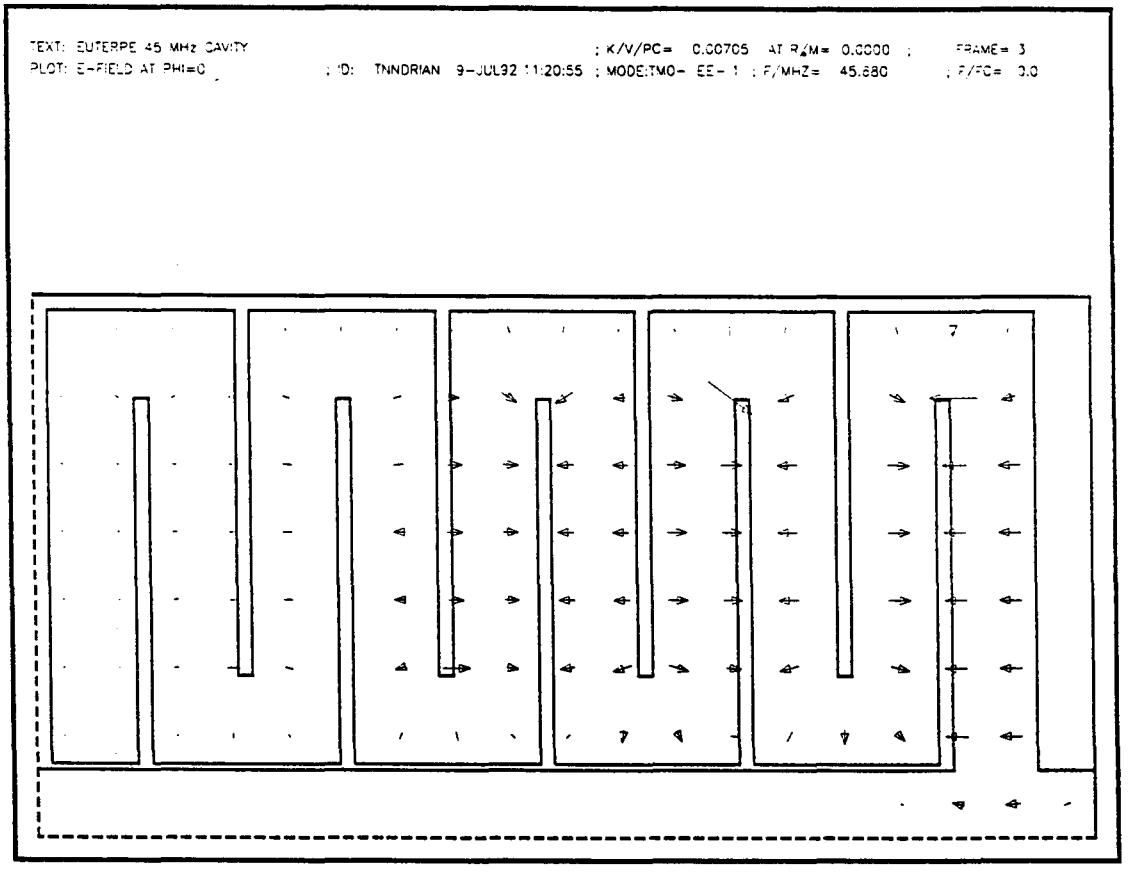

Figure 3.1: An URMEL-T plot of the electric fields in the initially proposed EUTERPE accelerating cavity, employing radial transmission line folding.

These main parameters were calculated analytically as well as numerically using the computer code URMEL-T [URM 87].

Parameters	Analytical	URMEL-T
f_0 (MHz)	45.00	45.68
Q_0	2573	2744
R_{sh} (kΩ)	145.2	135.0
P_{dis} (kW) (V_g=50 kV)	17.2	18.5
P_{dis} (kW) (V_g=100 kV)	68.9	74.1

Table 3.1: Main parameters of the initial design of the EUTERPE cavity.

As can be seen in Fig. 3.1 the construction of this cavity would become rather complicated. Furthermore the quality factor and the shunt impedance are low. This means that the dissipated power in the walls of the cavity is high. Therefore we looked for different designs of the cavity, with a higher quality factor and, which is more important, a higher shunt impedance.
The solution was found by employing longitudinal transmission line folding. This new design is easier to construct and, as we will see, the quality factor and the shunt impedance are essentially higher than in the first design. In the subsequent paragraphs of this chapter, analytical equations are derived, using transmission line theory for the cavity length, the dissipated power, the shunt impedance, the stored energy and the quality factor. Finally results of numerical and analytical calculations are given and compared. Furthermore conclusions are given.

3.2 Transmission line matrix theory.

The properties of a ¼λ cavity can be conveniently described by using matrix multiplication. In this method, a general cavity is decomposed into separate sections with each section characterised by a matrix A, which relates the voltage and the current at the exit of the section to the voltage and current at the entrance of the section, i.e

$$\begin{pmatrix} V \\ I \end{pmatrix}_{exit} = A \begin{pmatrix} V \\ I \end{pmatrix}_{entr.} \quad . \tag{3.1}$$

The total transformation of the voltage/current vector from the shorting plate to an arbitrary point along the cavity is then obtained by multiplication of all the matrices involved. If we take the transformation matrix from the shorting plate to the accelerating gap then the resonance condition is simply obtained by putting the right/under element of this matrix to zero. The reason for this is that at the shorting plate the voltage must be zero and at the accelerating gap the current must be zero.

In Fig. 3.2 a general design of the EUTERPE cavity is drawn. This simple two layer cavity consists of cylinders positioned concentric around the beam axis, which is the symmetry axis, a shorting plate and a return section plate. So the cavity consists of coaxial layers and a return section.

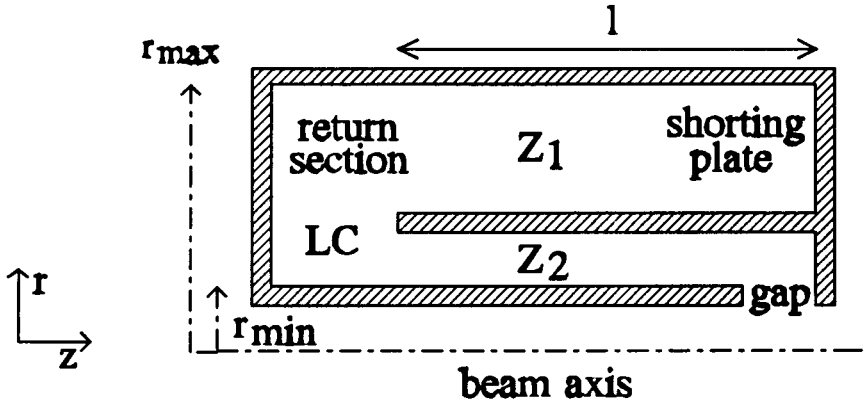

Figure 3.2: A general layout of a 2-layer coaxial cavity.

So for the EUTERPE cavity the separate elements are coaxial transmission line sections connected by a return section. The transformation matrix for a lossless transmission line section is calculated from Eqs.(1.5) and (1.6) (by putting R=G=0) and is given by [GRI 70],[SAN 86],[GEN 87].

$$A=\begin{pmatrix} \cos\beta z & -jZ_0\sin\beta z \\ -\frac{j}{Z_0}\sin\beta z & \cos\beta z \end{pmatrix}, \tag{3.2}$$

where Z_0 is the characteristic impedance and β=k the wave factor.
We model a return section by a lumped element circuit consisting of a series inductance and a shunt capacitance as given in Fig. 3.3. This will be a good approximation as long as the dimensions of the return section are small compared to the wavelength.

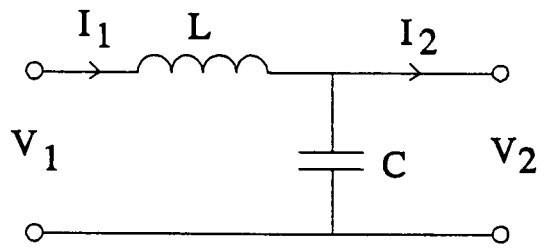

Figure 3.3: Lumped-element circuit representation of a return section.

The transfer matrix for this circuit is given by:

$$B = \begin{pmatrix} 1 & -j\omega L \\ -j\omega C & 1-\omega^2 LC \end{pmatrix}. \tag{3.3}$$

3.2.1 Analytical calculations of the cavity length.

The cavity can be described by using the transmission line matrix formalism. In order to illustrate the method, we assume a two cell cavity. In the simplest approximation one just can ignore the return section, and the equation for the length is given by Eq.(E.16) in appendix E, which is

$$l = \frac{1}{\beta}\arctan\sqrt{\frac{Z_2}{Z_1}}\ , \tag{3.4}$$

where Z_1 and Z_2 are the characteristic impedances of the two transmission line parts.
If we take the return section into account then the transmission line configuration of Fig. 3.4 can be used.

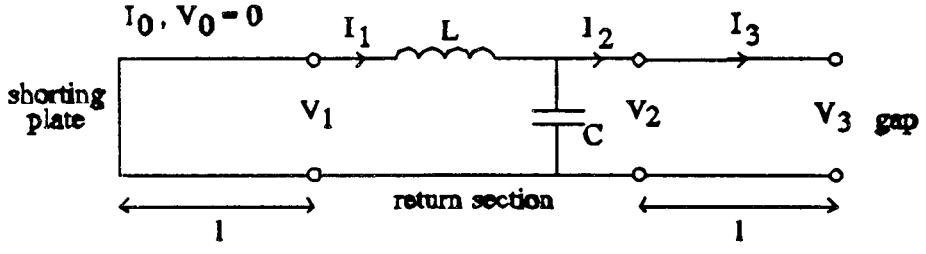

Figure 3.4: Transmission line configuration of a two layer cavity.

This network can be decomposed into three components: two lines with length l and a return section. The total network then is represented by three transfer matrices. The transformation for the total system is

$$\begin{pmatrix} V_3 \\ I_3 \end{pmatrix} = \begin{pmatrix} \cos kl & -jZ_2\sin kl \\ -\frac{j}{Z_2}\sin kl & \cos kl \end{pmatrix} \begin{pmatrix} 1 & -j\omega L \\ -j\omega C & 1-\omega^2 LC \end{pmatrix} \begin{pmatrix} \cos kl & -jZ_1\sin kl \\ -\frac{j}{Z_1}\sin kl & \cos kl \end{pmatrix} \begin{pmatrix} V_0 \\ I_0 \end{pmatrix}, \tag{3.5}$$

where Z_1 and Z_2 are the characteristic impedances of the outer layer and inner layer respectively. For the overall transfer matrix we have the following matrix equation

$$\begin{pmatrix} V_3 \\ I_3 \end{pmatrix} = \begin{pmatrix} a_{11} & a_{12} \\ a_{21} & a_{22} \end{pmatrix} \begin{pmatrix} V_0 \\ I_0 \end{pmatrix} . \tag{3.6}$$

The cavity is a ¼λ-resonator and so we have the " boundary conditions" $V_0=0$ and $I_3=0$. Therefore the matrix component a_{22} must be zero. This then gives the resonance condition:

$$(1-\omega^2 LC)\cos^2 kl - \left(\frac{\omega L}{Z_2}+\omega C Z_1\right)\sin kl \cos kl - \frac{Z_1}{Z_2}\sin^2 kl = 0 . \tag{3.7}$$

When divided by $\cos^2 kl$, the equation becomes

$$\frac{Z_1}{Z_2}\tan^2 kl + \left(\frac{\omega L}{Z_2}+\omega C Z_1\right)\tan kl - (1-\omega^2 LC) = 0 , \tag{3.8}$$

which gives the solution for the physical length l of the cavity as

$$\tan kl = -\frac{1}{2}\frac{\omega L}{Z_1} - \frac{1}{2}\omega C Z_2 + \frac{1}{2}\frac{Z_2}{Z_1}\sqrt{4\frac{Z_1}{Z_2}+\omega^2\left(\frac{L}{Z_2}-C Z_1\right)^2} , \tag{3.9}$$

where $-\frac{1}{2}\omega L/Z_1 - \frac{1}{2}\omega C Z_2$ and $\omega^2(L/Z_2 - CZ_1)^2$ are perturbation terms which take the return section into account. If L=C=0 (no return section) we get Eq.(3.4).
The inductance L of the return section is easily calculated with

$$L = \frac{\mu_0}{2\pi} g \ln\frac{r_{max}}{r_{min}} , \tag{3.10}$$

where g the gap, and r_{max} the outer radius of the outer layer and r_{min} the inner radius of the inner layer. The capacitance C can be calculated in three ways, namely by using the fringing field capacity formulas in appendix A.1, the conformal mapping formulas in appendix C or the computer code RELAX3D [REL 88] calculations in appendix B.

3.2.2 Dissipated power and shunt impedance.

The shunt impedance is defined by Eq.(2.5). In order to calculate it we need an analytical expression for the dissipated power. For this we use a model of a 2-layer cavity as given in Fig 3.5: the middle cylinder has zero thickness and the current on the shorting plate and in the return section are assumed constant. There are four contributions to the dissipated power, namely from the shorting plate, the outer coaxial layer, the return section and the inner coaxial layer.

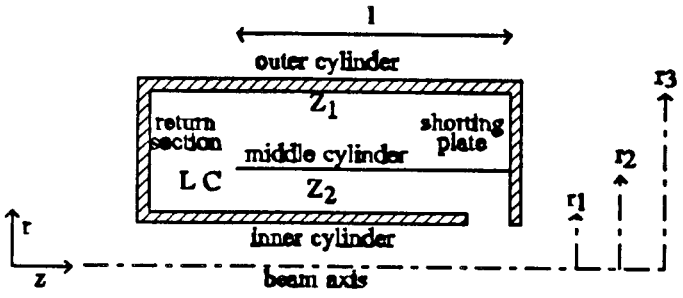

Figure 3.5: Assumed cavity geometry for calculating the shunt impedance. The middle cylinder has zero thickness.

We first consider the shorting plate. The infinitesimal resistance dR of a radial layer with thickness dr at radius r is given by

$$dR = \frac{\rho dr}{2\pi r \delta} , \tag{3.11}$$

where ρ is the specific resistance of the wall material and δ is the skin depth:

$$\delta = \left(\frac{2\rho}{\mu_0 \omega} \right)^{1/2} , \tag{3.12}$$

with μ_0 the magnetic permeability of vacuum and ω the angular rf frequency.
So assuming constant current along the shorting plate, the total dissipated power is

$$P_{short} = \frac{1}{2} \frac{\rho}{2\pi\delta} \int_{r_2}^{r_3} \frac{1}{r} |I_0|^2 dr = \frac{\rho I_0^2}{4\pi\delta} \ln \frac{r_3}{r_2} , \tag{3.13}$$

where r_2 and r_3 are the inner and outer radii of the outer coaxial layer respectively and I_0 is the shorting plate current.
Next we consider the outer coaxial layer. From the transformation matrix Eq.(3.2) we obtain the voltage and current profile along the outer layer by putting the voltage V_0 at the shorting plate equal to zero. Then

$$V_1(z) = -jZ_1 I_0 \sin kz , \tag{3.14}$$

$$I_1(z) = I_0 \cos kz , \tag{3.15}$$

with Z_1 the characteristic impedance of the outer layer.

Now consider a small section dz of the outer layer at position z. The infinitesimal resistance of this layer is:

$$dR=\frac{\rho dz}{2\pi\delta}\left(\frac{1}{r_2}+\frac{1}{r_3}\right), \tag{3.16}$$

where the first contribution comes from the inner cylinder and the second contribution from the outer cylinder respectively. So, the total power dissipated in the outer coaxial layer is

$$\begin{aligned} P_{coaxl}&=\frac{1}{2}\int_0^l I_1^2(z)\,dR=\frac{1}{2}\frac{\rho}{2\pi\delta}\int_0^l\left(\frac{1}{r_2}+\frac{1}{r_3}\right)|I_1|^2dz \\ &=\frac{\rho I_0^{\,2}}{4\pi\delta}\left(\frac{1}{r_2}+\frac{1}{r_3}\right)\left(\frac{1}{4k}\sin 2kl+\frac{l}{2}\right), \end{aligned} \tag{3.17}$$

where l is the length of the outer coaxial layer.
Next we consider the return section. For simplicity we ignore the thickness of this section and only take into account its radial plate. The current in the return section is

$$I_1=I_0\cos kl\ , \tag{3.18}$$

and so the dissipated power is

$$P_{plate}=\frac{1}{2}\frac{\rho}{2\pi\delta}\int_{r_1}^{r_3}\frac{1}{r}I_1^{\,2}dr=\frac{\rho I_0^{\,2}}{4\pi\delta}\cos^2 kl\ \ln\frac{r_3}{r_1}\ , \tag{3.19}$$

where r_1 is the inner radius of the inner coaxial layer.
To determine the current for the second coaxial layer we take the return section into account. This because the current profile is not exactly a cosine, but due to the return section, there is some deviation from it. After multiplying three matrices (coax1 transfer matrix with z=l, simple return section matrix and coax2 transformation matrix) we get for the voltage and the current profiles on the inner layer

$$V_3=-jI_0[(Z_1\sin kl+\omega L\cos kl)\cos kz+Z_2((1-\omega^2LC)\cos kl-\omega CZ_1\sin kl)\sin kz]\ , \tag{3.20}$$

$$I_3=I_0[((1-\omega^2LC)\cos kl-\omega CZ_1\sin kl)\cos kz-\left(\frac{Z_1}{Z_2}\sin kl+\frac{\omega L}{Z_2}\cos kl\right)\sin kz]\ . \tag{3.21}$$

And thus for the dissipated power in the second coaxial layer

$$P_{coax2}=\frac{1}{2}\frac{\rho}{2\pi\delta}\int_0^l\left(\frac{1}{r_1}+\frac{1}{r_2}\right)|I_3|^2dz$$

$$=\frac{\rho I_0^2}{4\pi\delta}\left(\frac{1}{r_1}+\frac{1}{r_2}\right)\left[A\left(\frac{1}{4k}\sin 2kl+\frac{l}{2}\right)+B\left(-\frac{1}{4k}\sin 2kl+\frac{l}{2}\right)-D\frac{1}{2k}\sin^2 kl\right], \tag{3.22}$$

with

$$A=((1-\omega^2LC)\cos kl-\omega CZ_1\sin kl)^2\ ,$$

$$B=\left(\frac{Z_1}{Z_2}\sin kl+\frac{\omega L}{Z_2}\cos kl\right)^2\ , \tag{3.23}$$

$$D=2((1-\omega^2LC)\cos kl-\omega CZ_1\sin kl)\left(\frac{Z_1}{Z_2}\sin kl+\frac{\omega L}{Z_2}\cos kl\right).$$

The total dissipated power in the cavity is

$$P_{tot}=P_{short}+P_{coax1}+P_{plate}+P_{coax2}\ . \tag{3.24}$$

To find the shunt impedance we need the relation between the shorting plate current I_0 and the gap voltage V_g. This equation has already been derived in Eq.(3.20), namely $V_g=V_3(z=l)$, so

$$V_g=-jI_0[\omega L\cos^2 kl-\omega CZ_1Z_2\sin^2 kl+(Z_1+Z_2(1-\omega^2LC))\cos kl\sin kl]\ . \tag{3.25}$$

The analytical shunt impedance of the cavity is then (assuming a transit time factor equal to one):

$$R_{sh}=\frac{|V_g|^2}{P_{tot}}\ . \tag{3.26}$$

The length l in these equations is given by equation (3.9). For convenience we assume that:

$$\omega CZ_1\ll 1 \quad , \quad \frac{\omega L}{Z_2}\ll 1\ . \tag{3.27}$$

The Eq.(3.9) can be simplified by making a Taylor expansion up to first order. If we further assume that $Z_1=Z_2=Z$ we get the following expression for the length l.

$$l=\frac{\pi}{4}\frac{c}{\omega}\left[1-\frac{1}{\pi}\left(\omega CZ+\frac{\omega L}{Z}\right)\right], \tag{3.28}$$

where c is the speed of light.

When we would ignore the effect of the return section on the voltage and current profiles completely (L=C=0) then the length of the cavity would simply become

$$l=\frac{\pi}{4}\frac{1}{k}\,, \tag{3.29}$$

which equals $l=\frac{1}{8}\lambda$.
Furthermore the approximation for the shunt impedance would simplify to:

$$R_{sh}=\frac{4\pi\delta Z^2}{\rho}\left[\ln\frac{r_3}{r_2}+l\left(\frac{1}{r_2}+\frac{1}{r_3}\right)\left(\frac{1}{2}+\frac{1}{\pi}\right)+\frac{1}{2}\ln\frac{r_3}{r_1}+l\left(\frac{1}{r_1}+\frac{1}{r_2}\right)\left(\frac{1}{2}-\frac{1}{\pi}\right)\right]^{-1}. \tag{3.30}$$

All these calculations can be done in the same way for a multi-layer cavity.

3.2.3 Stored energy and quality factor.

The quality factor is given by Eq. (2.7). In order to calculate Q analytically for the two layer cavity shown in Fig. 3.5, we first have to calculate the stored energy in the cavity. We assume that the stored energy of the entire cavity can be calculated by separating it into two coaxial parts with length l as defined previously. There are two contributions to the stored energy namely from the magnetic field and from the electric field.

$$W_{st}=W_{magn}+W_{elec}\,. \tag{3.31}$$

If we once more consider a small section dz at position z, then the energy stored in this section is

$$W_{st}=\frac{1}{2}LI^2(z)\,dz+\frac{1}{2}CV^2(z)\,dz\,, \tag{3.32}$$

where L is the inductance per unit length, C the capacitance per unit length, I(z) the wall current at position z and V(z) the voltage at position z. The inductance and capacitance for a coaxial transmission line are given by

$$L=\frac{\mu_0}{2\pi}\ln\frac{r_b}{r_a}\,,\qquad C=\frac{2\pi\varepsilon_0}{\ln\frac{r_b}{r_a}}\,, \tag{3.33}$$

where r_a and r_b are the inner and outer radii of the coax respectively.

For the outer coaxial layer we find

$$W_{magn\ coax1}=\frac{1}{4}\int_0^l L|I|^2dz=\frac{\mu_0 I_0^2}{8\pi}\ln\frac{r_3}{r_2}\int_0^l\cos^2 kz dz$$
$$=\frac{\mu_0 I_0^2}{8\pi}\ln\frac{r_3}{r_2}\left(\frac{1}{4k}\sin 2kl+\frac{l}{2}\right). \tag{3.34}$$

For the stored magnetic energy of the second coaxial layer we get

$$W_{magn\ coax2}=\frac{1}{4}\int_0^l\frac{\mu_0}{2\pi}\ln\frac{r_2}{r_1}|I_3|^2dz$$
$$=\frac{\mu_0 I_0^2}{8\pi}\ln\frac{r_2}{r_1}\left[A\left(\frac{1}{4k}\sin 2kl+\frac{l}{2}\right)+B\left(-\frac{1}{4k}\sin 2kl+\frac{l}{2}\right)-D\frac{1}{2k}\sin^2 kl\right], \tag{3.35}$$

in which A,B and D are given by Eqs.(3.23), I_3 is the current in the second coaxial layer, where in this case the influence of the return section on the current profile is not yet ignored. The total stored magnetic energy is

$$W_{magn}=W_{magn\ coax1}+W_{magn\ coax2}\ . \tag{3.36}$$

Similarly we can calculate the stored electrical energy in the outer coaxial layer as

$$W_{elec\ coax1}=\frac{1}{4}\int_0^l C|V_1|^2dz=\frac{1}{4}\int_0^l\frac{2\pi\varepsilon_0}{\ln\frac{r_3}{r_2}}V_1V_1^*dz$$
$$=\frac{\mu_0 I_0^2}{8\pi}\left(-\frac{1}{4k}\sin 2kl+\frac{l}{2}\right)\ln\frac{r_3}{r_2}\ , \tag{3.37}$$

where we used Eq.(3.14) for V_1 and

$$Z_1=\frac{1}{2\pi}\sqrt{\frac{\mu_0}{\varepsilon_0}}\ln\frac{r_3}{r_2}\ , \tag{3.38}$$

for the characteristic impedance of the line.
Furthermore,

$$W_{elec\ coax2}=\frac{1}{4}\int_0^l\frac{2\pi\varepsilon_0}{\ln\frac{r_2}{r_1}}|V_3|^2dz$$

$$=\frac{\pi\varepsilon_0 I_0^2 Z_2^2}{2\ln\frac{r_2}{r_1}}\left[A\left(-\frac{1}{4k}\sin 2kl+\frac{l}{2}\right)+B\left(\frac{1}{4k}sin2kl+\frac{l}{2}\right)+D\frac{1}{2k}\sin^2 kl\right], \tag{3.39}$$

where A,B and D are given by Eqs.(3.23).
The total stored electric energy is

$$W_{elec}=W_{elec\ coax1}+W_{elec\ coax2}\ . \tag{3.40}$$

After some calculation we find for the total stored energy

$$W_{tot}=\frac{\mu_0 I_0^2 l}{8\pi}\left(\ln\frac{r_3}{r_2}+(A+B)\ln\frac{r_2}{r_1}\right). \tag{3.41}$$

Then the quality factor is, with $\delta=(2\rho/\mu_0\omega_0)^{1/2}$,

$$Q=\frac{l}{\delta}\ \frac{\ln\frac{r_3}{r_2}+(A+B)\ln\frac{r_2}{r_1}}{X}\ , \tag{3.42}$$

with X

$$X=\ln\frac{r_3}{r_2}+\left(\frac{1}{r_2}+\frac{1}{r_2}\right)\left(\frac{1}{4k}\sin 2kl+\frac{l}{2}\right)+\ln\frac{r_3}{r_1}\cos^2 kl$$

$$+\left(\frac{1}{r_1}+\frac{1}{r_2}\right)\left[A\left(\frac{1}{4k}\sin 2kl+\frac{l}{2}\right)+B\left(-\frac{1}{4k}\sin 2kl+\frac{l}{2}\right)-D\frac{1}{2k}\sin^2 kl\right], \tag{3.43}$$

where A,B and D are given in Eqs.(3.23).
If we now also ignore the influence of the return section on the current and voltage profiles in the second layer, as we have done with the approximation of the shunt impedance, then we obtain for the approximation of the quality factor

$$Q=2\frac{l}{\delta}\ln\frac{r_3}{r_2}\left[\ln\frac{r_3}{r_2}+l\left(\frac{1}{r_2}+\frac{1}{r_3}\right)\left(\frac{1}{2}+\frac{1}{\pi}\right)+\frac{1}{2}\ln\frac{r_3}{r_1}+l\left(\frac{1}{r_1}+\frac{1}{r_2}\right)\left(\frac{1}{2}-\frac{1}{\pi}\right)\right]^{-1}, \tag{3.44}$$

where we have used $kl=\pi/4$ and L=C=0.

3.3 Analytical and numerical calculations; conclusions.

The analytical results for the length, the quality factor and the shunt impedance are compared with numerical results that are obtained by the computer code SUPERFISH [POI 87]. We therefore choose once more a simple geometry for a two layer longitudinally folded cavity, for which the middle cylinder has zero thickness as used in the analytical calculations. The radial dimensions are r_1=2.6 cm, r_2=5.9 cm and r_3=13.4 cm . They are chosen in such a way that the characteristic impedances of the first and the second layer are equal. The inductance of the return section was calculated with Eq.(3.10), where $r_{max}=r_3$, $r_{min}=r_1$ and g=5 cm for the gap of the return section, which results in L=16.4 nH. The capacitance C=3.6 pF was calculated with RELAX3D. This is a numerical program which solves the 3-dimensional Laplace equation (see appendix C). In Fig. 3.6 the comparison between analytical and numerical results is shown.

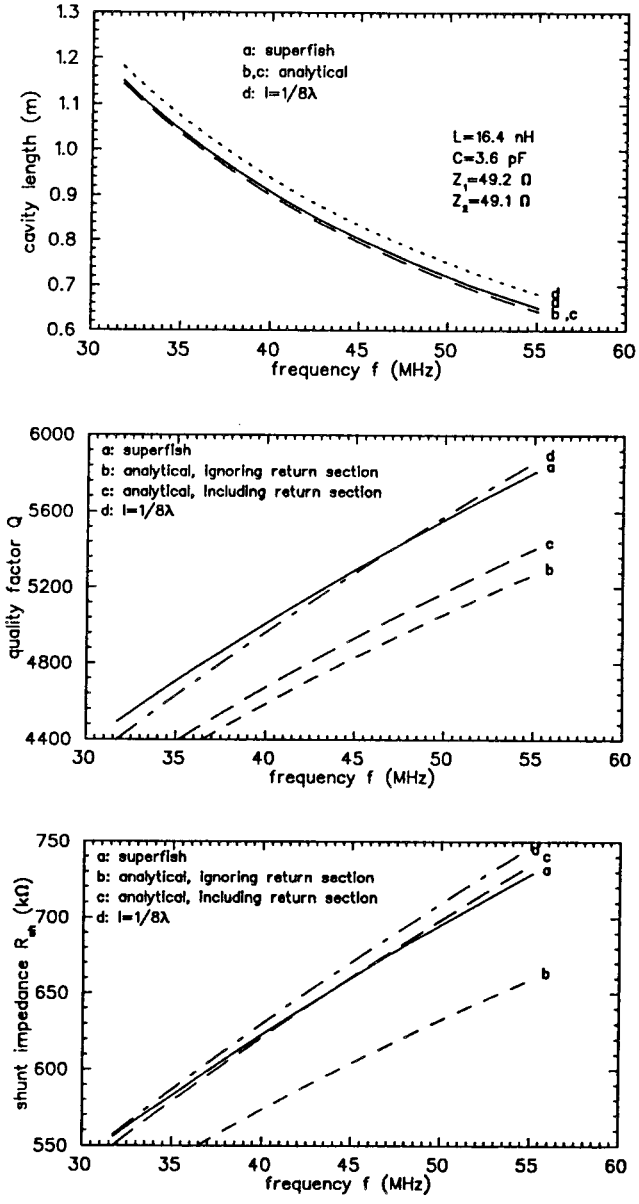

Figure 3.6: Comparison between analytical and SUPERFISH results as a function of the frequency, for a 2-layer cavity employing longitudinal transmission line folding.

Curve a represents the SUPERFISH calculations. Curve b is calculated by using the simple equations (3.28), (3.44), and (3.30), respectively. These curves show already quite good agreement. A further improvement of the analytical results is obtained if the influence of the return section on the current and voltage profiles in the inner layer is taken into account. Curve c is obtained when using Eqs. (3.9), (3.42), and (3.26), respectively. As expected the analytical results give even better agreement with the numerical SUPERFISH results. The quality factor approximation can even be more improved when l is taken as $\frac{1}{8}\lambda=c/8f$. The results are represented by curve d. This occurs because now we take the entire volume of the cavity into account, instead of only the parts defined by the length l used in the transmission line matrix theory, without the return section. This means that the calculated stored energy increases, and thus the quality factor.

We can therefore conclude that the transmission line matrix formalism is a valuable method for analytically estimating the length, the quality factor and shunt impedance.
The calculations shown in this chapter have been done for a two layer cavity employing longitudinal transmission line folding, but the theory can be also used be used for multi-layer cavities.

We now look at some construction parameters of the cavity employing longitudinal transmission line folding. In Fig. 3.7 a general layout of the cavity is drawn. This cavity consists of three layers. The more layers a cavity has the smaller the physical length will be. The cavity consists of coaxial parts and return sections. For the coaxial parts the characteristic impedance is only a function of the outer and inner radii,respectively r_b and r_a, given by Eq.(3.38). In the cavity of Fig. 3.7 the radii are chosen in such a way, that the characteristic impedances of the coaxial layers are equal.
The cavity has three gaps, two gaps between layers and one accelerating gap. By using the computer code URMEL-T we calculated the effect on the length, the quality factor and the shunt impedance of the cavity when changing the width of the gaps. The gaps are chosen such that they are equal to the distances between the cylinders of a layer, denoted by s_1, s_2, s_3. In these calculations the frequency was kept constant at about 45 MHz, and the outer radius at 31.14 cm.

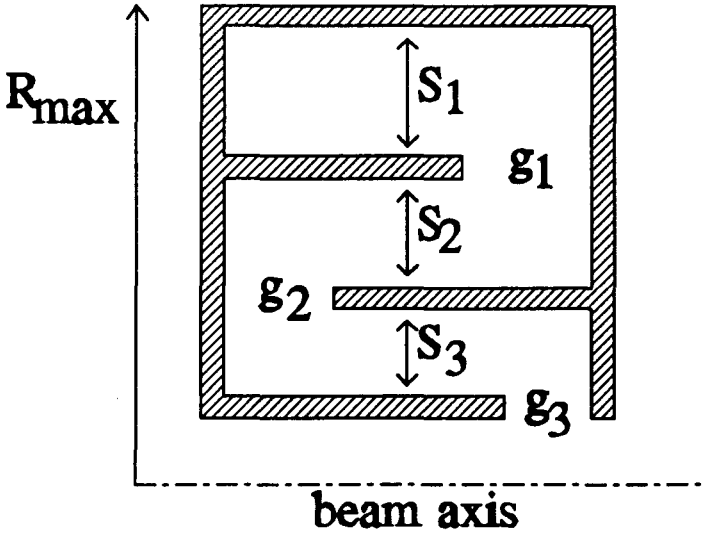

Figure 3.7: A general layout of a 3-layer coaxial cavity.

The results of the numeral calculations are listed in table 3.2.

gap 1	gap 2	gap 3	f_0 (MHz)	Q_0	R_{sh} (kΩ)	l (cm)
s_3	s_3	s_3	45.2	8355	1406.8	52.0
s_2	s_3	s_3	45.6	8362	1448.4	52.5
s_1	s_2	s_3	45.5	8380	1611.0	55.0

Table 3.2: Numerical calculations of the effect of changing the distances of the gaps. The outer radius is kept constant at R_{max}=31.14 cm

By going down in the table the total surface of the cavity becomes smaller. The quality factor doesn't change much, but the shunt impedance does, and becomes larger. This is the result of the decrease of the dissipated power in the cavity walls, while the volume and therefore the stored energy remains the same.

We now look at the effect of changing the outer radius. For these calculations we use a simpler model consisting of two cells (see Fig 3.8). In order to keep the characteristic impedance the same for the two layers, the outer radius of the outer layer must also be increased, when the outer radius of the inner layer is increased.

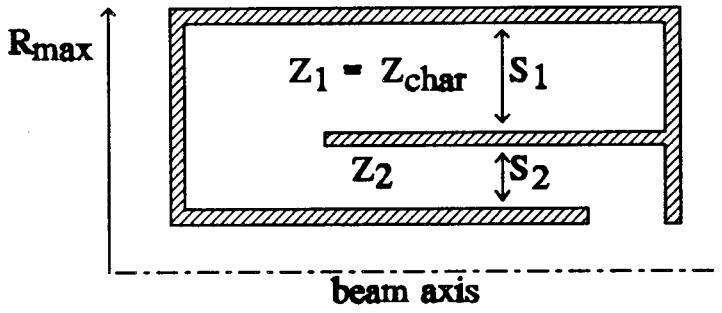

Figure 3.8: A 2-layer cavity.

In table 3.3 the results of the URMEL-T calculations are given when changing s_2, while keeping the frequency more or less constant.

s_2 (cm)	s_1 (cm)	f_0 (MHz)	Q_0	R_{sh} (kΩ)	l (cm)	R_{max} (cm)	Z_{char} (Ω)
1.5	2.7	45.8	2451	165.4	83.7	8.2	28.2
3.0	7.2	44.5	5087	664	83.0	14.2	47.3
5.0	16.0	44.0	9356	1590	81.3	25.0	65.9

Table 3.3: URMEL-T calculations of the effect of changing the width of the layers and thereby the characteristic impedance.

If we increase the radial dimensions, the length of the cavity must be decreased slightly. The quality factor and the shunt impedance become much larger. If we would apply this to a cavity consisting of three layers, R_{max} would increase considerably when increasing s_2. For s_2=3.0 cm, R_{max} would become 30.6 cm.
In the calculations above we kept the characteristic impedances of the different layers constant. Now the effect of different characteristic impedances of the layers is determined. The results are given in table 3.4. We again use a two cell geometry as in Fig. 3.8, with a characteristic impedance of the inner layer of Z_2=47.3 Ω as a reference. Again we must adjust the length in order to keep the resonance frequency constant at 45 MHz.

Z_1 (Ω)		f_0 (MHz)	Q_0	R_{sh} (kΩ)	l (cm)	R_{max} (cm)
30.8	$Z_1<Z_2$	48.3	3692	324	88.3	10.5
47.3	$Z_1=Z_2$	44.5	5087	664	81.6	13.7
58.9	$Z_1>Z_2$	44.5	6220	962	75.3	16.5
69.2	$Z_1>Z_2$	44.9	7254	1236	71.0	19.5

Table 3.4: URMELT-T calculations of the effect of varying the characteristic impedance of the outer layer.

The result is that if the characteristic impedance of the outer layer increases, the cavity becomes shorter (see resonance condition described in appendix E), while the quality factor and the shunt impedance increase. This is a desired effect, because less power is needed to build up an accelerating voltage of 50 kV. We can therefore conclude that it is favourable to choose s_1 and s_3 as large as possible (large R_{max}). In reality this will be limited because of practical construction limitations.

Chapter 4

Coupling rf Power into the Cavity

4.1 Introduction.

To generate an accelerating voltage at the gap power has to be coupled into the cavity. This can be done in different ways. One solution is by directly connecting the inner conductor of the input transmission line to the inner conductor of the cavity. This is shown in Fig. 4.1a and is described in detail in appendix B. There it is shown that in order to have matched coupling, the coupling point must be very close to the shorting plate. A disadvantage of this is that the VSWR (Voltage Standing Wave Ratio, described in paragraph 4.4) is sensitive to changes of the coupling position. This leads to the necessity of a movable connection with the inner conductor. The current on the inner conductor is high near the shorting plate, so losses can occur which lead to undesired heating.
A second solution is based on inductive coupling with a loop. This is described in paragraph 4.2, where the matching conditions are derived. In paragraph 4.3 these conditions are used to find the required properties of the loop like area, number of windings, position and rotation angle.

4.2 Inductive coupling.

We have seen that direct coupling is not so convenient for a cavity employing longitudinal transmission line folding. The best solution is found in inductive coupling with a small loop. This is shown in Fig. 4.1b.

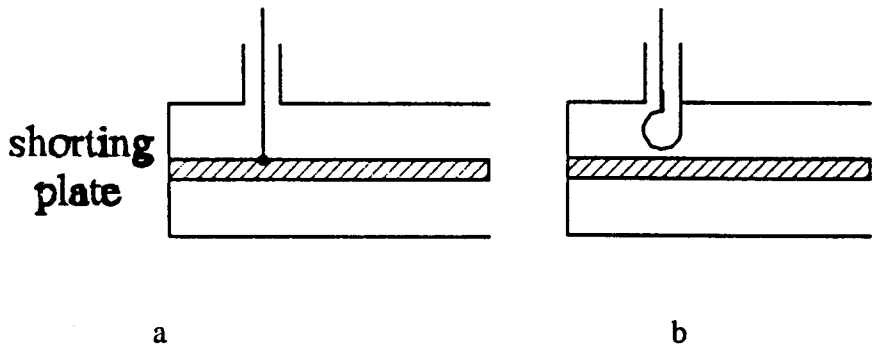

Figure 4.1: a: Direct coupling to the inner conductor. b: Inductive coupling with a little loop.

The complete rf system can be simulated by the equivalent circuit, given in Fig. 4.2. The rf generator is represented by an ideal rf voltage V_0 in series with the characteristic impedance R_0 of the input transmission line. The resonator is represented by a series resonant RLC lumped-element circuit. The quantity I_0 is chosen to represent the current at the shorting plate.

The coupling between the input line and the resonator is represented by the mutual inductance M. First we calculate the input impedance seen by the generator.

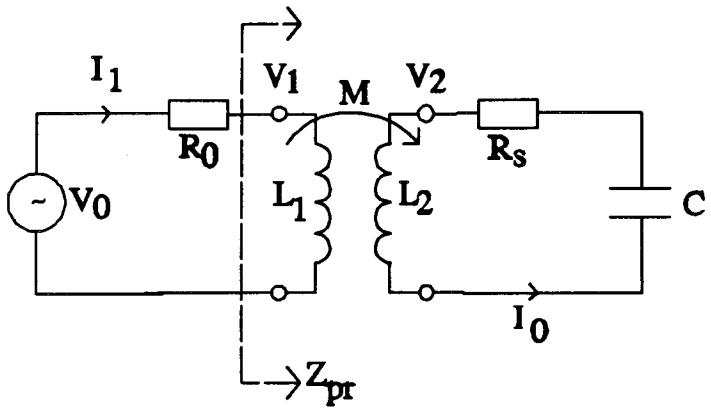

Figure 4.2: Equivalent circuit for the complete rf system.

For the primary circuit we get the following equation

$$V_1 = j\omega L_1 I_1 + j\omega M I_0 \ , \tag{4.1}$$

and for the secundary circuit

$$V_2 = j\omega M I_1 + j\omega L_2 I_0 \ . \tag{4.2}$$

Also

$$V_2 = -I_0 R_s - \frac{I_0}{j\omega C} \ , \tag{4.3}$$

where R_s is the series resistance in the circuit. Elimination of V_2 gives

$$j\omega M I_1 + I_0 \left(j\omega L_2 + \frac{1}{j\omega C} + R_s \right) = 0 \ . \tag{4.4}$$

Next, elimination of I_0 gives

$$V_1 = I_1 \left(j\omega L_1 + \frac{\omega^2 M^2}{j\omega L_2 + \frac{1}{j\omega C} + R_s} \right) , \tag{4.5}$$

and with substitution of the angular resonance frequency

$$\omega_0=\frac{1}{\sqrt{L_2C}}\ , \tag{4.6}$$

Eq. (4.5) becomes

$$V_1=I_1\left(j\omega L_1+\frac{\omega^2M^2}{R_s\left[1+\frac{jL_2}{\omega R_s}(\omega^2-\omega_0^2)\right]}\right). \tag{4.7}$$

Now the impedance as seen from the generator can, with the use of

$$Q_0=\frac{1}{R_s}\sqrt{\frac{L_2}{C}}\quad ,\quad \delta=\frac{\omega-\omega_0}{\omega_0}=\frac{\Delta\omega}{\omega_0}\ , \tag{4.8}$$

be written as (assuming $\delta<<1$)

$$Z_{pr}=j\omega L_1+\frac{\omega^2M^2}{R_s(1+2jQ_0\delta)}\ . \tag{4.9}$$

In Fig. 4.3 Z_{pr} is drawn in the complex plane.

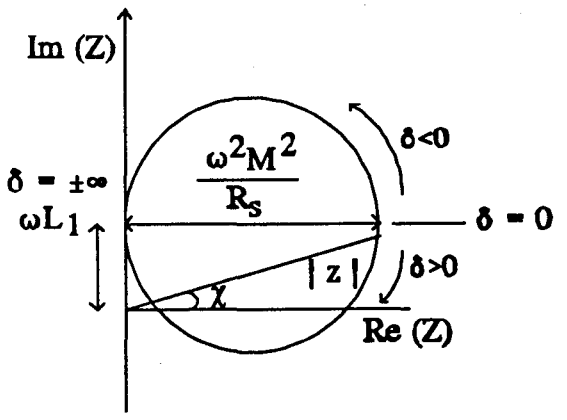

Figure 4.3: The complex input impedance seen by the generator.

The diameter of the circle is ω^2M^2/R_s. The quantity $\omega^2M^2/R_s(1 + 2jQ_0\delta)$ is the impedance of the cavity transformed to the primary circuit. The primary impedance is a complex quantity, having resistive and reactive components. If we compare this with the input impedance for an isolated resonator given in Eq. 2.16 and drawn in Fig. 2.5 we see that the circle has a vertical displacement due to the reactance ωL_1 of the coupling loop.
To obtain impedance matching of the cavity seen from the transmission line, the voltage reflection coefficient Γ as measured on the transmission line $\Gamma=(Z_{pr}-R_0)/(Z_{pr}+R_0)$ must be zero. Thus $Z_{pr}=R_0\approx 50\ \Omega$.

From Eq. (4.9) two conditions for zero reflection can be derived. The imaginary part of Z_{pr} must be equal to zero, and the real part of Z_{pr} must be equal to R_0. This leads to a requirement for the detuning factor

$$\delta=\frac{\omega L_1}{2Q_0R_0}\ , \tag{4.10}$$

and for the mutual induction

$$M=\frac{\sqrt{R_0R_s}}{\omega}\left(1+\left(\frac{\omega L_1}{R_0}\right)^2\right)^{\frac{1}{2}}\ . \tag{4.11}$$

The first condition can be satisfied if the resonator is detunable. The second condition can be satisfied for example if the loop is rotatable, such that the mutual induction M can be varied from zero to a maximum. This maximum must be larger than M given in Eq. (4.11)

4.3 Requirements for the coupling loop.

The power dissipated in the lumped element circuit of Fig. 4.2 is

$$P_{diss}=\frac{1}{2}I_0^2R_s\ , \tag{4.12}$$

which must be equal to the power dissipated in the cavity

$$P_{diss}=\frac{V_g^2}{R_{sh}}=\frac{1}{2}\frac{V_g^2}{R_{sh}^*}\qquad ,\qquad R_{sh}=2R_{sh}^*\ . \tag{4.13}$$

From these two equations and with the use of Eq. (4.11) we get

$$M=\frac{1}{\omega}\frac{V_g}{I_0}\left(1+\left(\frac{\omega L_1}{R_0}\right)^2\right)^{1/2}\left(\frac{R_0}{R_{sh}^*}\right)^{1/2}\ . \tag{4.14}$$

The mutual induction M is determined by the equation

$$\Phi=MI_0\ , \tag{4.15}$$

where Φ is the magnetic flux enclosed by the coupling loop. If we assume that the loop is not too large, then the magnetic field can be taken constant across the loop. This gives us another equation for the flux

$$\Phi = B_c A = \mu_0 H_c A \ , \tag{4.16}$$

with A the area of the loop and B_c the magnetic induction at the position of the loop at a distance z from the shorting plate. The magnetic field strength is determined by

$$\oint H_c \, ds = 2\pi r H_c = I_c \ , \tag{4.17}$$

where I_c is the current on the inner conductor at a distance z from the shorting plate, where the loop is located, and r the radial distance from the cavity axis to the middle of the loop. Together with Eqs. (4.15) and (4.16) we get for M

$$M = \frac{\mu_0 A}{2\pi r} \frac{I_c}{I_0} \ . \tag{4.18}$$

For the matching condition we get by using Eq. (4.14)

$$\frac{\mu_0 f_0 A}{r} \frac{I_c}{V_g} = \left(\frac{R_0^2 + (\omega L_1)^2}{R_{sh}^* R_0} \right)^{1/2} \ . \tag{4.19}$$

Suppose we rotate the loop over an angle θ, and the loop consists of N windings, Eq. (4.16) becomes

$$\Phi = B_c A N \cos\theta \ , \tag{4.20}$$

and the matching condition becomes

$$\frac{\mu_0 f_o A N \cos\theta}{r} \frac{I_c}{V_g} = \left(\frac{R_0^2 + (\omega L_1)^2}{R_{sh}^* R_0} \right)^{1/2} \ . \tag{4.21}$$

In order to be able to produce always matched coupling the area of the loop must be larger than A given by Eq. (4.21) with $\theta=0$.
The ratio I_c/V_g can again be calculated with the transmission line matrix theory treated in chapter 3. When coupling close to the shorting plate $I_c \approx I_0$. If we approximate the cavity by an ideal ¼λ-system with a characteristic impedance Z_0, the ratio I_c/V_g is $1/Z_0$.

4.4 Voltage standing wave ratio.

The quantity $V_{max}/V_{min} = I_{max}/I_{min} = VSWR$ is called the voltage standing wave ratio and is a measure of the mismatch between a line and its terminating impedance. It is related to the

voltage reflection coefficient by

$$VSWR=\frac{1+|\Gamma|}{1-|\Gamma|}\ , \tag{4.22}$$

The VSWR is a real quantity and since $0\leq|\Gamma|\leq 1$, $1\leq VSWR\leq\infty$, where VSWR=1 implies a matched load. The magnitude of the reflection coefficient on the line is found from the standing wave ratio as

$$|\Gamma|=\frac{VSWR-1}{VSWR+1}\ . \tag{4.23}$$

Chapter 5

Design and Construction of a Cold Model

5.1 Introduction.

A "cold" model was built in order to test the analytical equations derived in chapter 3 and 4 involving the cavity parameters and the coupling of power into the cavity, and the numerically calculated parameters. These numerical calculations have been carried out using the computer codes SUPERFISH and URMEL-T. The aim of these calculations was to obtain information about the resonance frequency, electric and magnetic fields, shunt impedance and quality factor. Both programs calculate azimuthally symmetric modes in a three-dimensional geometry with cylindrical symmetry [URM 85], [POI 87]. URMEL-T is the most complex program of the two, since it can also calculate azimuthally asymmetric modes. In the next sections the results of numerical calculations are presented which lead to the building of a 1:1 "cold" copper model of the EUTERPE accelerating cavity employing longitudinal transmission line folding. Cold means that it will only operate at low voltages and currents. The cavity consists of two layers.

5.2 URMEL-T calculations.

A scale 1:1 two layer model cavity employing longitudinal transmission line folding was built. The radial dimensions were determined by the commercially available copper pipe, with the requirement that the characteristic impedances of the two layers were more or less equal. In Fig. 5.1 the final layout of the model cavity is drawn, and in table 5.1 the dimensions are given.

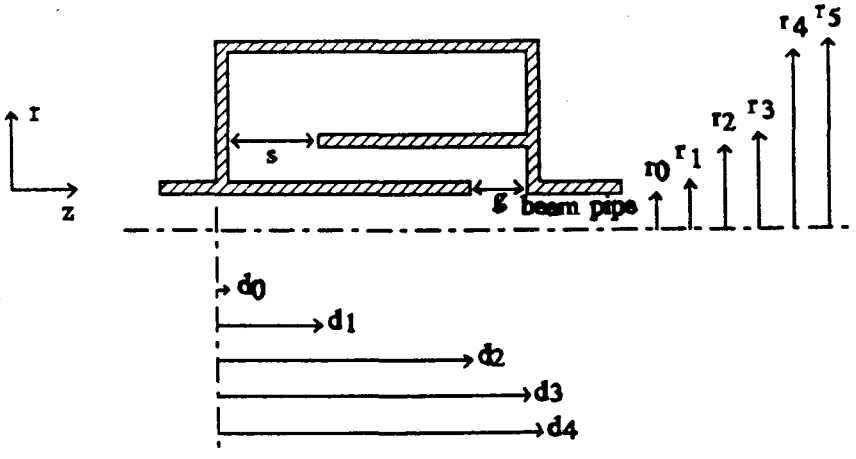

Figure 5.1: Lay-out of the scale 1:1 cavity measuring model.

Radial	Longitudinal
r_0= 23.0 mm	d_0= 10.0 mm
r_1= 25.0 mm	d_1= 76.5 mm
r_2= 52.5 mm	d_2=836.5 mm
r_3= 55.5 mm	d_3=864.0 mm
r_4=122.0 mm	d_4=934.0 mm
r_5=125.0 mm	s=66.5 mm
	g=27.5 mm

Table 5.1: Dimensions of the 1:1 model cavity.

An example of the input file for URMEL-T is given in appendix G. In order to calculate this very long geometry with thin cylinder walls it was necessary to use the maximum number of mesh points. URMEL-T needs about 30 min CPU time on a VAX-station (Digital 3100 M38) for this geometry. The cavity parameters calculated by URMEL-T are listed in table 5.2. The results obtained with SUPERFISH are also included as a comparison.

Parameter	URMEL-T	SUPERFISH
Frequency f_0	43.0 MHz	44.0 MHz
Quality factor Q_0	4590	4746
Shunt impedance R_{sh}	552 kΩ	573 kΩ
Dissipated power P_{dis} (V_g=50 kV)	4.5 kW	4.4 kW

Table 5.2: Parameters of the cavity in Fig. 5.1 obtained from URMEL-T and SUPERFISH.

There is good agreement between both calculations. In Fig. 5.2 a plot of the electric and magnetic field of the ground mode is shown. This is a TM mode, which means that the magnetic field is transverse to the propagation direction of the wave, (B_z=0 everywhere). URMEL-T has the possibility to calculate higher order modes of a cavity. With this a possible frequency spectrum of the model cavity can be predicted. These frequencies are also calculated analytically. The results of the first ten modes are listed in table 5.3.

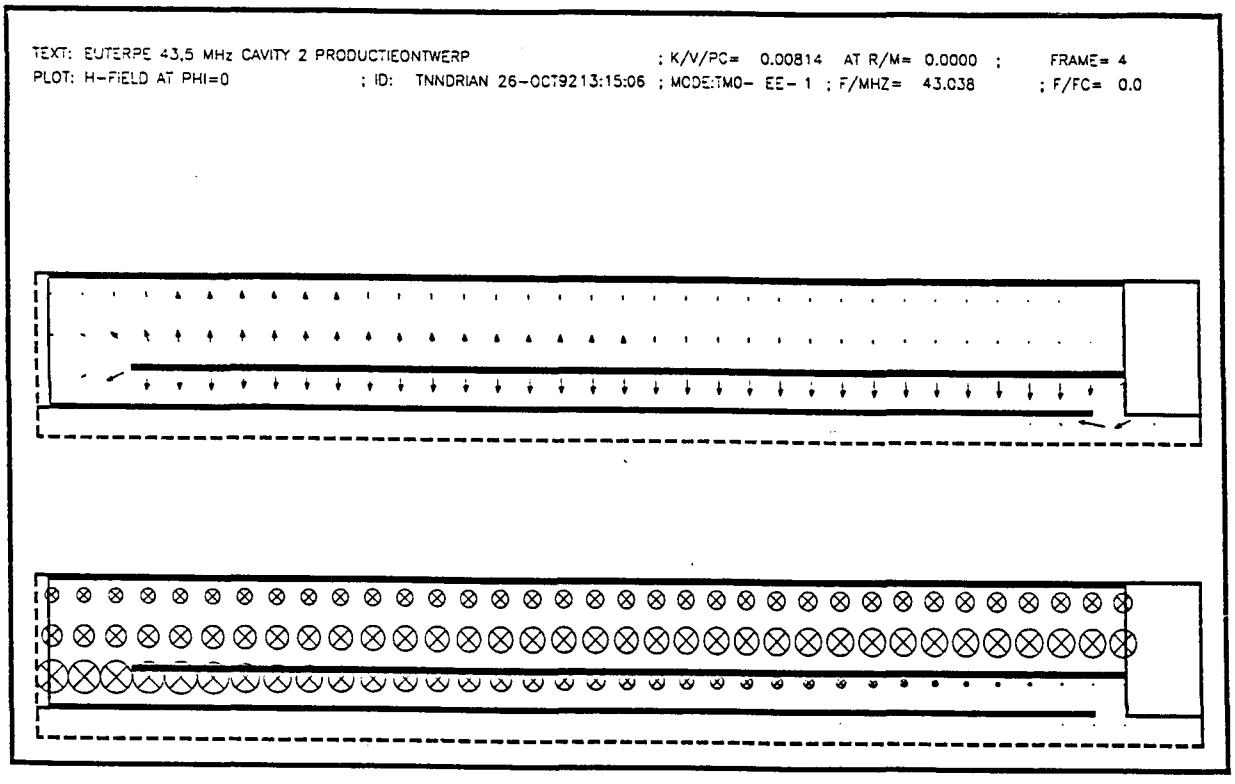

Figure 5.2: Top: The electric field. Bottom: The magnetic field of the ground mode, calculated by URMEL-T.

Freq. (MHz) URMEL-T	Freq. (MHz) Analytical
43.083	43.083
133.09	129.25
217.16	215.42
309.01	301.58
391.09	387.75
485.63	473.91
564.49	560.08
662.69	646.25
737.36	732.41
839.93	818.58

Table 5.3: Resonance frequencies calculated by URMEL-T and analytical.

In chapter 4 a matching condition was derived, described by Eq. (4.10). This condition can be satisfied if the cavity is detunable. From Eq. (4.10) we find that the cavity must be detunable by about 0.01 MHz. The cavity is detunable by moving the beam pipe into the cavity such that the capacitance of the accelerating gap is changed. When shifting the beam pipe into the cavity the capacitance is increased. The resonance frequency is related to the total capacitance of the cavity by $\omega_0=1/\sqrt{(LC)}$, thus the frequency will be decreased. In Fig. 5.3 the results of the URMEL-T calculations are shown with a gap decreased by 10 mm. In table 5.4 results are given for various gap sizes between 27.5 mm and 7.5 mm.

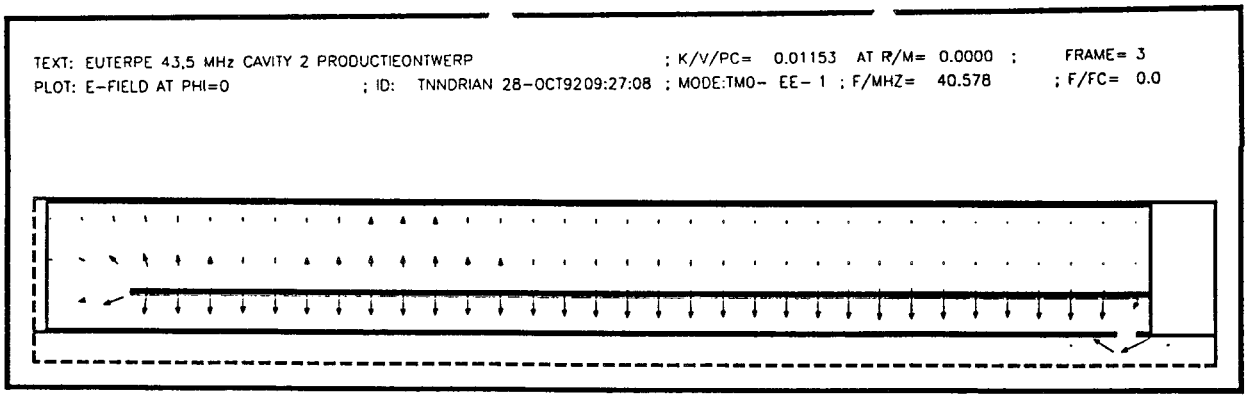

Figure 5.3: The effect on the electrical field when decreasing the gap with 10 mm, by a movable beam pipe.

gap (mm)	freq. (MHz)	Q_0	R_{sh} (kΩ)
27.5	43.04	4590	552
22.5	42.93	4582	555
17.5	40.58	4707	852
12.5	41.45	4642	856
7.5	42.81	4552	524

Table 5.4: URMEL-T results of the effect of decreasing the gap with a movable tube to detune the cavity.

Instead of a continuous decrease of the frequency when decreasing the gap, it rises again when the gap becomes 12.5 mm. Furthermore we see a modulation in the electrical field in Fig. 5.3. This modulation is better seen in Fig. 5.4 where we have taken the value of the electrical field given by URMEL-T in the middle of the outer layer of the cavity at a radius of 8.4 cm from the symmetry axis. The shorting plate is at 86.3 cm, and at 0 cm the return section plate is situated.

Curve a represents the situation when the gap is maximum, while curve b is calculated when the gap is decreased with 10 mm (situation in Fig. 5.3). Suspecting that this modulation could be due to the machine inaccuracy of the computer we altered URMEL-T in such a way that we could calculate with double precision. The cavity parameters, when the beam pipe is moved inward by 10 mm, are shown in table 5.5.

	URMEL-T	URMEL-T double
freq. (MHz)	40.58	39.95
Q_0	4707	4746
R_{sh} (kΩ)	852	904

Table 5.5: Cavity parameters calculated with URMEL-T and the adjusted URMEL-T employing double precision. The gap is decreased by 10 mm.

There is not much difference between the results of the calculations with or without double precision. If we look at the electrical field calculated with URMEL-T employing double precision, we see from curve c in Fig. 5.4 that the modulation is still present. As a result of these calculations we can conclude that URMEL-T isn't the optimal program to be used for this particular geometry of a cavity. Therefore we will use the computer code SUPERFISH in the next paragraph.

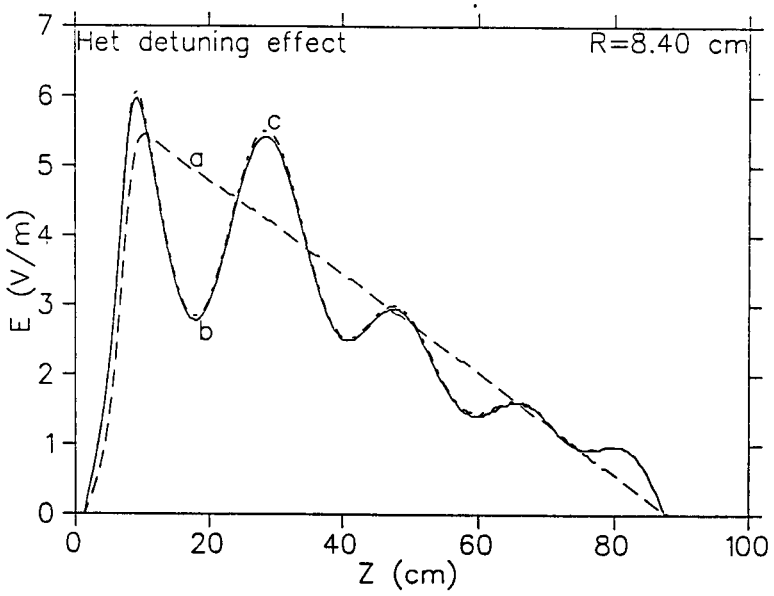

Figure 5.4: a: URMEL-T calculations of the electric field at a radial distance of 8.4 cm from the symmetry axis, with the complete gap distance of 27.5 mm.
b: URMEL-T calculations with a gap of 17.5 mm showing modulation.
c: URMEL-T double precision calculations with a gap of 17.5 mm.

The same calculations have been done with URMEL. This program also gave a modulation in the electric fields, and is therefore also not suitable for this geometry.

5.3 SUPERFISH calculations.

The same geometry of the cavity as used for the URMEL-T calculations, shown in Fig. 5.1, is used for SUPERFISH. A SUPERFISH input file is given in appendix G. The following step sizes were used: Δz=3.11 mm and Δr=2.03 mm. This makes a total of about 18000 mesh points. The plots of electrical field lines of a cavity with the full gap of 27.5 mm, and of a detuned cavity with a gap of 17.5 mm are shown in Fig. 5.5, and in table 5.5 the main parameters of the cavity are given.

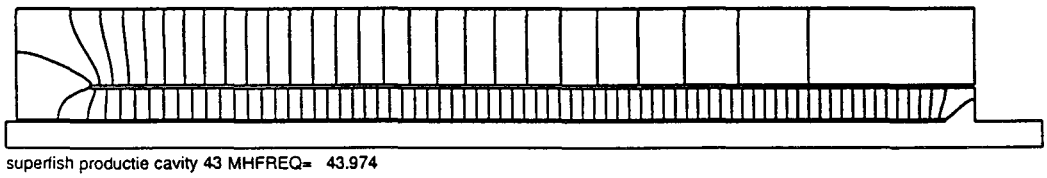

a

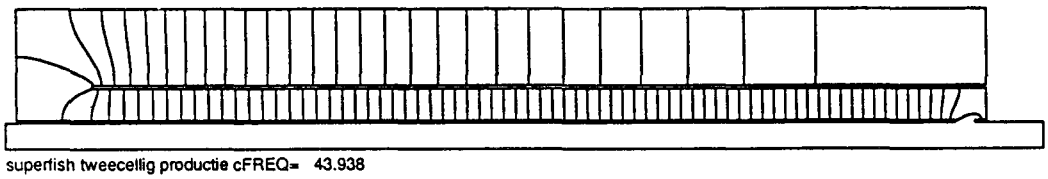

b

Figure 5.5: Plot of the electric field lines of a: cavity with a gap of 27.5 mm, b: detuned cavity with a gap of 17.5 mm.

SUPERFISH calculations	gap 27.5 mm	gap 17.5 mm
freq. (MHz)	43.97	43.94
Q_0	4746	4742
R_{sh} (kΩ)	573	573

Table 5.6: SUPERFISH calculations of the effect of a change in the width of the gap.

The frequency is lower when the capacitance is increased by shifting the tube inwards, as expected. If we compare the SUPERFISH and URMEL-T results in table 5.2 for the geometry with a complete gap of 27.5 mm we see good agreement. In the data given by SUPERFISH no modulation of the electric fields can be seen. We conclude that for these geometries SUPERFISH is superior to URMEL-T.
In Fig. 5.6 the electric field profiles on the symmetry axis of the cavity are given for a gap of 27.5 mm and a gap of 17.5 mm.

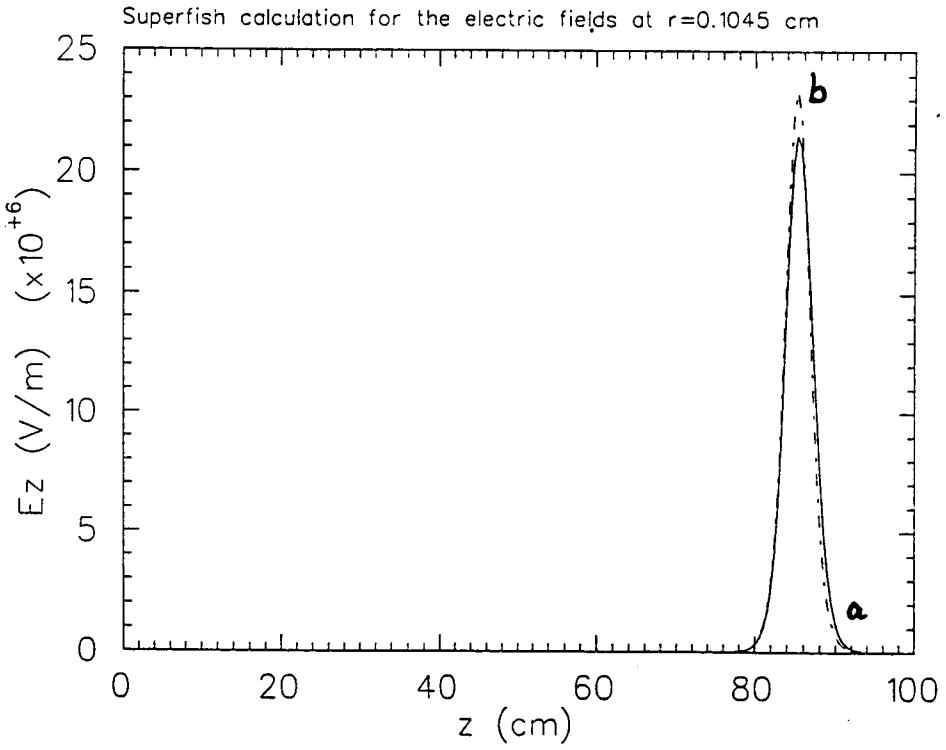

Figure 5.6: Electric field profile along the axis of a cavity with a: a gap of 27.5 mm and b: the tube shifted inward resulting in a gap of 17.5 mm.

The definition of the transit time factor used in SUPERFISH is

$$T=\frac{\int_{-\infty}^{\infty} E_z(z,r=0)\cos kz\, dz}{\int_{-\infty}^{\infty} E_z(z,r=0)\, dz}. \qquad (5.1)$$

Here it is assumed that z=0 corresponds with the middle of the gap.
The electric field profiles in Fig. 5.6 can be approximated by a Gauss function

$$f(z)=he^{-\left(\frac{z}{\sigma}\right)^2}, \qquad (5.2)$$

where h is the height of the function and σ the FWHM (full width at half maximum). If we use this function for E_z we get

$$T=\frac{\int_{-\infty}^{\infty} e^{-\left(\frac{z}{\sigma}\right)^2}\cos kz\,dz}{\int_{-\infty}^{\infty} e^{-\left(\frac{z}{\sigma}\right)^2}dz}=e^{-\left(\frac{k\sigma}{2}\right)^2}\approx 1-\frac{1}{4}\left(\frac{\omega\sigma}{v}\right)^2. \qquad (5.3)$$

To solve the integral we used a table of integrands [GRA 71].
This can be compared with the approximation of the electric field by a step used in chapter 2. Here the transit time factor was given by

$$T=\frac{\sin\frac{\theta}{2}}{\frac{\theta}{2}}\approx 1-\frac{1}{3}\left(\frac{\omega g}{v}\right)^2. \qquad (5.4)$$

Because $\sigma>g$

$$\frac{1}{4}\left(\frac{\omega\sigma}{v}\right)^2\approx\frac{1}{3}\left(\frac{\omega g}{v}\right)^2. \qquad (5.5)$$

With v=c the velocity of light, f≈43 MHz, g=2.75 cm, and σ≈3.9 cm the transit time factor for the cavity is T=1 (the deviation from unity is less than 10^{-3}).

5.4 Construction of the model cavity.

The cold model cavity employing longitudinal transmission line folding was constructed out of copper. The construction consists of three coaxial cylinders brazed on two flanges. The wall thickness of the outer and middle cylinders is 3 mm, that of the inner cylinder 2 mm. Because of the weight and the length of the middle cylinder and because it is brazed at one end to the flange it is necessary to calculate the deformation of this cylinder due to its own weight. In Fig. 5.7 the situation is schematically drawn. The parameters are: D the outer diameter and d the inner diameter of the middle cylinder, G the centre of mass, l the distance of the flange to G (half length of the cylinder), and x the deviation from the symmetry axis at a distance $2\cdot l$ from the flange. For this deviation the following equation holds [MAG 93]

$$x=\frac{P\,l^3}{3\,E\,I}\quad (cm)\ , \qquad (5.6)$$

with P the mass of the cylinder (kg), E the modulus of elasticity (kg/cm^2), and I the moment of inertia

$$I=\frac{D^4-d^4}{20}\quad (cm^4)\ . \qquad (5.7)$$

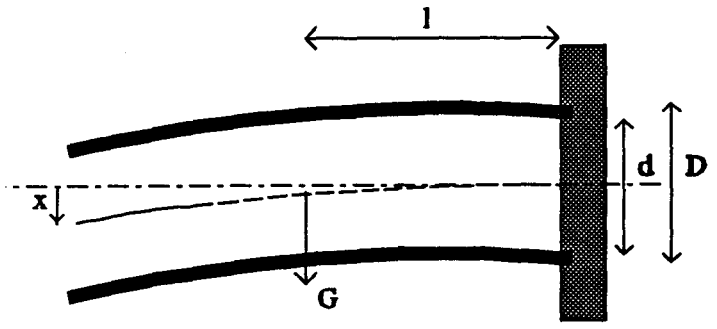

Figure 5.7: Deformation of the middle cylinder.

Using the data given in table 5.6 we get for the deformation $x \approx 1 \cdot 10^{-3}$ mm.

D=11.1 cm
d=10.5 cm
l=42.0 cm
P=10 kg
$E_{Cu}=1.2 \cdot 10^{6}$ kg/cm^2

Table 5.7: Data of the copper middle cylinder.

This means that there will be no deviation from the axis of symmetry that will be larger than the construction inaccuracy. The largest cylinder doesn't have this problem because it is brazed on two sides to the flanges. The smallest cylinder is light compared with the middle cylinder, so the deviation from the symmetry axis will even be smaller than that of the middle cylinder. Because this is a "cold" model, it is not necessary to braze it with silver. The dimensions of the cavity are given in table 5.1. The complete drawing of the cavity is given in Fig. 5.8.
For the decreasing of the gap in order to be able to detune the cavity the criterion of Kilpatrick [SCH 81] holds. The Kilpatrick field limit for any frequency is

$$f = 1.64\, E^2 e^{-\frac{8.5}{E}}, \tag{5.8}$$

where f is the frequency in MHz below which sparking is possible for surface peak electric field E in MV/m. Suppose the gap voltage V_g=50 kV over a gap of 1 cm, then E_g=50 kV/cm so E_g=5 MV/m. The frequency limit is then f=7.49 MHz. Because the cavity will operate at a frequency of ≈45 MHz there will be no sparking when employing 50 kV over 1 cm, even when there are peak electrical fields.
In order to couple power into the cavity three openings were made into the cavity: one at the shorting plate, one at the middle of the outer cylinder and one at the return section plate. Power will be coupled in at one of the locations at a time. The other two unused couple points will be closed with two little flanges. For the one used, a special flange is constructed with a BNC with a reading on it for the orientation angle. To this BNC the coupling loop will be soldered. The entire flange can be rotated 360 °, in order to adjust the amount of power coupled into the cavity. On the other side of the BNC the generator will be connected.

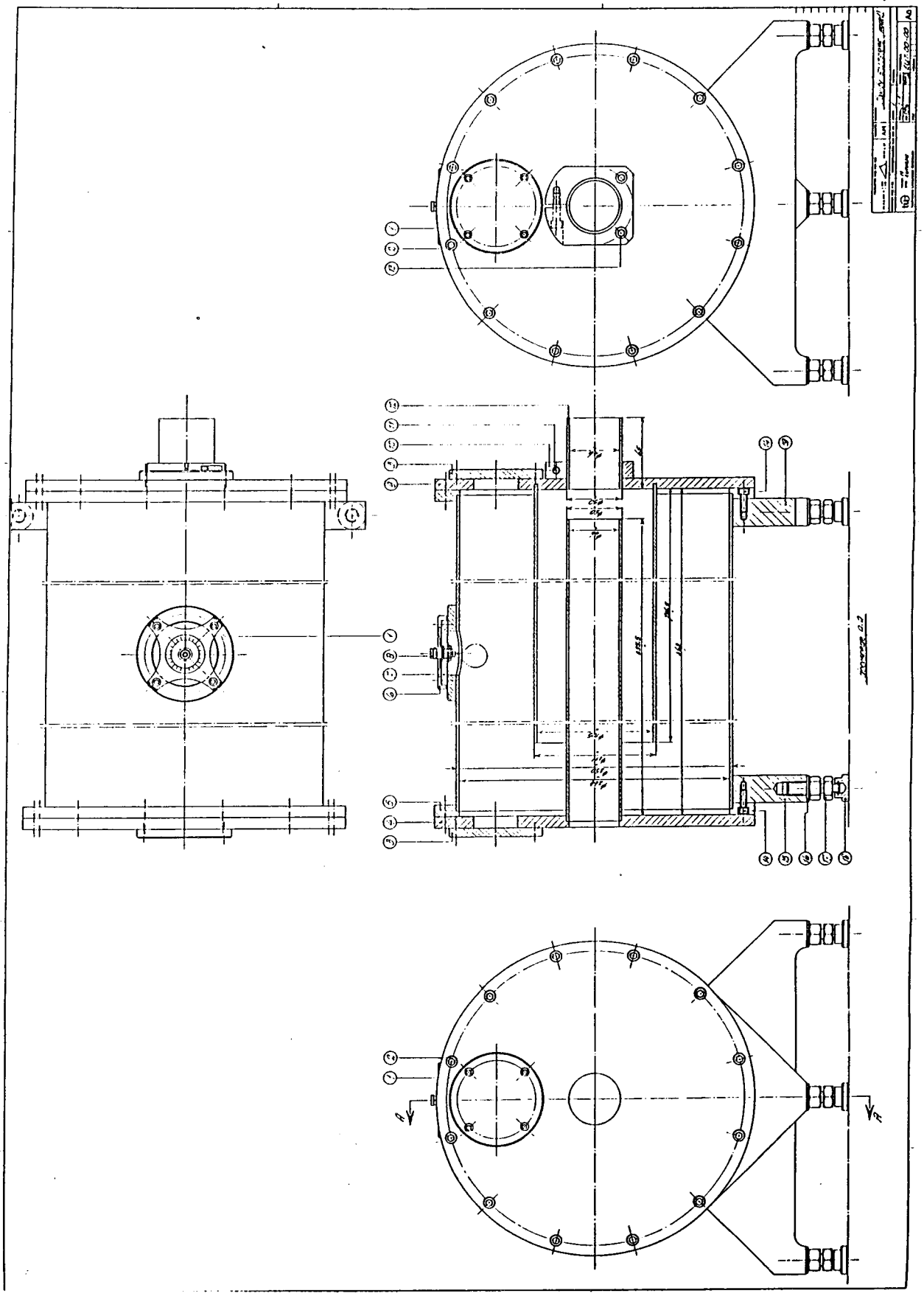

Figure 5.8: Construction drawing of the complete cavity.

Chapter 6

Measurements on the Model Cavity

6.1 Introduction.

A scale 1:1 copper "cold" model of a two layer accelerating cavity employing longitudinal transmission line folding has been built. A photograph of the cavity with its measuring equipment is shown in Fig. 6.1.
Measurements on the cavity were done in order to obtain the resonance frequency, frequency spectrum, quality factor and the shunt impedance. Also impedance matching was investigated and the VSWR on the input line was measured. In paragraph 6.2 the experiments done to measure the quality factor are presented. The results are compared with analytical predictions and with the numerical calculations done with URMEL-T and SUPERFISH. In paragraph 6.3 the measured cavity impedance is presented and compared with curves obtained by the analytical model derived in chapter 4. Paragraph 6.4 describes the determination of the shunt impedance of the cavity, from the data obtained in paragraph 6.3. These results will also be compared with the numerically and analytically obtained results. In paragraph 6.5 the detuning effects due to changes of the accelerating gap are presented. The measured VSWR curve will be presented in paragraph 6.6. Finally in paragraph 6.7 some conclusions will be given.

6.2 The quality factor.

To measure the unloaded quality factor Q_0, power has to be coupled into the cavity at one side, and a measuring signal must be coupled out of the cavity at the other side. The quality factor Q_0 is determined by Eqs. (2.17) and (2.18). Therefore the resonance curve of the cavity has to be determined. The resonance frequency is determined by sweeping the input frequency over a certain range. Resonance occurs when the amplitude of the measuring signal reaches a maximum.
The power will be coupled into the cavity by an inductive loop, as shown in Fig. 6.2. The loop can be mounted at three different places: at the shorting plate, at the return section plate, and at the middle of the outer cylinder. For strong coupling, the position of the loop should be at a place where the magnetic field is high. This will be at the shorting plate. Also for strong coupling the loop must be oriented perpendicularly to the magnetic field. Then the mutual induction M will be high.
The cavity signal is measured with a stripped piece of coaxial cable, acting as an antenna that is placed on the symmetry axis near the accelerating gap.

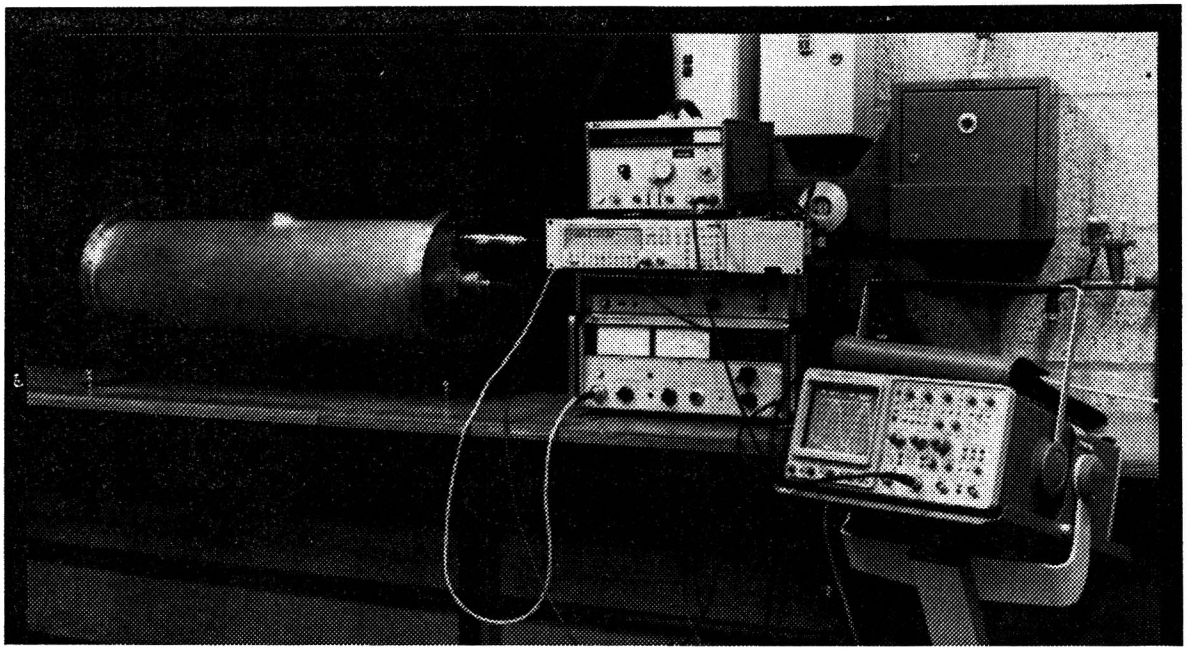

a

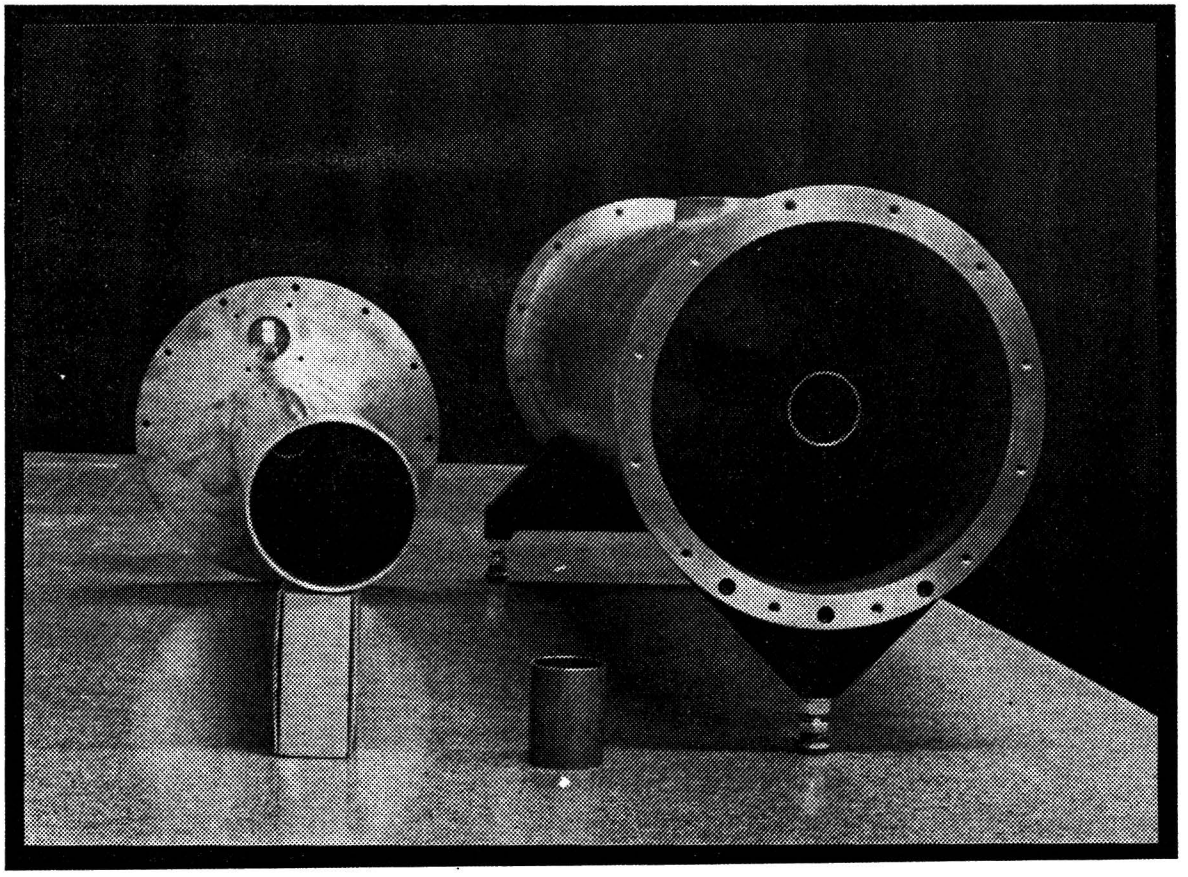

b

Figure 6.1: Photographs of the "cold" cavity model. a: The cavity with the measuring equipment. b: The disassembled cavity. Clearly seen are the different cylinders.

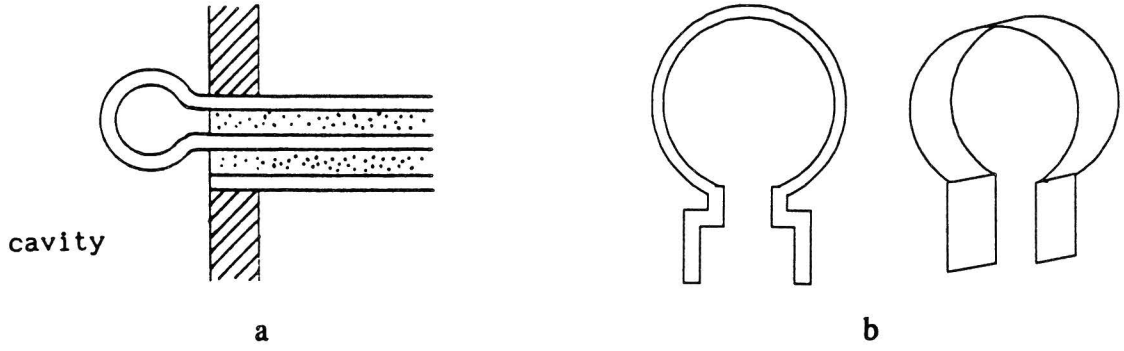

Figure 6.2: a) Coupling of rf-power into the cavity with an inductive loop. b) Some different coupling loops: one made of copper wire and the other one made of copper strip.

In Fig 6.3 a layout of the experimental setup is given. The output of the rf generator is amplified by a 27 dB amplifier. This amplifier was necessary to obtain a high enough cavity signal even when the major part of the input power is reflected due to cavity detuning or loop mismatch.

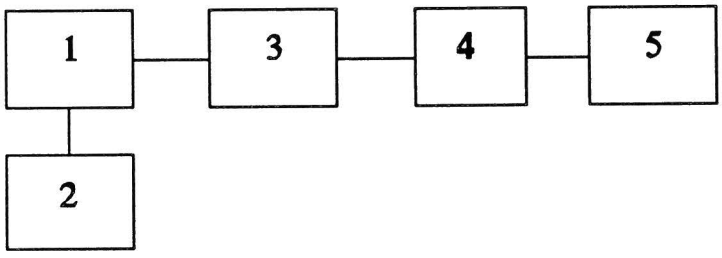

Figure 6.3: Schematic layout of the experimental setup, to measure the frequency spectrum, resonance curve and the quality factor of the cavity.
1: rf signal generator (HP 8654 A), 2: frequency counter (PM 6680),
3: 27 dB amplifier, 4: cavity, 5: oscilloscope (Tektr.2445).

We measured the frequency spectrum from 10 to 320 MHz. This range is limited to 320 MHz by the operational frequency range of the oscilloscope. In this range we found 14 resonances. They are listed in table 6.1. The measured results are compared with frequencies of the first 4 modes numerically calculated with URMEL-T and also with the analytical frequency predictions of these modes. The signal coupled out of the cavity has a strong maximum for the resonance frequencies corresponding with the 1st harmonic. These measured resonance frequencies agree well with the calculated frequencies.

Resonance[1)] freq. (MHz)	Signal[2)] freq. (MHz)	Harmonic number	Mode number	URMEL-T freq.(MHz)	analytical freq. (MHz)
14.61	45	1/3	1		
21.91	40	1/2	1		
43.83	44	1	1	43.08	43.83
55.69	222	1/4	3		
62.59	320	1/5	4		
67.39	133	1/2	2		
74.25	222	1/3	3		
104.34	222	1/3	3		
111.38	314	1/2	4		
134.77	133	1	2	133.1	131.5
156.51	314	1/2	4		
200.91	400	1/2	5		
222.75	222	1	3	217.2	219.2
313.03	314	1	4	309.0	306.8

Table 6.1: Frequency spectrum of the cavity compared with the numerically and analytically calculated frequencies. [1)] rf generator frequency [2)] frequency as established from the oscilloscope signal.

In Fig. 6.4 the measured resonance curves of the ground mode are shown. Curve a is obtained when the loop is placed at the shorting plate perpendicular to the magnetic field. In curve b the loop rotated 90 °.

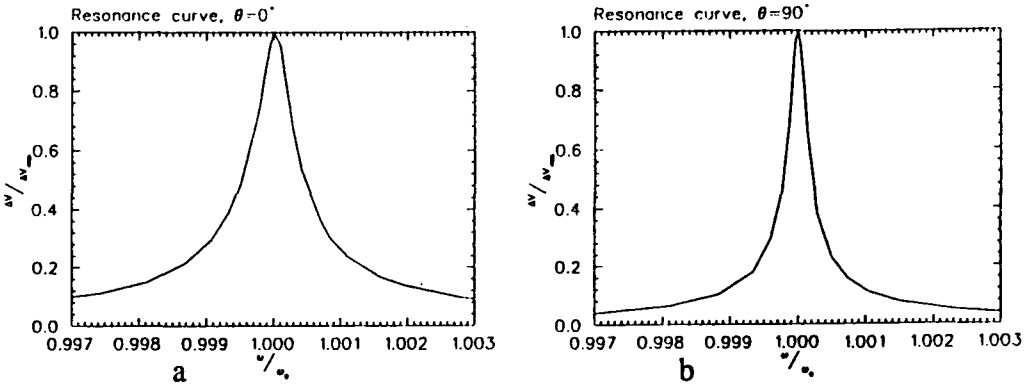

Figure 6.4: Resonance curve of the ground mode. a: Loop perpendicular to the magnetic field. b: Loop rotated 90°. The area of the loop is 15 cm².

From these curves the quality factor can be determined, if the bandwidth BW is measured. The quality factor is the reciprocal of the bandwidth, as was shown in chapter 2. This means that if the curve is narrow, Q is high. In Fig. 6.4 curve b is narrower than curve a. For a good measurement of Q_0 as little power as possible should be coupled in and out of the cavity by the loop. This can be achieved by introducing a mismatch between the power source and the cavity, in such a way that almost all power is reflected. When the loop is positioned perpendicularly to the magnetic field much power is coupled into the cavity because of the large dimensions of the loop and therefore much power is coupled out by the loop. This means that the measured quality factor is low. Therefore, the best estimate of Q_0 is obtained when the loop is rotated 90°. In table 6.2 the measured Q-values are given as a function of the rotation angle θ.

Rotation angle θ ± 5 (Degr.)	Resonance frequency f_0 (MHz)	Quality factor Q_0
0	43.864	1954
15	43.861	2130
30	43.858	2475
45	43.855	3043
60	43.853	3810
75	43.851	4075
85	43.852	4274
90	43.854	4217

Table 6.2: The measured quality factor as a function of the rotation angle of the loop.

In Fig. 6.5 the quality factor is drawn as a function of the rotation angle. If the loop is placed at the return section plate, the curve of the quality factor as a function of the rotation angle is more or less the same.

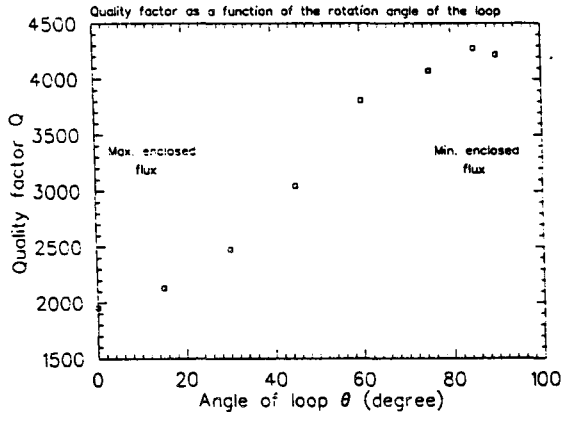

Figure 6.5: The quality factor as a function of the rotation angle.

From table 6.2 and Fig. 6.5 it can be seen that the maximum value doesn't occur at a rotation angle of 90° but at 85°. This is the result of a slight deformation of the loop.
In table 6.3 the quality factors obtained by measurement and by analytical and numerical calculations are compared.

Method	Q_0
Measured	4274
URMEL-T	4590
SUPERFISH	4746
Analytical without return section	4399
Analytical with return section	4625

Table 6.3: Comparison of Q_0 obtained by different methods.

The measured and calculated Q_0-values differ from each other by about 8%, so there is good agreement.

Also the normalized amplitude of the signal coupled out the cavity as a function of the rotation angle θ was measured. In all cases the frequency was adjusted so that the signal was maximal. The results are shown in table 6.4 and Fig. 6.6.

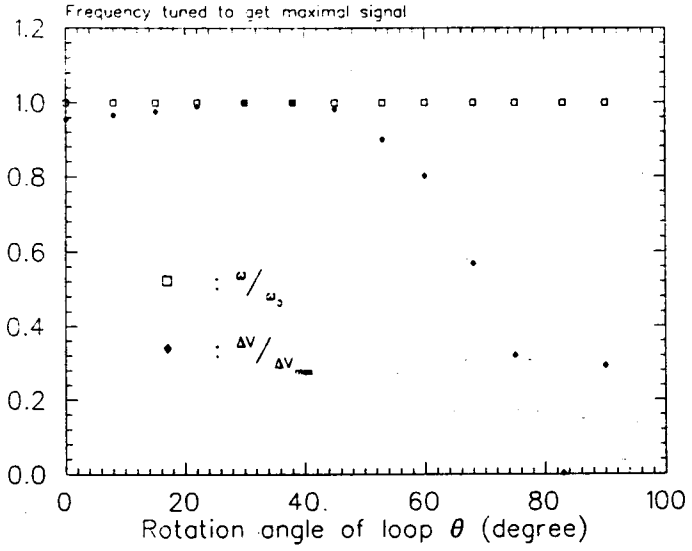

Figure 6.6: The normalized signal coupled out of the cavity as a function of the rotation angle of the loop.

θ ±5 (degr.)	$\Delta V/V_{max}$	f_0 (MHz)
0	0.95	43.860
8	0.97	43.861
15	0.98	43.860
22	0.99	43.859
30	1.00	43.858
38	1.00	43.857
45	0.98	43.855
53	0.90	43.854
60	0.80	43.853
68	0.57	43.852
75	0.32	43.852
83	$2.02 \cdot 10^{-3}$	43.851
90	0.29	43.852

Table 6.4: The normalized output signal as a function of the rotation angle of the loop.

As expected, the signal coupled out of the cavity decreases if less signal is coupled into the cavity. This occurs when the rotation angle of the loop increases. From the table it is seen that the resonance frequency decreases when less power is coupled into the cavity. The inductance and the capacitance of the cavity are slightly changed when the loop is rotated.

6.3 Measurements of the cavity input impedance.

With the vector impedance meter HP 4815A the absolute value of the complex input impedance of a cavity seen by the generator can be measured as a function of the frequency and the argument χ. The frequency of the measuring signal generated by the impedance meter is obtained with the frequency counter. The probe of the impedance meter has a BNC connector which can be attached directly to the BNC connector of the coupling loop. The coupling loop was positioned perpendicularly to the magnetic field.
In Fig. 6.7 the results are shown when the power is coupled into the cavity at the shorting plate and at the return section plate for the same thin loop with an area of A=15 cm^2.

From the data obtained by the vector impedance meter the complex impedance circles are simply constructed with the equations

$$ReZ = |Z|\cos\chi \ ,$$
$$ImZ = |Z|\sin\chi \ , \qquad (6.1)$$

with $-90 \leq \chi \leq 90$ the angle between |Z| and the real impedance axis.

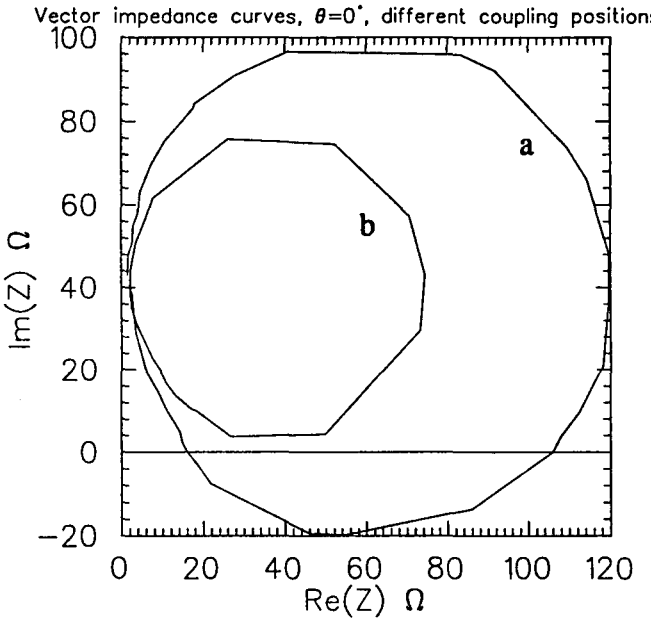

Figure 6.7: Complex cavity impedance curves for a thin coupling loop with an area of 15 cm².
Circle a: power coupled in at the shorting plate.
Circle b: power coupled in at the return section plate.

From the intersection of the two curves with the imaginary axis the reactance of the loop can be determined: $\omega L_1 \approx 41 \pm 3\ \Omega$. Furthermore by measuring the diameter of the circles the factor $\omega^2 M^2/R_s$ in Eq. (4.9) of the input impedance can be determined.
Circle a) intersects with the real impedance axes at $106 \pm 1\ \Omega$. There is matched coupling when Im Z=0 and $|Z|=Z=R_0$. The generator and the coaxial cables all have a characteristic impedance of 50 Ω. This means that for a matched circuit the impedance circle should intersect the real impedance axis at 50 Ω. It is possible to obtain perfect matching for the loop placed at the shorting plate. The loop then needs to be rotated over approximately 35°. An other possibility is by exchanging the loop for a smaller one (radius of the circle decreases) and/or a thicker one (the reactance of the loop decreases).
For circle b, representing the loop placed at the return section plate, no perfect matching can be accomplished by rotating the loop. The circle will never intersect the real axis for the loop used in this situation. A solution is a larger and/or thicker loop.
In Fig. 6.8 the results of choosing a different loop to couple power into the cavity at the shorting plate are shown. The larger circle is the same as seen in Fig. 6.7.a. The smaller circle is obtained with a coupling loop with an area of 11 cm² made of a strip of 1 cm width . These different dimensions have the result that the diameter of the circle in the impedance

plot is smaller as well as the offset in the vertical direction. This because the reactance ωL_1 has become smaller.

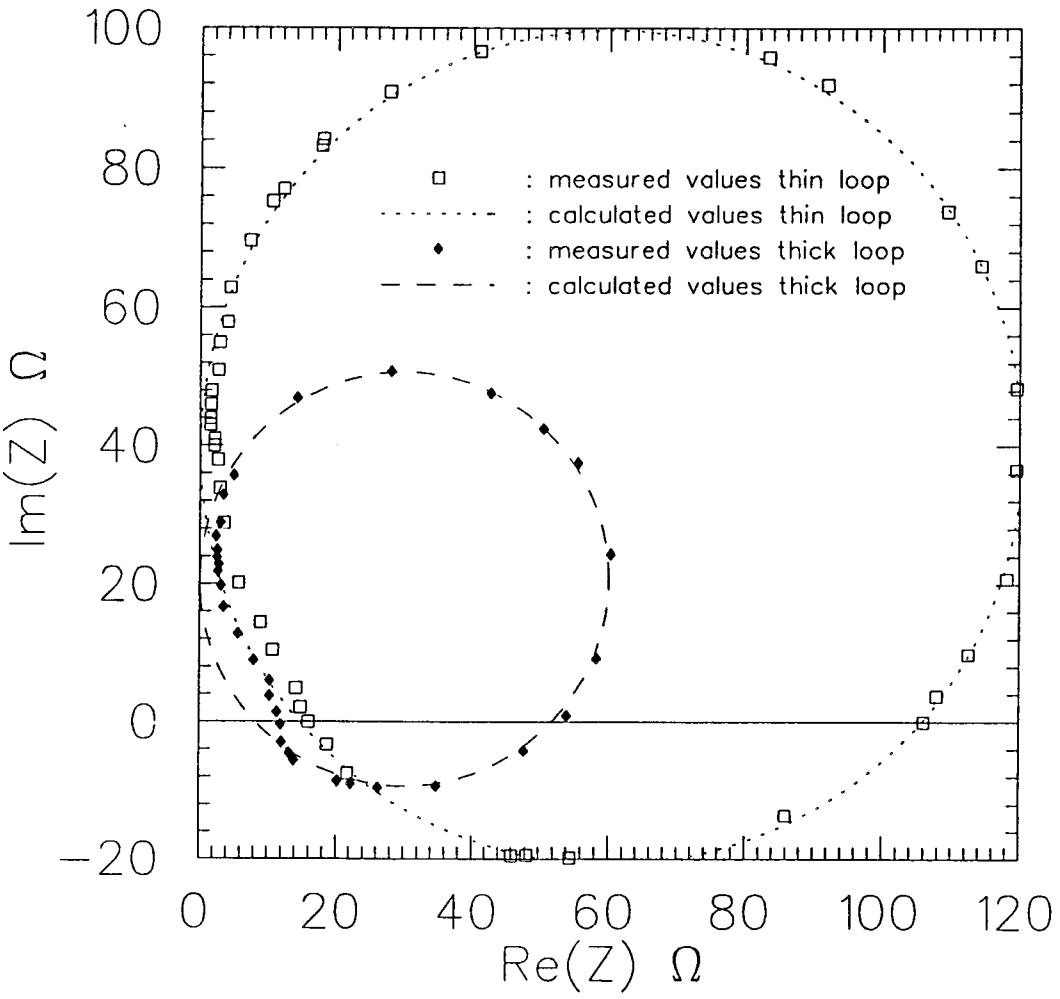

Figure 6.8: Cavity impedance curves. Large circle: large thin loop.
Small circle: small thick loop.

From Fig. 6.8 we find that for the small loop $\omega L_1 \approx 21 \pm 3\ \Omega$, and that the circle intersects the real axis at almost 50 Ω, namely 53 Ω. Thus for the small thick loop almost perfect matching has been accomplished. For perfect matching the loop only has to be rotated by a few degrees. We can conclude that it is possible to achieve matched coupling with a correctly chosen loop. From the data supplied by the vector impedance meter it is possible to deduce the resonance frequency, the quality factor and the reactance of the loop. For this we have fitted the curves in Fig. 6.9, representing the absolute value of the cavity impedance as a function of the frequency.

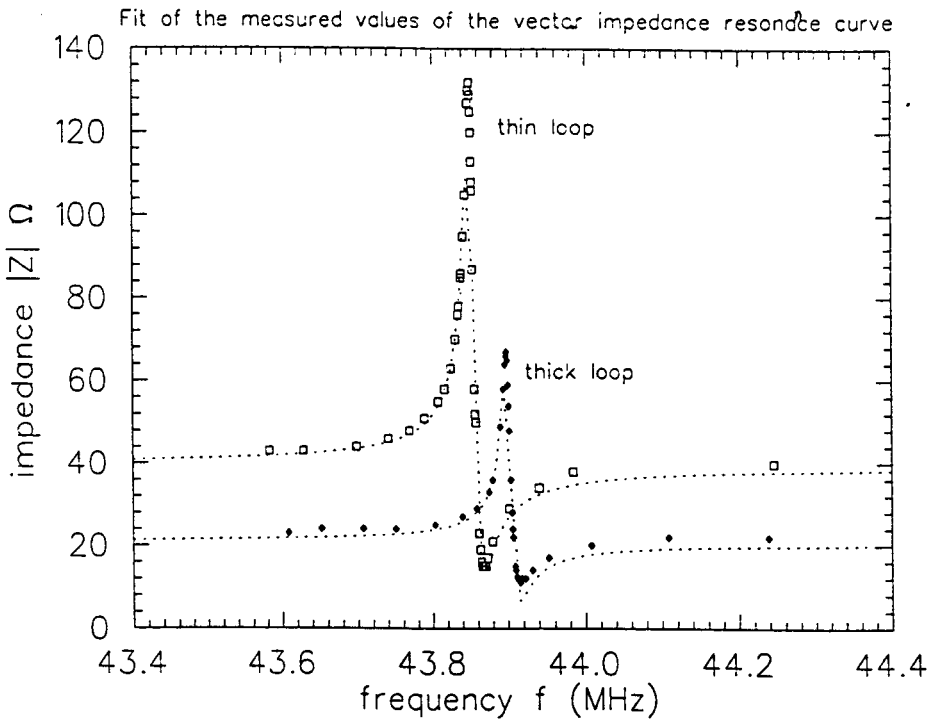

Figure 6.9: The measured vector impedance as a function of the frequency.

The primary impedance seen by the generator is given by Eq. (4.9)

$$Z_{pr}=j\omega L_1+\frac{\omega^2 M^2}{R_s(1+2jQ_0\delta)} . \tag{6.2}$$

We can define a detuning angle ψ (as in chapter 2)

$$\tan\psi=-2Q_0\delta , \tag{6.3}$$

so that Z_{pr} can be written as, with $R_z=\omega^2M^2/R_s$,

$$Z_{pr}=R_z\cos^2\psi+j(\omega L_1+R_z\cos\psi\sin\psi) , \tag{6.4}$$

with the absolute value equal to

$$|Z_{pr}|=\left\{R_z^2\cos^4\psi+(\omega L_1+R_z\cos\psi\sin\psi)^2\right\}^{\frac{1}{2}} , \tag{6.5}$$

and

$$\psi=\arctan\left(2\frac{f_0-f}{f_0}Q_0\right) . \tag{6.6}$$

By using Eqs. (6.5) and (6.6) to fit the data points in Fig. 6.9 with the computer code PLOTDATA [PLO 92] using the least squares method, we get the following results

Parameter	Thin loop	Error	Thick loop	Error
f_0 (MHz)	43.851	$5.9 \cdot 10^{-5}$	43.900	$1.3 \cdot 10^{-4}$
Q_0	4175	39	4245	79
ωL_1 (Ω)	39.5	0.6	20.7	0.8
R_z (Ω)	120.5	0.7	60.0	0.8

Table 6.5: Results of fitting the vector impedance curves in Fig. 6.9.

The values of the resonance frequencies and the quality factor are in good agreement with the values measured in the previous paragraph.

6.4 Shunt impedance.

From the data obtained in the previous paragraph we now can calculate the shunt impedance of the cavity. With R_s the series impedance in the equivalent circuit of paragraph 4.2, and I_0 the current at the shorting plate, we have for the dissipated power

$$P_{diss} = \frac{1}{2} I_0^2 R_s = \frac{V_{gap}^2}{R_{sh}} , \tag{6.7}$$

so

$$R_{sh} = \frac{2V_{gap}^2}{R_s I_0^2} . \tag{6.8}$$

With

$$R_z = \frac{\omega^2 M^2}{R_s} , \tag{6.9}$$

and if we approximate the cavity by a ideal ¼λ-resonator ($V_{gap}=I_0 Z_0$ with Z_0 the characteristic impedance) we get

$$R_{sh} \approx \frac{2R_z Z_0^2}{\omega^2 M^2} . \tag{6.10}$$

For the mutual inductance we found in chapter 4

$$M=\frac{\mu_0 I_c A}{2\pi r I_0}\approx\frac{\mu_0 A}{2\pi r}\ , \tag{6.11}$$

where we have used $I_c \approx I_0$ because the location where the power is coupled into the cavity is close to the shorting plate. Together with Eq. (6.10) we get an expression for the shunt impedance

$$R_{sh}\approx\frac{2R_z Z_0^2 r^2}{\mu_0^2 f_0^2 A^2}\ . \tag{6.12}$$

When we substitute the data for f_0, A, and R_z obtained in the previous paragraph for the thin and the thick loop, and use $Z_0 \approx 50\ \Omega$, r=8.85 cm and compare these results with those calculated numerically and analytically, we get

Method	R_{sh} (kΩ)
Measured (thin loop)	579±80
URMEL-T	552
SUPERFISH	573
Analytical without return section	509
Analytical with return section	556

Table 6.6: Measured shunt impedance compared with calculated values.

For the thick loop we get a measured shunt impedance R_{sh}=537 kΩ with an error of 80 Ω due to the inaccuracy in determining the area of the loops. The shunt impedances measured for the two types of loops agree well. Furthermore there is a good agreement between the numerical and analytical values and the measured value of the shunt impedance of the thin loop.

6.5 Detuning.

The cavity can be detuned by shifting inward a beam pipe at the accelerating gap, decreasing the gap. With this action the total capacity of the cavity is increased and therefore the frequency decreased. In chapter 5 URMEL-T calculations have been performed yielding the results shown in table 5.4.
Now the detuning of the cavity is measured using the same setup used to measure the quality factor. The large thin coupling loop is placed near the shorting plate, perpendicular to the magnetic field in order to get a strong output signal on the oscilloscope. Gradually the gap

distance is decreased. The results are shown in table 6.7.

gap (mm)	Resonance freq. (MHz)
27.5	43.88
25.0	43.87
22.5	43.85
20.0	43.83
17.5	43.80
15.0	43.76
12.5	43.71
10.0	43.62
7.5	43.53
5.0	43.31
2.5	42.81

Table 6.7: Detuning of the cavity by decreasing the accelerating gap.

With a quality factor of 4500 the necessary detuning is about 0.01 MHz in order to obtain impedance matching. But due to small inaccuracies in the construction of the cavity the minimal detuning must be about 0.1 MHz. From the results given in table 6.7 it is seen that with detuning by capacitive loading this can be reached on signal level. Detuning of the cavity is limited by sparking. This occurs when the gap is less than 1 cm with a gap voltage of 50 kV and a frequency of ≈45 MHz. If we compare these results with the SUPERFISH results in table 5.5 we see good agreement.

6.6 Voltage standing wave ratio.

A measure for the mismatch of a line is the VSWR. From Eq. (4.22) it is seen that the VSWR is a real quantity such that $1 \leq VSWR \leq \infty$. The VSWR on the input line of the cavity can be measured by placing a VSWR-meter between the generator and the cavity, as is shown in the experimental setup in Fig. 6.10.

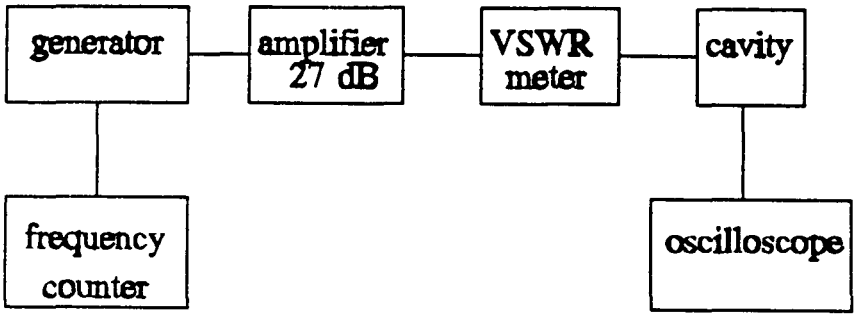

Figure 6.10: Schematic layout of the experimental setup to measure the VSWR.

First the VSWR-meter was tested with loads having a known real impedance. The characteristic impedance of the generator and the coaxial cables is 50 Ω. We therefore made one load 50 Ω and one (consisting of two parallel 50 Ω impedances) 25 Ω load. The results of the test are shown in table 6.8.

Load	VSWR expected	VSWR measured
50 Ω	1	1.2
25 Ω	2	1.8

Table 6.8: Test of the VSWR-meter. The expected and the measured VSWR as a function of a known load.

For the actual measurements we rotated the loop 17±5° in order to obtain a maximum output signal on the oscilloscope. In Fig. 6.11 the results of the measurements are shown. Also the resonance curve is shown, in Fig. 6.11. Due to the limit of the VSWR-meter only a small range of the resonance curve can be scanned. The resonance frequency measured with the oscilloscope is off the frequency scale. The minimum in the VSWR occurs at a frequency of 43.854 MHz, while the resonance frequency lies at 43.861 MHz. At this minimum the VSWR=1.9 with an expected error derived from table 6.8 of 0.2. There isn't perfect matching due to the fact that the power is coupled into the cavity by the thin loop, without being rotated 35° as discussed in paragraph 6.3. From this value of the VSWR we can calculate the absolute value of the load (cavity plus loop) with Eq.(4.23). The load is $|Z|=95\pm9$ Ω. At a frequency of 43.854 MHz where this minimum of the VSWR occurs the measurements of the vector impedance in paragraph 6.3 gave $|Z|=106\pm1$ Ω with $\theta=0°$. These two results give good agreement.

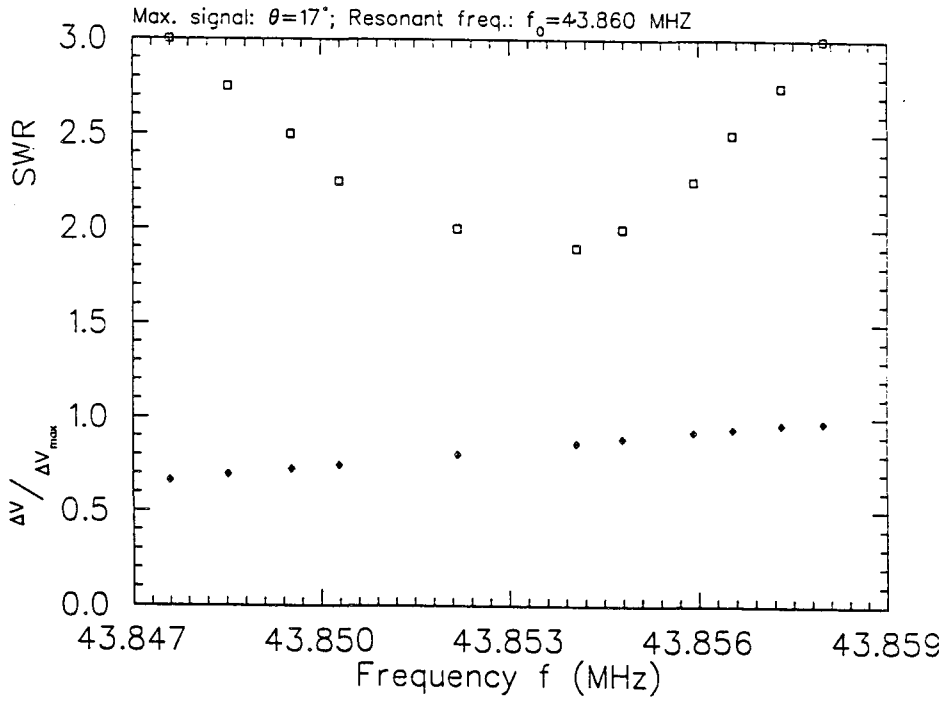

Figure 6.11: The voltage standing wave ratio.

6.7 Conclusions.

The frequency spectrum of the cavity showed more resonance frequencies than predicted by URMEL-T and analytical calculations. This is due to higher harmonics in the rf signal. Resonance curves were measured from which the quality factor was calculated. The quality factor is dependent on the place where power is coupled into the cavity and the rotation angle of the loop. The less power is coupled into and out of the cavity the more accurate the unloaded quality factor can be determined. The measured Q_0 is about 8% lower than the numerically and analytically calculated values. They all show good agreement.

It is possible to obtain matched coupling with a loop. Good results for the resonance frequency and the quality factor were obtained from fits of the cavity impedance curves. The small difference in resonance frequency that occurs when power is coupled in with two different loops is due to the inductance of the loops. In order to create matched coupling the loops can be rotated, which changes the mutual inductance, and/or the inductance of the loop can be lowered by using thick wire.

From the cavity impedance measurements the shunt impedance can be determined experimentally. The analytical and numerical calculations are in good agreement with the experimentally obtained values.

The cavity must be 0.1 MHz detunable. By pushing the beam pipe into the accelerating gap, decreasing the distance of the gap to 1 cm, a detuning was reached of ≈0.3 MHz.

The absolute cavity impedance can be obtained from a VSWR measurement although this method is not so accurate due to the inaccuracy of the VSWR meter.

We have seen that all the important parameters of a cavity, resonance frequency, quality facor and shunt impedance can be determined experimentally, analytically and numerically.

Chapter 7

An Alternative Design of an Accelerating Cavity

7.1 Introduction.

The construction of the cavity treated in the previous chapters becomes rather complicated because more than two coaxial layers are needed to reduce its length to 0.5 m. In the search for a simple design of a cavity with a physical length several times shorter than its electrical length, we found at the end of this graduate study a third design which is described in this chapter. In paragraph 7.2 analytical calculations are performed on this new cavity, using the transmission line matrix theory described in chapter 3. These calculations will be compared with numerical calculations performed by SUPERFISH. In paragraph 7.3 conclusions will be drawn.

7.2 Analytical calculations.

The latest design of an accelerating cavity for the EUTERPE storage ring is depicted in Fig. 7.1. It consists of an inner cylinder serving as beam pipe, an outer cylinder, two flanges and a large plate acting as a large capacitor. Due to the large capacitance of the total cavity, the length is small.

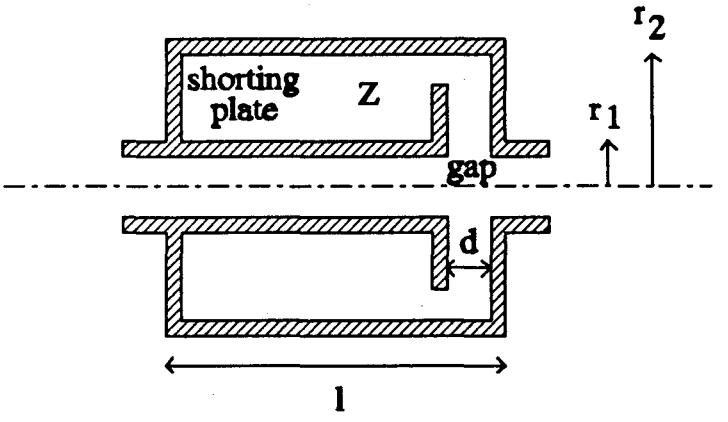

Figure 7.1: A ¼λ transmission line cavity employing capacitive loading.

This cavity can be represented by a transmission line terminated with a capacitance, see Fig. 7.2.

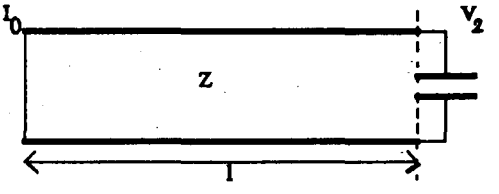

Figure 7.2: The cavity represented by a transmission line terminated with a capacitance.

The current and voltage profiles are determined by the matrix description in Eq. (3.2). The capacitive loading is taken into account with a matrix as in Eq. (3.3), but with the inductance L put to zero, because the currents are almost zero this close to the accelerating gap. The matrix equation for the entire cavity then becomes

$$\begin{pmatrix} V_2 \\ I_2 \end{pmatrix} = \begin{pmatrix} 1 & 0 \\ -j\omega C & 1 \end{pmatrix} \begin{pmatrix} \cos kl & -jZ\sin kl \\ -\frac{j}{Z}\sin kl & \cos kl \end{pmatrix} \begin{pmatrix} V_0 \\ I_0 \end{pmatrix}, \tag{7.1}$$

with Z the characteristic impedance, C the loading capacitance, and l the total length of the coaxial line. This equation gives (when using $V_0=0$ and $I_2=0$) the following two equations

$$\begin{aligned} V_2 &= -jZI_0\sin kl \ , \\ I_0(\cos kl - \omega CZ\sin kl) &= 0 \ . \end{aligned} \tag{7.2}$$

From the second equation we get the resonance condition

$$\tan kl = \frac{1}{\omega CZ} \ . \tag{7.3}$$

If we assume that the inner radius r_1 is much smaller than the outer radius r_2 ($r_1 << r_2$) then in good approximation the capacitance C is

$$C = \frac{\varepsilon_0 A}{d} = \frac{\pi \varepsilon_0 r_2^2}{d} \ , \tag{7.4}$$

where d is the accelerating gap. As in chapter 3 the shunt impedance and the quality factor can be calculated by first calculating the dissipated power and the stored energy. The analytical shunt impedance and the unloaded quality factor are

$$R_{sh} = \frac{4\pi\delta}{\rho} \frac{Z^2 \sin^2 kl}{\ln\frac{r_2}{r_1} + \left(\frac{1}{r_1}+\frac{1}{r_2}\right)\left(\frac{l}{2}+\frac{\sin 2kl}{4k}\right)} \ , \tag{7.5}$$

$$Q_0 = \frac{2kl+\sin 2kl}{8\sin^2 kl}\frac{R_{sh}}{Z} \ , \tag{7.6}$$

where l is determined by Eq. (7.3).
These analytical results are compared with numerical results obtained by SUPERFISH calculations for a cavity with r_1=2.5 cm, r_2=15 cm and d=1 cm. These results are shown in Fig. 7.3. There is good agreement. As can be seen from Fig. 7.3 for a cavity operating at 45 MHz the length would be 45 cm. Furthermore a quality factor of 6600 and a shunt impedance of 580 kΩ can be achieved. For a gap voltage of 50 kV, the required rf power would be 4.3 kW, compared to 1.8 kW for a 3-layer cavity employing longitudinal transmission line folding with a length of ±50 cm.

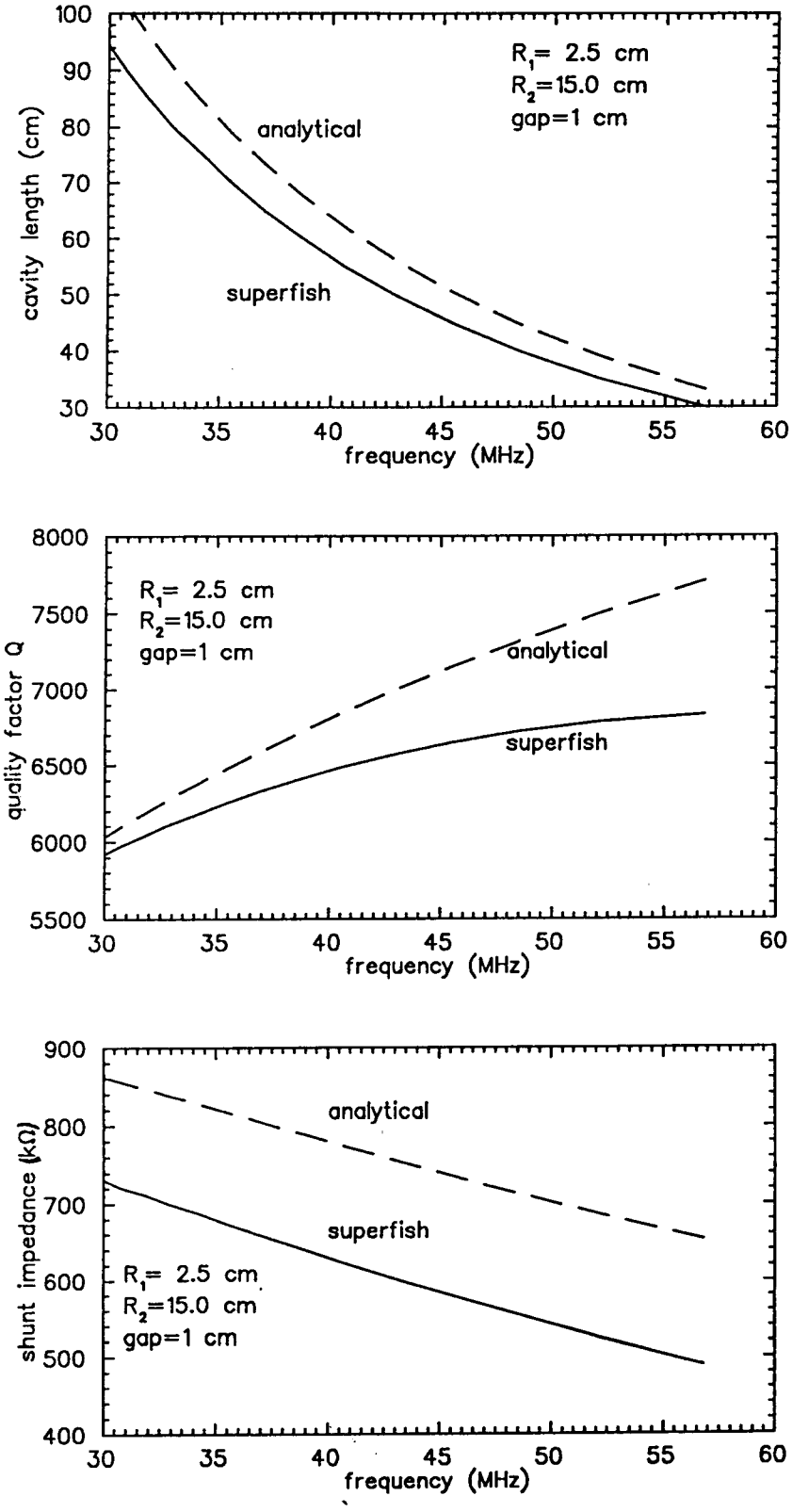

Figure 7.3: Analytical calculations of the length, the quality factor and the shunt impedance compared with the numerical calculations of SUPERFISH [HEI 93].

7.3 Conclusions.

The alternative cavity, employing capacitive loading is much simpler of construction than a 3-layer cavity employing longitudinal transmission line folding. The important parameters of the cavity (such as length, quality factor and shunt impedance) can be calculated analytically. They agree well with numerical calculations done with SUPERFISH.
If we compare the quality factor and the shunt impedance with a cavity employing longitudinal transmission line folding with a length of about 50 cm and a characteristic impedance of the layers of 50 Ω (table 3.2) large differences can be seen. The quality factor of a 3-layer cavity is ≈8300, the shunt impedance ≈1400 kΩ and the power 1.8 kW, compared to $Q_0 \approx 6600$, $R_{sh} \approx 580$ kΩ and $P_{diss}=4.3$ kW of the alternative cavity. The larger R_{sh} the less power is needed to obtain an accelerating voltage of 50 kV.
The design of a cavity employing capacitive loading came up late in this graduate study, so more research has to be done on this subject.

Chapter 8

The Tetrode Power Source

8.1 The tetrode.

Tetrode vacuum tubes are well established as high power rf sources in the VHF (30-300 MHz) band. The tetrode consists of an evacuated tube containing four electrodes: a cathode, a control grid, a screen grid and an anode. It is also known as a screen-grid tube.
The tetrode that is going to be used as the power source for the EUTERPE accelerating cavity will be the Eimac 4 CW 10,000 A power tetrode, shown in Fig. 8.1. The electrodes in this tube are positioned as coaxial spirals. The thoriated tungsten cathode is placed at the centre. The cathode is surrounded by the control grid and the screen grid. The anode is forming the outside of the tube.

OUTLINE

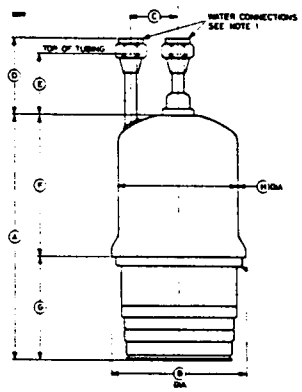

Ref	Inches	Millimetres
A	8.375 ± 0.250	212.7 ± 6.4
B	4.656 max	118.3 max
	4.524 min	114.9 min
C	1.625 ± 0.125	41.28 ± 3.18
D	2.562 ± 0.250	65.07 ± 6.35
E	2.062 ± 0.125	52.37 ± 3.18
F	4.903 ± 0.122	124.5 ± 3.1
G	3.500 ± 0.150	88.90 ± 3.81
H	4.156 max	105.6 max
	4.000 min	101.6 min

Millimetre dimensions have been derived from inches.

Figure 8.1: Outline of the Eimac 4 CW 10,000 A power tetrode with in the table its dimensions.

In order to understand the operation of the tube the behaviour of the anode and the cathode is considered first, and the effects of the grid and the screen are added later. Suppose the cathode, grid and screen are grounded and the anode is held at a positive voltage, then the tube behaves as a diode. By passing a current (75 A) through the cathode, it emits electrons. The anode collects the electrons when its voltage V_a is positive, and repels them when it is negative. The current flow in the diode for $V_a>0$ is limited by space charge of the electrons moving between the cathode and anode. The result is a current I_a which is space-charge limited and is given by Child's law [ZIE 74]

$$I_a = k V_a^{3/2} , \tag{8.1}$$

where the coefficient k is expressed in amperes per volt$^{3/2}$ and is called the perveance, and is determined by the geometry of the tube. For very low anode voltages, V_a has to be corrected [TER 55]. For very high anode voltages the anode collects all the electrons emitted by the cathode and the diode is said to be saturated, see Fig. 8.2.

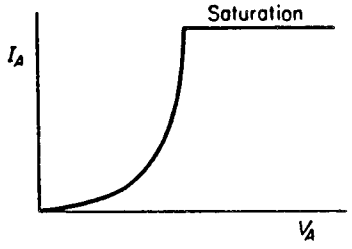

Figure 8.2: Characteristic showing space-charge limited and saturated regime.

Now the control grid is added between the cathode and the anode. The function of this helix wire is to control the current flowing from the cathode to the anode independent of the voltage between the two. The control grid voltage is negative, so no electrons can arrive at the grid. Thus the grid current I_g is zero. The number of electrons that reach the anode in a triode tube under space-charge limited conditions is therefore almost solely determined by the electrical field in the cathode-grid space; once the electrons have passed the grid, they travel so rapidly to the anode plate that space-charge effects in the grid-plate space can be neglected. The negative voltage applied to the grid causes an electric field at the cathode which will lower the overall attractive field at the cathode, reducing the anode current. Beyond some critical value of the grid voltage, called the cut-off point, no anode current will flow. If the grid voltage is positive the anode current is increased but also electrons are attracted to the grid, leading to a grid current. Excessive grid current can overheat the grid.
The electrical field in the vicinity of the cathode is proportional to the quantity (V_g+V_a/μ), where V_g is the grid voltage. The quantity μ is the ratio of the effectiveness of the grid and the anode in producing electric fields at the cathode and is called the amplification factor, [TER 43].

$$\mu = -\left(\frac{\partial V_a}{\partial V_g}\right)_{I_a} . \tag{8.2}$$

The amplification factor μ is determined by the geometry of the tube. If the grid has a regular geometrical construction, then μ depends only weakly on the adjustment of the tube i.e. the grid voltage and can be seen as a constant.
The anode current depends upon an effective voltage (V_g+V_a/μ) and equals

$$I_a = k\left(V_g + \frac{V_a}{\mu}\right)^{3/2} , \tag{8.3}$$

where k is about the same as in Eq. (8.1). This is a good approximation if in Fig. 8.3 the ratio w/d is relatively small (not larger than 5), and if w/d_{cg} is less than unity. In that case the field distribution near the cathode is more or less uniform. However, if w/d is relatively large and w is relatively large in comparison with d_{cg}, the field distribution near the cathode is very inhomogeneous and the anode current comes mostly from the cathode regions near the middle of the spaces between the grid wires. It is found that the anode current can then be represented as [ZIE 74]

$$I_a = k' \left(V_g + \frac{V_a}{\mu} \right)^2 . \qquad (8.4)$$

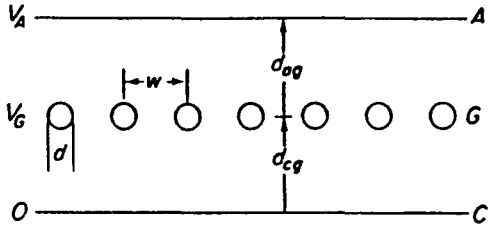

Figure 8.3: Cross section of a triode.

Eq. (8.3) doesn't hold for small I_a. The characteristic of I_a as a function of V_g is somewhat more curved than expected from Eq. (8.3) due to the fact that the field distribution near the cathode becomes inhomogeneous. This can mean that the grid voltage needed to completely cut off the anode current is more negative than predicted by Eq.(8.4).
Also when I_a is small, especially when also V_g is strongly negative, μ decreases with 10 to 20%. This is also due to the inhomogeneous field distribution. Davidse [DAV 70] calls this "eilandvorming".

Next we consider the behaviour of the complete tetrode. The grid added to a triode is called screen-grid or screen, as a result of its screening or shielding action. It acts as an electrostatic shield between the grid and the anode. The screen grid is maintained at a positive voltage with respect to the cathode, and maintained at ground potential with respect to rf by means of a capacitor. It serves to increase or accelerate the flow of electrons to the anode. Because there are large openings in the screen mesh, most of the electrons pass through it and arrive on the anode. Due also to the screen, the anode current is largely independent of the anode voltage over the usual operating range. This increases the amplification factor μ.
There is a disadvantage in using a screen grid. When electrons from the cathode approach the anode with sufficient velocity, they dislodge electrons on striking the anode. This gives rise to the condition of secondary emission. The screen is close to the anode and maintained at a positive potential, thus the screen will attract these electrons, particularly when the anode voltage falls to a lower value than the screen voltage. The result is that the anode current is lowered and the amplification is decreased. It is therefore necessary to operate the anode at a high voltage in relation to the screen in order to overcome these effects of secondary emission. In Fig. 8.4 some anode current characteristics are drawn for a tetrode. The ratio of the effectiveness of the grid and the screen in producing electric fields at the cathode is known as the screen grid amplification factor μ_s.

$$\mu_s = -\left(\frac{\partial V_s}{\partial V_g}\right)_{I_a} . \tag{8.5}$$

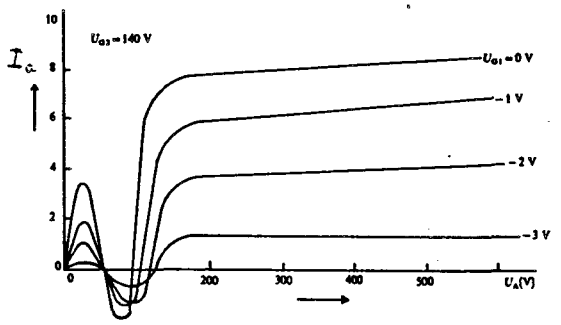

Figure 8.4: I_a-V_a characteristics of a tetrode.

The relation between the anode, grid and screen voltages and the total cathode current of the tetrode is now [ORR 75]

$$I_k = I_a + I_s + I_g = k\left[V_g + \left(\frac{V_a}{\mu}\right) + \left(\frac{V_s}{\mu_s}\right)\right]^{3/2} , \tag{8.6}$$

where $I_g=0$ if the control grid is negative with respect to the cathode.
It is generally assumed that the cathode current is independent of the anode voltage. Below the normal operating range of the anode voltage, the anode current and the screen current are not constant. This equation also has to be corrected for very low anode voltages [TER 55].

8.2 Fits of the Eimac tube current characteristics.

The manufacturers supplied constant current characteristics of the tetrode, shown in appendix F. The total cathode current I_k can be obtained from these curves as a function of V_a, V_g and V_s. The equation chosen to model I_k is an adaptation of Eq. (8.6)

$$I_k = k\left[V_g + \left(\frac{V_a}{\mu}\right) + \left(\frac{V_s}{\mu_s}\right)\right]^{\alpha} . \tag{8.7}$$

The exponent $^3/_2$ is now replaced by the variable α. This because some of the problems mentioned in connection with this equation can be taken into account if a higher value than $^3/_2$ is chosen for the exponent α. Consider the cross section of the tetrode in Fig. 8.5. The exponent is about $^3/_2$ for w/d relatively small and where w/d_{cg} is not too large. The exponent can become 2 (k changes too) if w/d and w/d_{cg} are both large [ZIE 74].

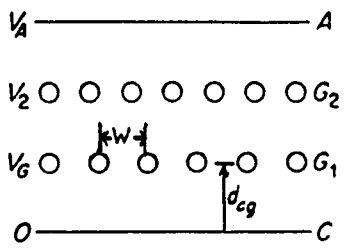

Figure 8.5: Cross section of a tetrode.

So, letting α be variable as a fit parameter, a better fit of the current characteristics can be obtained even more because μ and μ_s are not really constant. The cathode current I_k is calculated by adding the anode current and the screen current. The grid current is zero over the entire operating range.

The operating screen voltage will be 1500 V. This means that the operating range of the anode must be chosen higher than 1500 V in order to prevent secondary electron emission. The cathode current curves that will be fitted with Eq. 8.7 are chosen in such a way that the anode voltage is constant. This results in one variable namely V_g and four parameters, k, μ, μ_s and α. A command file was written for the VAX software package PLOTDATA, to fit I_k curves with different constant V_a using a least squares fitting method. The command file also produces graphs of the actual and calculated values of I_k as a function of V_g for different values of V_a.
First it was assumed that μ and μ_s were constants. This resulted in values for α calculated between 2.1 and 2.5. Next we assumed μ a function of I_a and thus of V_g. This resulted in $2.1 \leq \alpha \leq 2.8$. Finally we assumed that μ and μ_s are a function of V_g. This resulted in the expected values of α distributed around 1.5. The complete results of the calculations of k, μ, μ_s and α are shown in table 8.1. The input values of μ and μ_s when they are taken constant are the average values of the μ's and μ_s's calculated with Eqs. (8.2) and (8.5) from the current characteristics in appendix F. The amplification factor μ calculated with I_a=constant is constant over the entire range of the anode voltage, but is a function of the grid voltage. This is shown in Fig. 8.6.

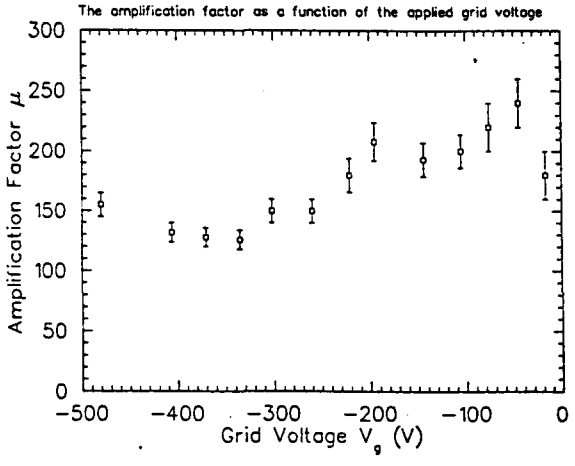

Figure 8.6: The amplification factor μ as a function of the grid voltage (V_a=7 kV and V_s=1500 V).

V_a (kV)	2	3	4	5	6	7
μ en μ_s	fit	param.				
k	$2.9 \cdot 10^{-5}$	$2.3 \cdot 10^{-5}$	$9.6 \cdot 10^{-6}$	$1.5 \cdot 10^{-5}$	$3.2 \cdot 10^{-5}$	$4.3 \cdot 10^{-6}$
μ	182.3	182.0	181.8	170.0	155.5	161.4
μ_s	4.1	4.0	3.9	3.8	3.8	3.7
α	2.2	2.2	2.4	2.3	2.1	2.5
μ	function	of I_a				
k	$5.6 \cdot 10^{-5}$	$4.9 \cdot 10^{-5}$	$1.1 \cdot 10^{-5}$	$1.8 \cdot 10^{-5}$	$3.0 \cdot 10^{-5}$	$7.4 \cdot 10^{-7}$
μ_s	4.3	4.2	4.0	3.9	3.9	3.7
α	2.1	2.1	2.4	2.3	2.2	2.8
μ en μ_s	functions	of I_a				
k	$3.4 \cdot 10^{-3}$	$3.4 \cdot 10^{-3}$	$1.3 \cdot 10^{-3}$	$6.1 \cdot 10^{-4}$	$1.3 \cdot 10^{-3}$	$6.5 \cdot 10^{-5}$
α	1.4	1.4	1.6	1.8	1.7	2.3

Table 8.1: Results of fitting I_k with Eq. 8.7.

The screen grid amplification factor μ_s is a function of V_a and I_a, and therefore a function of V_a and V_g. In table 8.2 the results are given.

$I_a \setminus V_a$ (A) (kV)	2	3	4	5	6	7
14	4.3	4.6	4.9	5.2	5.4	5.7
12	4.6	4.8	5.1	5.3	5.6	5.9
10	5.1	4.9	5.3	5.6	5.7	5.9
8	5.2	5.5	5.6	5.7	5.8	5.9
6	5.1	5.5	5.4	5.5	5.6	5.7
4	5.2	5.2	5.3	5.3	5.4	5.4
3	5.2	5.2	5.2	5.3	5.3	5.3
2	5.0	5.0	5.0	5.0	5.0	5.0
1	4.7	4.7	4.7	4.7	4.7	4.7
0.5	4.5	4.4	4.5	4.4	4.4	4.4
0	3.3	3.4	3.4	3.4	3.4	3.4

Table 8.2: Screen grid amplification factors μ_s as a function of V_a and I_a (V_g).

In Fig. 8.7 the results in table 8.2 are shown in a three dimensional plot.

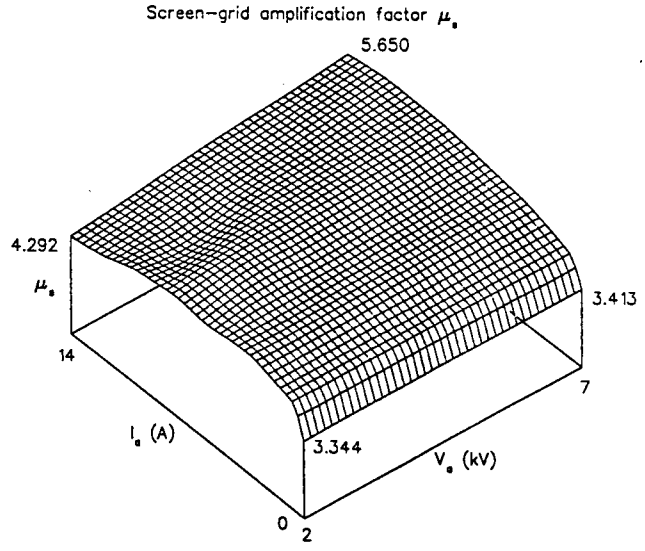

Figure 8.7: Three dimensional plot of μ_s as a function of V_a and I_a.

As an example the actual and the calculated values of I_k with V_a=4 kV are shown in Figs. 8.8, 8.9 and 8.10.

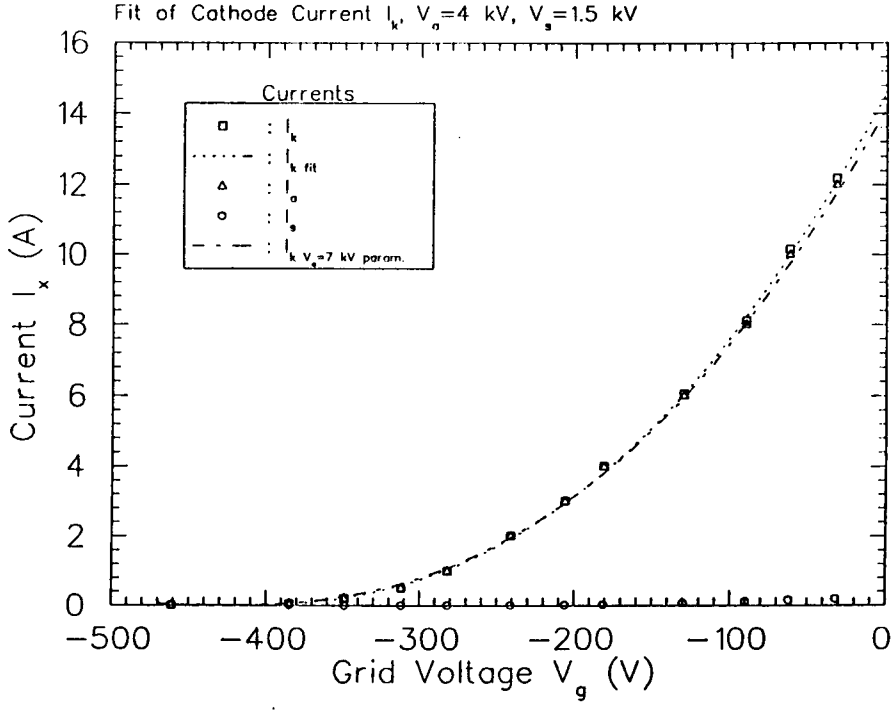

Figure 8.8: Fit of cathode current with μ and μ_s constants. The contributions of I_a and I_s are split up, and the fitted curve of I_k with V_a=7 kV is plotted for comparison.

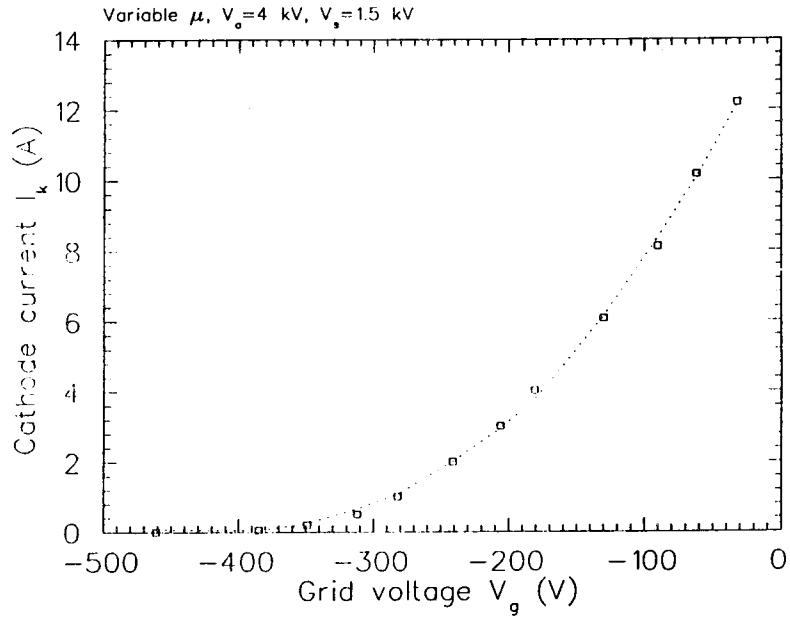

Figure 8.9: Fit of the cathode current with μ a function of I_a and V_a=4 kV.

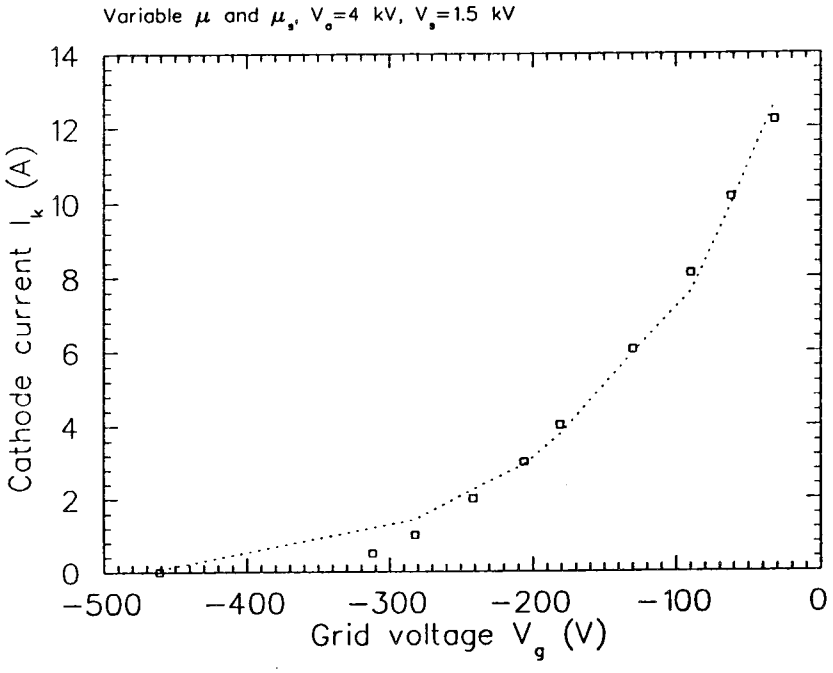

Figure 8.10: Fit of the cathode current with μ and μ_s functions of I_a.

The fit in Fig. 8.10 isn't accurate for low cathode currents. This is due to the fact that Eq. (8.7) doesn't hold for small values of I_k. Also inaccuracy in the determination of μ and μ_s is a cause of the fit being not perfect.

8.3 The operating line.

For our purpose the tetrode will operate in class C. The tube is then biased so that it is cut-off for more than half of the rf cycle as shown in Fig. 8.11. The slope of the operating line is determined by the maximum admissible anode dissipation. The maximum ratings for the tetrode operating in this mode are given in table 8.3 [EIM 69].

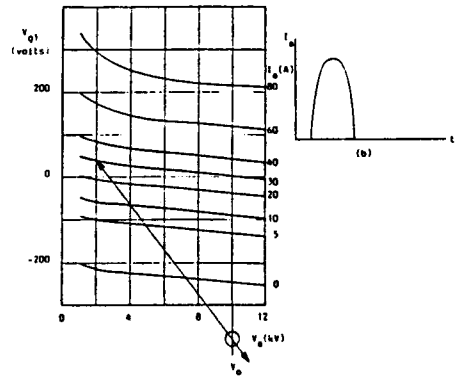

Figure 8.11: Class C amplification.

	30-60 MHz
Anode voltage	7.0 kV max
Anode current	2.8 A max
Anode dissipation	10 kW max
Screen voltage	1.5 kV max
Screen dissipation	250 W max
Grid dissipation	75 W max

Table 8.3: Maximum ratings of the Eimac 4 CW 10,000 power tetrode.

Because the anode circuit of the tetrode will be tuned to the signal frequency, the voltages on the operating line in Fig. 8.11 vary sinusoidally in antiphase with each other. The operation throughout the rf cycle is therefore represented by points on the straight load-line or operating line shown. The anode current is not quite a part of a pure sinusoid because of the non-linearity of the tube characteristics. The so called Q (quiescent) point shown by the little circle in Fig. 8.11 is found when the tube is biased so that in absence of rf drive it sits at this point.
The operating line is determined by two points, the Q-point which represents the cut-off end of the line and the peak anode current end of the line. The selection of an operating line can be a process of successive approximation since the peak anode current end of the line may require several test calculations to be carried out before the optimal position is selected.

The dc anode current should not exceed the maximum value of $I_{0\,(max)}$=2.8 A. The maximum dc input power is determined by this value. The bias dc anode voltage determines the Q-point. The Q-point must lay beneath the I_a=0 A current characteristic so that the tetrode is a class C amplifier. The maximum dc input power needed is therefore

$$P_{in(max)}=V_0 I_{0(max)} \,, \tag{8.8}$$

and the maximum output power

$$P_{out(max)}=\eta P_{in(max)} \,, \tag{8.9}$$

where η is the efficiency.
By choosing the Q-point, one end of the operating line is determined. The other end is determined by the peak anode current. The value of the peak anode current is estimated by

$$I_{pk}=aI_0 \,, \tag{8.10}$$

where a is a factor which determines the ratio of peak to dc anode current, with $3.5 \le a \le 4.5$. Next the operating line is constructed on the characteristic curves in appendix F by choosing the minimum anode voltage. We must ensure that the anode voltage is always greater than the screen grid voltage, and that the peak positive grid voltage is minimized for a low grid current. It is even better to construct the operating line in such way that the peak grid voltage is always negative. The left-hand end of the operating line is then fixed by this voltage and the peak anode current.
To find the anode current waveform we carry out the construction shown in the lower part of Fig. 8.12. (Here class A amplification is shown, but the method is the same for class C amplification.) From the anode current waveform we can calculate the dc anode current and the peak current value of the first harmonic component. The radius of the arc is equal to the length of the load line from the Q-point to the other end. From the arc we construct lines from which the anode current can be found at 15° phase intervals of the anode voltage. The 15° interval points are called A (0°) to F (75°). The dc and rf anode currents can be found by Fourier analysis of the current wave form using numerical formulas given by [PRE 70] and [CAS 92].

$$I_0=(0.5A+B+C+D+E+F)/12 \,, \tag{8.11}$$

and

$$I_1=(A+1.93B+1.73C+1.41D+E+0.52F)/12 \,. \tag{8.12}$$

I_0 can be compared with the value of I_0 assumed at the beginning. The result may differ appreciably and if it is not satisfactory another test calculation is carried out with a different minimum anode voltage. It may be necessary, if variations in the minimum anode voltage do not give the desired result, to modify the assumed value of the peak anode current, by modifying the factor in Eq. (8.10).

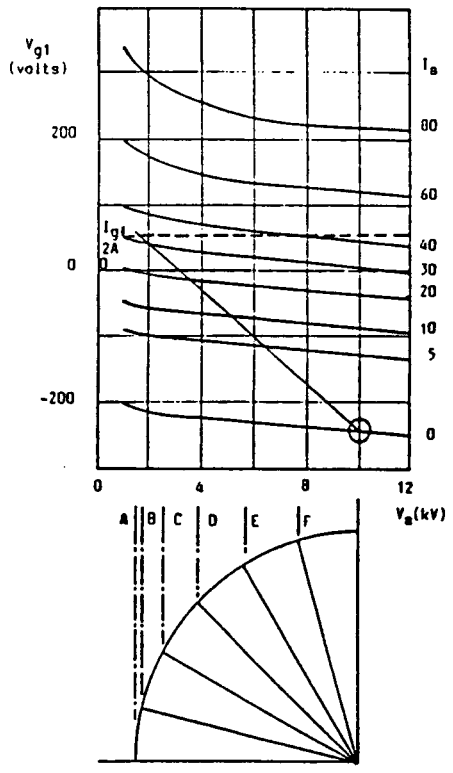

Figure 8.12: Current characteristics with an operating line (class A), plus the arc construction to calculate the anode current waveform.

The amplitude of the rf anode voltage is

$$V_1 = V_{Q\text{-}point} - V_{a(\min)} \ . \tag{8.13}$$

Thus the dc input power and the rf output power are then

$$P_{dc\ input} = V_0 I_0 \ , \tag{8.14}$$

$$P_{rf\ output} = 0.5 V_1 I_1 \ . \tag{8.15}$$

From these two equations the efficiency can be calculated.

The input and output resistances of the tube can be calculated. The output resistance is

$$R_{out} = \frac{V_1}{I_1} \ , \tag{8.16}$$

which is often called the load resistance. Because of the high Q_0 value of the resonant circuit (cavity), only the fundamental frequency component of the signal of the power supply will be dissipated in the accelerating system itself. The rest of the supplied power will be dissipated at the anode of the tube.
In order to find the input resistance of the tetrode, the amplitude of the rf control grid voltage must be determined

$$V_{in}=|V_{g\ Q\text{-}point}|-|V_{g\ peak}|\ , \tag{8.17}$$

and the rf input current is

$$I_{in}=I_1+I_{gl}\ . \tag{8.18}$$

I_{gl} is the control grid current obtained by reading the control grid currents off Fig. 8.12 at 15° intervals and employing Eq. (8.12). Then the rf input resistance is

$$R_{in}=\frac{V_{in}}{I_{in}}\ , \tag{8.19}$$

and the needed input power is

$$P_{in}=0.5V_{in}I_{in}\ . \tag{8.20}$$

From this it can be calculated that the power gain of the amplifier is

$$Gain=10\log\left(\frac{P_{rf\ out}}{P_{in}}\right). \tag{8.21}$$

From the values of the dc anode current I_0, the peak anode current I_{pk}, the amplitude of the first harmonic current component I_1, and the current opening angle we can find values for the exponent α in Eq. (8.7). This is done with the use of Fig. 8.13 [TER 43].

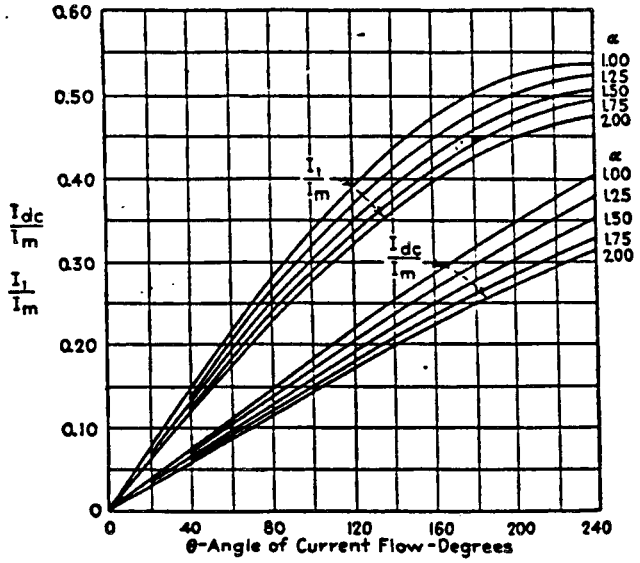

Figure 8.13: Curves giving the relation of direct-current $I_0=I_{dc}$ and the fundamental frequency I_1 components as a function of the opening angle and the peak amplitude $I_{pk}=I_m$.

An example of these calculations is shown below.

Estimated efficiency η=0.65.
dc anode voltage V_0=7 kV.
dc anode current I_0=1.2 A.
Min. anode voltage $V_{a\,(min)}$=1.8 kV.

Gives: $P_{in\,(max)}$=8.4 kW and $P_{out\,(max)}$=5.5 kW.

After trial and error we found: a=4.5 thus I_{pk}=5.4 A.

The results of the arc construction with the characteristic curves are

point	degrees	I_a (A)
A	0	5.4±0.1
B	15	5.0±0.1
C	30	3.9±0.1
D	45	1.9±0.1
E	60	0.55±0.02
F	75	0.049±0.002

Table 8.4: Anode currents at 15° phase intervals.

With Eqs. (8.11) and (8.12) we get: I_0=1.18±0.05 A and I_1=2.09±0.06 A. The dc anode current gives good agreement with the previously assumed value.

For the dc input power and the rf output power we get: $P_{dc\ input}$=8.2±0.4 kW and $P_{rf\ output}$=5.4±0.2 kW with η=0.66±0.01. This also gives good agreement.

The output resistance is: R_{out}=2.5 kΩ

The amplitude of the rf control grid voltage is V_{in}=500-130=370 V, and I_{g1}=0 because A=B=C=D=E=F=G=0. Thus the rf input current is $I_{in}=I_1$=2.09 A.

Then the input resistance is: R_{in}=177 Ω.

The input power is then P_{in}=386 W.

From this it follows that the power gain is: Gain=11.5 dB.

The opening angle is calculated from Fig. 8.14, showing the rf voltage and current characteristics: $\theta \approx 173°$. Together with the calculated values of I_0, I_1 and I_{pk} the approximation for the exponent in Eq. (8.7) is: α=2.3±0.1

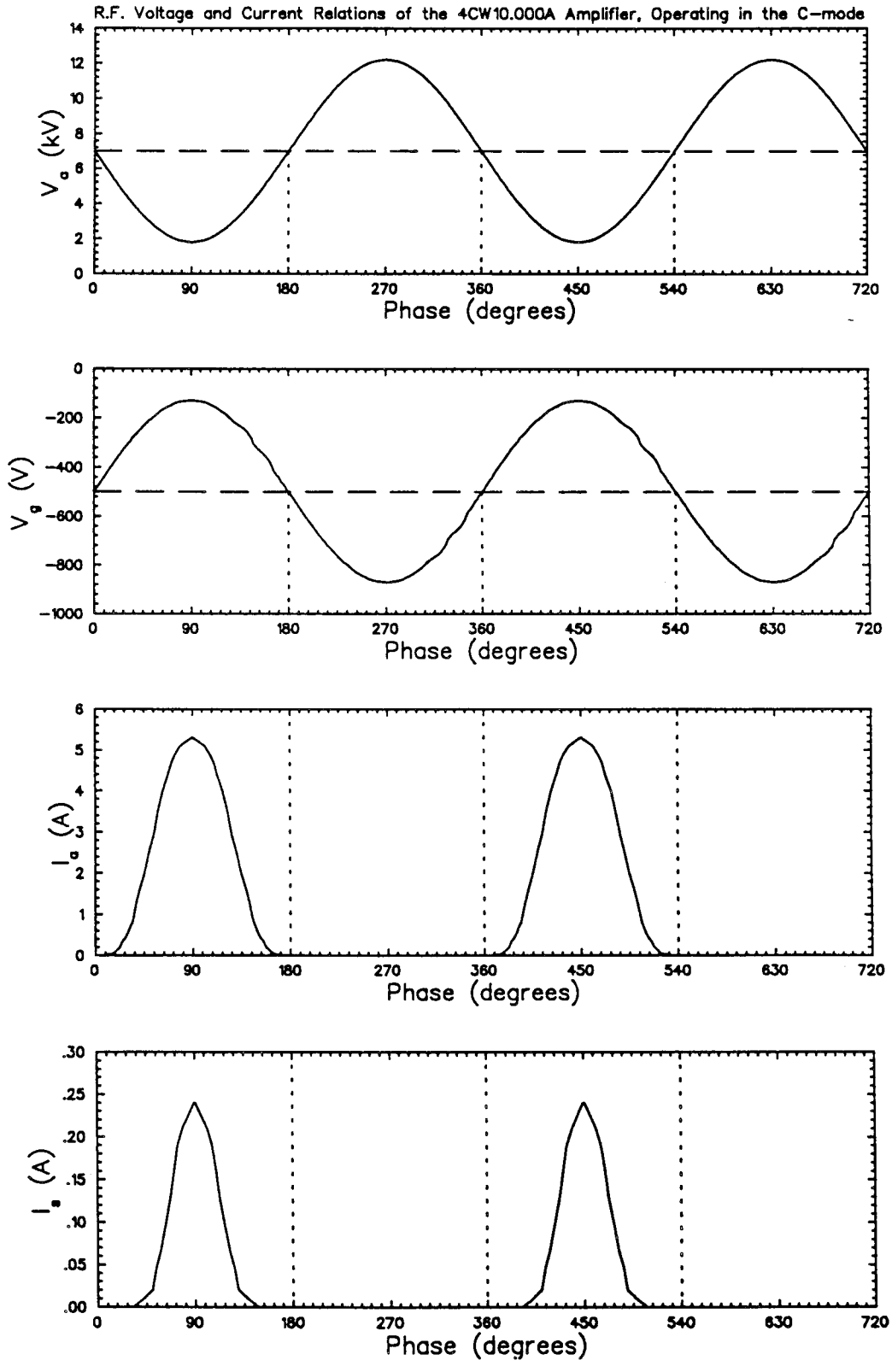

Figure 8.14: rf voltage and current characteristics of the operating line.

Final Conclusions and Recommendations

The aim of the graduate study was to find a design for an accelerating cavity resonant at 45 MHz and with a limited physical length of 50 cm. Three different designs have been considered, one employing radial transmission line folding, one employing longitudinal transmission line folding and finally one employing capacitive loading. For all the three cavities the physical length can be reduced to 50 cm.

The cavity employing radial transmission line folding has low values for its unloaded quality factor and shunt impedance and is complicated of construction. This design was therefore rejected.

Extensive research has been done on the cavity design employing longitudinal transmission line folding. Analytical equations have been derived to calculate all the important cavity parameters. In chapter 3 equations have been derived for the length, the dissipated power, the shunt impedance, the stored energy and the quality factor of a cavity consisting of two layers. To obtain these equations, matrix transmission line theory was used.
The analytically calculated cavity parameters showed good agreement with numerical calculations performed by the computer code SUPERFISH.

In order to check the analytical and numerical results a 1:1 "cold" copper model cavity was built of a two layer cavity. URMEL-T calculations of the resonance frequency differed about 2% from the measured frequency. For SUPERFISH this was less than 0.2%. The measured quality factor was only 8% lower than expected. Also the shunt impedance showed very good agreement with the measurements.

In order to establish matched coupling, the cavity must be detunable by 0.01 MHz.
However, it will be very difficult to construct the cavity such that its resonance frequency is within this small band, and therefore it is advisable to have more detuning available (in the order of ±0.1 MHz). Detuning by changing the accelerating gap from 27.5 mm to 10 mm allowed for a measured frequency band of 250 kHz.
Comparison between URMEL-T and SUPERFISH showed that the latter is the most reliable in predicting the cavity detuning from changing the accelerating gap.
Another way to detune the cavity is by changing the permeability of ferrites placed near the shorting plate of the cavity. The permeability of the ferrite is a function of the applied magnetic biasing field. The resonant frequency of a cavity depends on the permeability of the medium in it. Ferrites could also be used as a fourth alternative to shorten the cavity to less than 50 cm.

Power can be coupled into the cavity by a loop placed at a position where the magnetic fields are large. The coupling problem can be simulated with an equivalent LC-circuit. From an expression for the complex cavity input impedance, two conditions for matched coupling have been derived. This complex cavity impedance has been compared with measured values. They show good agreement. From the circuit model and also from the measurements we can conclude that perfect matching can always be achieved if the cavity is detunable and if the coupling loop can be rotated (for this, however, the loop should be large enough).

An alternative design of the accelerating cavity is based on capacitive loading. The main advantage of this cavity is, that it is very simple of construction. Also here transmission line matrix theory was used to calculate the cavity parameters. Once more these calculations showed good agreement with numerical calculations done with SUPERFISH. The quality factor is of the same order as that of a three layer cavity. However, the shunt impedance is a factor two lower. Nevertheless this design seems to be the best of the three types considered in this report.

The power source for the cavity will be a tetrode. An empirical equation is used which describes the total cathode current as a function of the anode voltage, control grid voltage and screen grid voltage. This equation contains parameters which have been obtained by fitting the cathode current characteristics of the tube as supplied by the manufacturer. There is good agreement between the fitted empirical equation and the actual current characteristics. The amplification factor μ and the screen grid amplification factor μ_s are no constants, but are a function of the anode current. The quantity μ_s is also a function of the anode voltage.
An operating line has been determined, and analytical calculations have been performed determining the dc anode current, the amplitude of the first harmonic of the anode current, the dc input power, the rf output power and the rf input power.
A solution has to be found in order to transport an output power of 5.4 kW to the resonator. A coaxial cable heats up due to the damping of the rf wave. Furthermore, impedance transformation will be necessary due to the difference of the characteristic impedance of the cable (which is 50 Ω) and the output impedance of the tetrode (which is $\approx$2.5 kΩ).

References

[CAS 92] R.G. Carter, "Review of RF Power Sources for Accelerators", RF Engineering for Particle Accelerators, CERN Accelerator School, CERN 92-03, Vol. I,Geneva, 1992.

[DAV 70] J. Davidse, "Grondslagen van de Electronica", Spectrum, Utrecht, 1970.

[EIM 69] Manufacturers specifications for the Eimac 4 CW 10,000 Power Tetrode, English Electric Valve Compagny Limited, 1969.

[GEN 87] W. van Genderen and J.A. van der Heide, "Calculation of Cyclotron RF Systems", Nucl. Instr. and Meth. in Phys. Res. A258, 1987, p.p. 161-169.

[GRA 71] I.S. Gradshteyn, "Table of Integrals, Series and Products", 4th edition, Academic Press, 1971.

[GRI 70] P. Grivet, "The Physics of Transmission Lines at High and Very High Frequencies", Vol 1, Academic Press, London/New York, 1970.

[HEI 93] J.A. van der Heide, M.J.A. Rubingh, W.J.G.M. Kleeven, "Calculations and Model Measurements for the Euterpe Cavity", Paper submitted to the 1993 Particle Accelerator Conference, Washington D.C., 1993.

[KOP 92] W. Koppens, "Berekeningen aan de Versnelcavity voor Euterpe", int. rep. VDF/NK 92-30, 1992.

[MAG 93] P. Magendans, gesprek, 1992.

[ORR 75] W.I. Orr, "Radio Handbook", Editors and Engineers, Indiana USA, 1975.

[PLO 92] Plotdata Users' Guide, J.L. Chuma, Triumf, Vancouver, 1992.

[POI 87] User's Guide for the POISSON/SUPERFISH group of codes, M.T. Menzel, H.K. Stokes, Accelerator Theory and Simulation Group, Los Alamos National Laboratory, Los Alamos USA, 1987.

[POZ 90] D.M. Pozar, "Microwave Engineering", Addison-Wesley Publishing Compagny Inc., London, 1990.

[PRE 70] Preamble, "Tetrodes", English Electric Valve Company Limited, 1970.

[REL 88] RELAX3D user's Guide and Reference Manual, version 2.0, C.J. Kost and F.W. Jones, TRIUMF, Vancouver, 1988

[SAN 86] K.F. Sander, G.A.L. Reed, "Transmission and Propagation of Electromagnetic Waves", 2nd edition, Cambridge University Press, Cambridge, 1986.

[SCH 81] S.O. Schriber, "Accelerator structure development for room-temperature linacs", IEEE Transactions on Nuclear Science, Vol. NS-28, No. 3, 1981.

[TER 43] F.E. Terman, "Radio Engineers' Handbook", McGraw-Hill Book Company Inc., New York/London, 1943.

[TER 50] F.E. Terman, "Radio Engineers' Handbook", 1st edition, McGraw-Hill Publishing Compagny, New York/London, 1950.

[TER 55] F.E. Terman, "Electronic and Radio Engineering", 4th edition, McGraw-Hill Book Compagny Inc., New York/London, 1955.

[URM 87] URMEL and URMEL-T user Guide, U. Lauströer, U. van Rienen, T. Weiland, 1987.

[WEB 92] G.A. Webers, "The use of Conformal Mapping to calculate the capacity of the 45 MHz EUTERPE cavity", int. rep., 1992.

[ZIE 74] A. van der Ziel, "Introductory Electronics", Prentice-Hall inc., New Jersey, 1974.

Appendix A: The EUTERPE cavity; the initial design.

Appendix A1: Analytical calculations.

In the cavity there is an electric field and a magnetic field which, by using $\vec{E}=Ee^{j\omega t}$ and $\vec{H}=He^{j\omega t}$, satisfy the Maxwell equations.

$$\nabla\times E=-j\omega\mu H\ , \tag{A.1}$$

$$\nabla\times H=j\omega\varepsilon E\ . \tag{A.2}$$

Only E_r,E_z and H_θ are different from zero. If we transform these equations to equations for a two dimensional rotationally symmetric system in z and r coordinates, we get

$$\frac{\partial^2 H_\theta}{\partial z^2}+\frac{\partial}{\partial r}\left(\frac{1}{r}\frac{\partial}{\partial r}(rH_\theta)\right)=-\omega^2\varepsilon\mu H_\theta\ . \tag{A.3}$$

And for the electrical field

$$\begin{aligned}\frac{\partial^2 E_r}{\partial z^2}-\frac{\partial^2 E_z}{\partial r\partial z}&=-\omega^2\varepsilon\mu E_r\ ,\\ \frac{1}{r}\frac{\partial}{\partial r}\left(r\frac{\partial E_r}{\partial z}-r\frac{\partial E_z}{\partial r}\right)&=\omega^2\varepsilon\mu E_z\ .\end{aligned} \tag{A.4}$$

These equations are difficult to solve analytically in order to get an expression for the capacitance of the cavity drawn in Fig. 3.1. We therefore use approximation methods.
One cell of the cavity is drawn in detail in Fig. A.1.

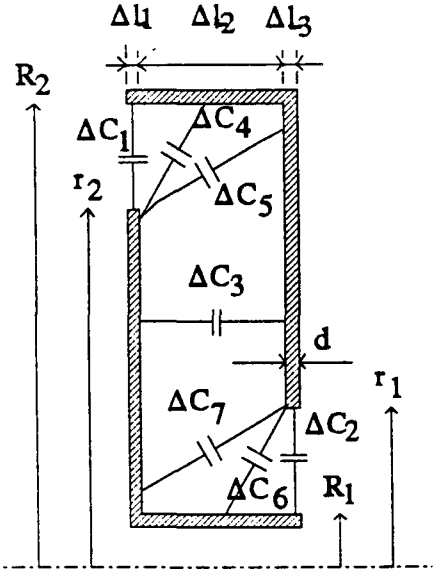

Figure A.1: One cell of the cavity in detail.

The inductance of this cell is the sum of the inductances of three parts of the cell

$$\Delta L=\Delta L_1+\Delta L_2+\Delta L_3=\frac{\mu_0}{2\pi}\left(\frac{1}{2}d\,\ln\frac{R_2}{r_2}+s\,\ln\frac{R_2}{R_1}+\frac{1}{2}d\,\ln\frac{r_1}{R_1}\right). \tag{A.5}$$

Because the E-field rotates twice over an angle of 90° in one cell, the capacitance is split up in seven contributing parts. The "coaxial" contributions are

$$\Delta C_1+\Delta C_2=2\pi\varepsilon_0\left\{\frac{1}{2}d\left(\ln\frac{R_2}{r_2}\right)^{-1}+\frac{1}{2}d\left(\ln\frac{r_1}{R_1}\right)^{-1}\right\}. \tag{A.6}$$

Between the vertical plates, supposing the current is constant over this short distance

$$\Delta C_3=\pi\varepsilon_0\frac{r_2^2-r_1^2}{s}. \tag{A.7}$$

There will be a concentration of the field lines near the corners of the inner conductor. This effect is taken into account by calculating the capacitances in the corners with fringing field capacitance formulas, given by [GEN 87]

$$\Delta C_4=\varepsilon_0\left\{\ln\frac{(R_2-r_2)^2+s^2}{4s^2}+\frac{2s}{R_2-r_2}\arctan\frac{R_2-r_2}{s}\right\}(R_2+r_2),$$

$$\Delta C_5=\varepsilon_0\left\{\ln\frac{(R_2-r_2)^2+s^2}{4(R_2-r_2)^2}+\frac{2(R_2-r_2)}{s}\arctan\frac{s}{R_2-r_2}\right\}(R_2+r_2),$$

$$\Delta C_6=\varepsilon_0\left\{\ln\frac{(r_1-R_1)^2+s^2}{4s^2}+\frac{2s}{r_1-R_1}\arctan\frac{r_1-R_1}{s}\right\}(r_1+R_1),$$

$$\Delta C_7=\varepsilon_0\left\{\ln\frac{(r_1-R_1)^2+s^2}{4(r_1-R_1)^2}+\frac{2(r_1-R_1)}{s}\arctan\frac{s}{r_1-R_1}\right\}(r_1+R_1). \tag{A.8}$$

The total capacitance of one cell is

$$\Delta C=\Delta C_1+\Delta C_2+\Delta C_3+\Delta C_4+\Delta C_5+\Delta C_6+\Delta C_7. \tag{A.9}$$

The speed of a travelling wave is

$$v=\sqrt{\frac{dz}{dL}\frac{dz}{dC}}\cong\sqrt{\frac{d+s}{\Delta L}\frac{d+s}{\Delta C}}\ , \tag{A.10}$$

and with ¼λ=N(d+s), the resonance frequency is with $f_0=v/\lambda$

$$f_0=\frac{1}{4N\sqrt{\Delta L\Delta C}}\ , \tag{A.11}$$

where N is the number of cells.
To calculate the higher modes of a cavity we use transmission line theory and represent the cavity by a network of lumped-circuit elements

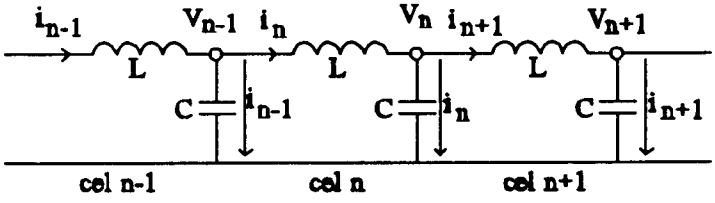

Figure A.2: Electrical circuit representing the cavity.

The expression for the frequency becomes [KOP 92]

$$f_p=2f_0\sin\left(\frac{2p-1}{2N+1}\cdot\frac{1}{2}\pi\right), \tag{A.12}$$

with p=1,2,...N. For large N and p=1 we get Eq. (A.11) again.

The resistance Ω of a circular plate with skin depth $\delta=1/\sqrt{\pi\mu\sigma f}$ is

$$\Omega=\int_{r_a}^{r_b}\frac{\rho}{2\pi r\delta}dr=\frac{\rho}{2\pi\delta}\ln\frac{r_b}{r_a}\ , \tag{A.13}$$

where r_a is the inner and r_b the outer radius of a vertically placed plate. The quantity ρ is the specific resistance. The resistance of a coaxial cylinder is

$$\Omega=\int_0^l\frac{\rho}{2\pi\delta}\left(\frac{1}{r_a}+\frac{1}{r_b}\right)dz\ , \tag{A.14}$$

with l the length of the conductors.

For one cell the resistance $\Delta\Omega$ is

$$\Delta\Omega=\frac{\rho}{2\pi\delta}\left\{\frac{1/2d}{r_2}+\ln\frac{r_2}{R_1}+\frac{s+1/2d}{R_1}+\frac{s+1/2d}{R_2}+\ln\frac{R_2}{r_1}+\frac{1/2d}{r_1}\right\}. \tag{A.15}$$

The quality factor is given by Eq. (2.7) with for the stored energy and the dissipated power

$$W_{st}=\frac{\mu_0}{2}\int H^2dV=\frac{\mu_0}{2}\int\left(\frac{I_n}{2\pi r}\right)^2dV\ , \tag{A.16}$$

$$P_{dis}=\frac{1}{2\sigma\delta}\int H^2dS=\frac{1}{2\sigma\delta}\int\left(\frac{I_n}{2\pi r}\right)^2dS\ , \tag{A.17}$$

with dV the volume of the cell, dS an infinitesimal surface part, I_n the current in a cell which is supposed to be constant, and σ the conductivity. The total stored energy and dissipated power summated over N cells become

$$W_{st}=\frac{\mu_0}{2}\frac{\sum I_n^2}{2\pi}\left\{\frac{1}{2}d\ \ln\frac{R_2}{r_2}+s\ \ln\frac{R_2}{R_1}+\frac{1}{2}d\ \ln\frac{r_1}{R_1}\right\}=\frac{1}{2}\Delta L\sum I_n^2\ , \tag{A.18}$$

$$P_{dis}=\frac{1}{2\sigma\delta}\frac{\sum I_n^2}{2\pi}\left\{\frac{d}{2r_2}+\ln\frac{R_2}{R_1}+\frac{s+1/2d}{R_1}+\frac{d}{2r_1}+\ln\frac{R_2}{r_1}+\frac{s+1/2d}{R_2}\right\}=\frac{1}{2}\Delta\Omega\sum I_n^2\ . \tag{A.19}$$

The equation for the quality factor becomes then (using Eq. (A.11))

$$Q=\frac{\pi}{2N\Delta\Omega}\sqrt{\frac{\Delta L}{\Delta C}}\ . \tag{A.20}$$

The shunt impedance is given by Eq. (2.5) where V_g is the gap voltage. So $V_g=U_0$. For one cell we have

$$U_0=\sqrt{\frac{\Delta L}{\Delta C}}\ I_0\ . \tag{A.21}$$

I_n has a cosine character so

$$\sum I_n^2 \approx \frac{1}{2} N I_0^2 \ , \tag{A.22}$$

which results by using Eq. (A.19) in

$$R_{sh} = \frac{4\Delta L}{\Delta C \Delta \Omega N} \ . \tag{A.23}$$

Appendix A.2: Results of numerical calculations.

The aim is to find a cavity design with the highest values for the quality factor and the shunt impedance, and that has a resonance frequency of 45.0 MHz. The cavity variables are

N	=	Number of cells
d	=	Thickness of plates
s	=	Distance between two plates
R_1	=	Outer radius beam pipe
R_2	=	Inner radius outer tube
r_1	=	R_1+s
r_2	=	R_2-s

A Turbo PASCAL program has been written that calculates the inner radius of the outer tube, the inductance, the capacitance, the resistance, the quality factor and the shunt impedance of a cavity as a function of the number of cells, the distance between plates and the outer radius of the beam pipe. Variation of d didn't have much effect on these calculated values. The frequency was kept constant at a value of 45.00±0.01 MHz. The results are given in Figs. A.3-A.8.

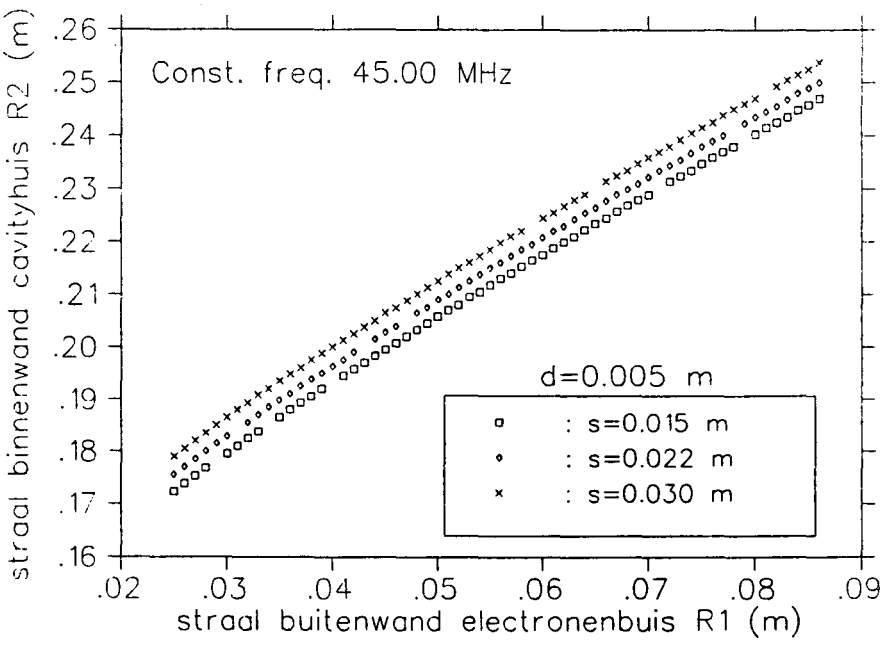

Figure A.3: R_2 as a function of R_1 and s.

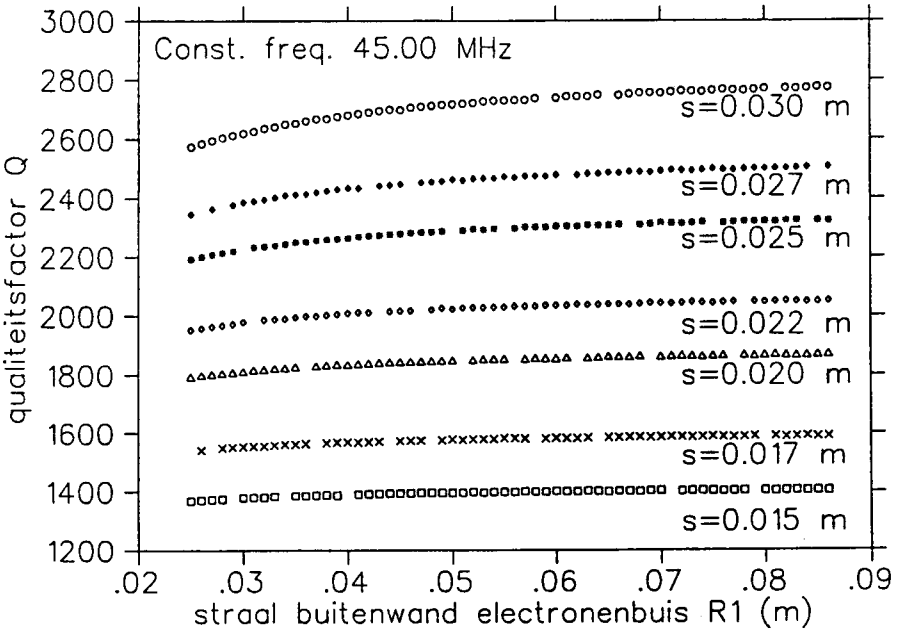

Figure A.4: The quality factor Q as a function of R_1 and s. d=5 mm and N=10.

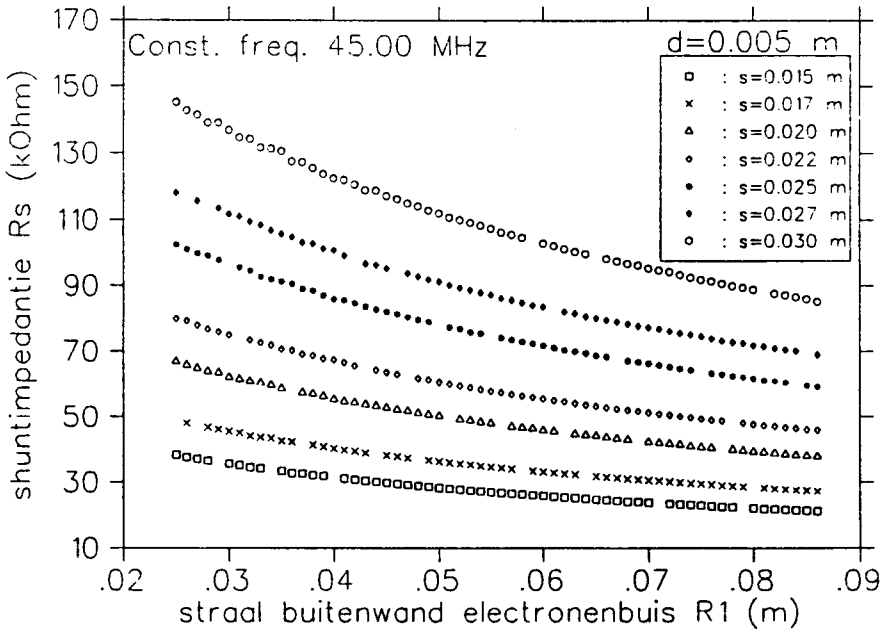

Figure A.5: The shunt impedance R_{sh} as a function of R_1 and s. N=10.

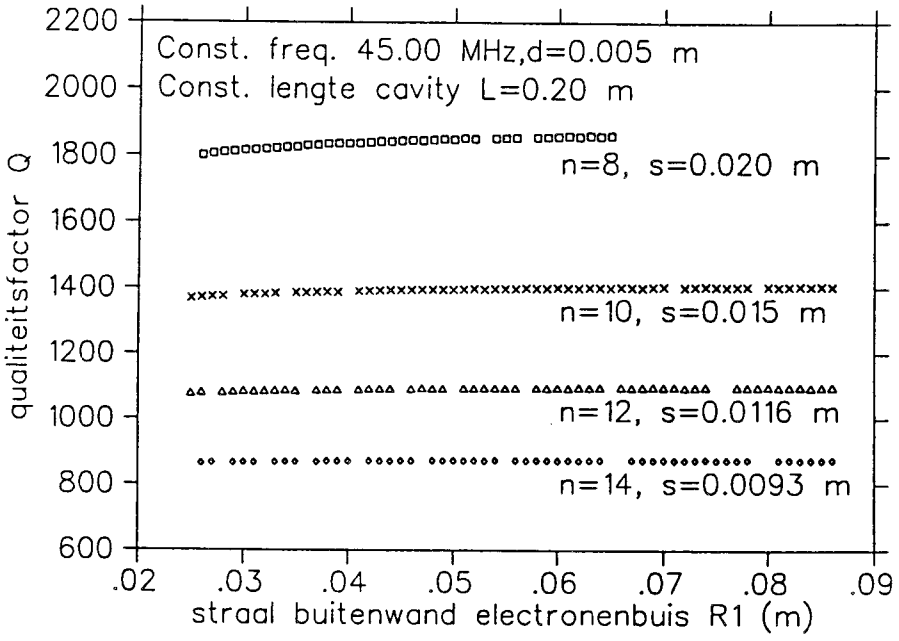

Figure A.6: Q as function of s and N, maintaining a constant length of 20 cm.

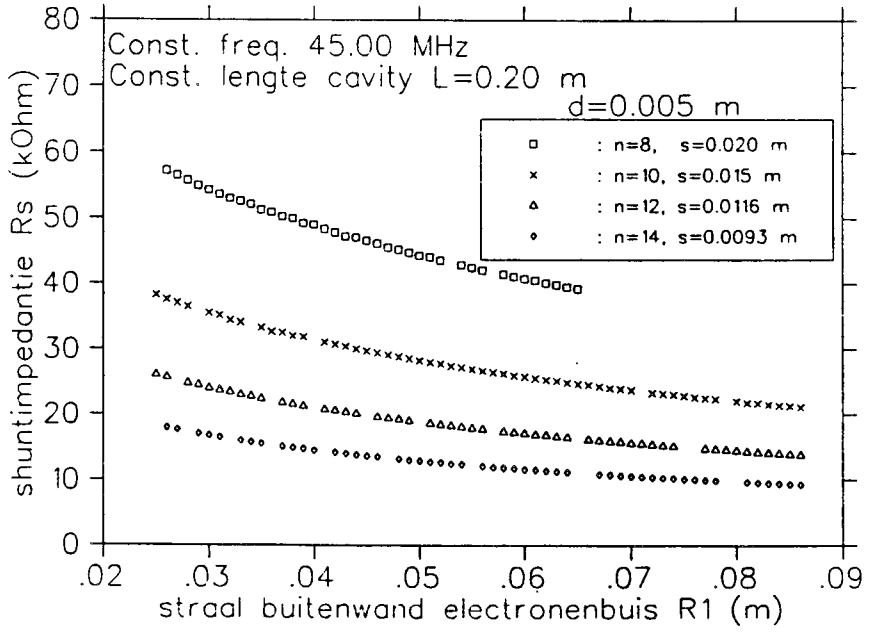

Figure A.7: R_{sh} as a function of N and s, maintaining a constant length of 20 cm.

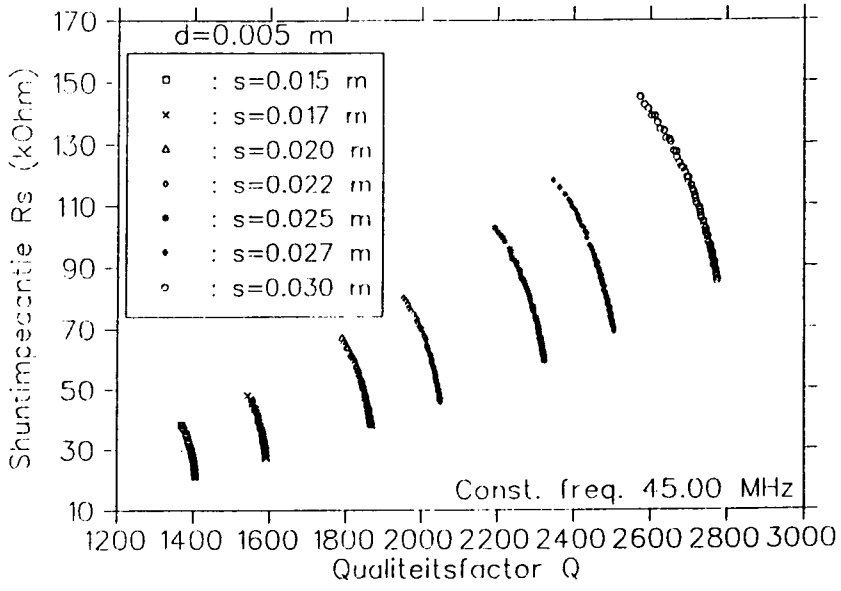

Figure A.8: The shunt impedance R_{sh} as a function of the quality factor Q.

The radius R_2 depends linearly on the outer radius of the beam pipe. Q differs only a little bit on increasing R_1, but changes dramatically if we increase the distance between the plates. This occurs because Q is a function of the stored energy, and the stored energy increases when the volume of the cavity increases. Increasing R_1 has the opposite effect on the shunt impedance R_{sh} as it has on Q. From Fig. A.5 we can see that R_{sh} increases when s increases. Furthermore, the fewer cells, the higher Q and R_{sh}, when maintaining a constant length of the cavity. In choosing the best cavity design we prefer a high shunt impedance because it is directly related to the dissipated power in the cavity walls. As a result the design will be a 10 cell cavity with dimensions given below.

r_0	=	2.3 cm
R_1	=	2.5 cm
r_1	=	5.5 cm
r_2	=	14.9 cm
R_2	=	17.9 cm
r_3	=	18.4 cm
s	=	3.0 cm
d	=	0.5 cm
l	=	37.0 cm
n	=	10

Table A.1: Dimensions of a 10 cell cavity.

This leads to f_0=45.00 MHz, Q_0=2573 and R_{sh}=145.2 kΩ. This means that 17.2 kW is needed to build up an accelerating voltage of 50 kV.

Appendix A.3: Coupling of rf power.

The power will be coupled into the cavity by a loop, see Fig. A.9. The equivalent circuit for the complete rf system is given by Fig. 4.2. The primary input impedance is

$$Z_{pr}=j\omega L_1+\frac{\omega^2 M^2}{R_s(1+2jQ_0\delta)} \quad . \tag{A.24}$$

When there is matched coupling the imaginary part of Z_{pr} is zero and the real part is equal to $R_0 \approx 50\ \Omega$. If the circuit is tuned, $\delta=0$. So the condition for matched coupling is

$$Z_{pr}=\frac{\omega^2 M^2}{R_s}=50\Omega \quad . \tag{A.25}$$

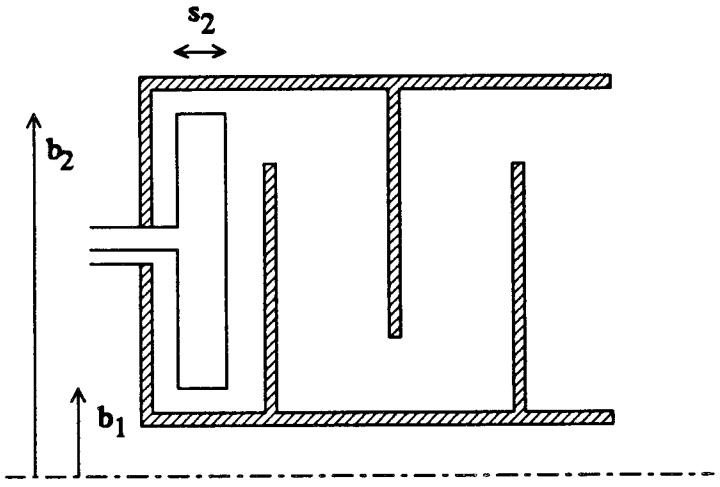

Figure A.9: Cavity with coupling loop near the shorting plate.

The mutual induction is

$$M=\frac{\phi_{12}}{I_0}=\frac{\mu_0}{2\pi}s_2 \ln\frac{b_2}{b_1} \quad , \tag{A.26}$$

where ϕ_{12} is the flux enclosed by the loop, generated by the current I_0 in the cavity.
R_s is calculated by equalizing the dissipated power in the equivalent circuit and the cavity, using Eq. (A.22)

$$\frac{1}{2}I_0^2 R_s=\frac{1}{2}\sum I_n^2 \Delta\Omega \quad , \tag{A.27}$$

$$R_s=\frac{1}{2}N\Delta\Omega=6.75\cdot10^{-3}\ \Omega \quad , \tag{A.28}$$

when we use the data of the cavity chosen in the previous paragraph.
For optimal coupling it is necessary that $\omega L_1 \ll R_0$. So for the mutual induction we get, when

the real part of Z_{pr}=50 Ω,

$$M=\frac{\sqrt{R_0 R_s}}{\omega}=2.05\,nH\ . \qquad \text{(A.29)}$$

This can be obtained by using s_2=0.70 cm, b_1=7.75 cm and b_2=16.25 cm for the dimensions of the coupling loop in Fig. A.9.
The inductance of this loop can be calculated by [TER 47]

$$L=0.004[(s_1+s_2)\ln\frac{4s_1s_2}{d}-s_1\ln(s_2+g)+\mu\,\delta'(s_1+s_2)+2(g+\frac{d}{2})-2(s_1+s_2)]\ , \qquad \text{(A.30)}$$

where δ' is the skin effect correction factor, and μ=1. In Fig. A.10 the loop with its parameters is drawn.

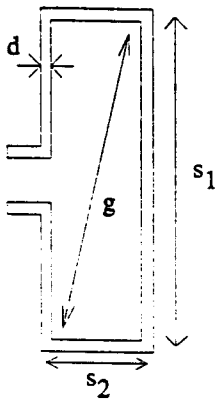

Figure A.10: Thin coupling loop with a thickness d.

Using the dimensions given above (s_1=12.51 cm, s_2=0.70 cm, g=12.53 cm, d=0.10 cm, δ'=0.003), the inductance is L=0.136 μH, and the impedance of the loop is ωL_1=38.48 Ω. To obtain matched coupling ωL_1 must be smaller then 25 Ω. A solution is found by taking a metal strip with width c, see Fig. A.11.

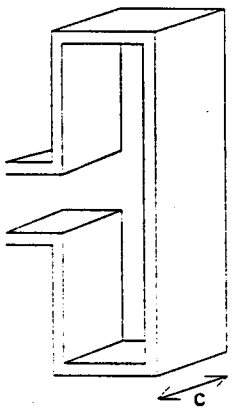

Figure A.11: Thick coupling loop with width c.

The inductance of this loop is given by [TER 50]

$$L=0.004[(s_1+s_2)\ln\left(\frac{2s_1s_2}{b+c}\right)-s_1\ln(s_1+g)-s_2\ln(s_2+g)+2g-\frac{s_1+s_2}{2}+0.447(b+c)] \quad . \tag{A.31}$$

Taking now c=2.50 cm and d=0.30 cm we get for the inductance 26.21 nH and ωL_1=10.23 Ω. By taking a thicker wire and keeping all the other dimensions the same, the mutual inductance is not changed. Only the self inductance of the loop is changed.

Appendix B: Direct rf coupling.

When we employ direct coupling, the power is coupled directly to the inner conductor of the cavity. This is shown schematically below.

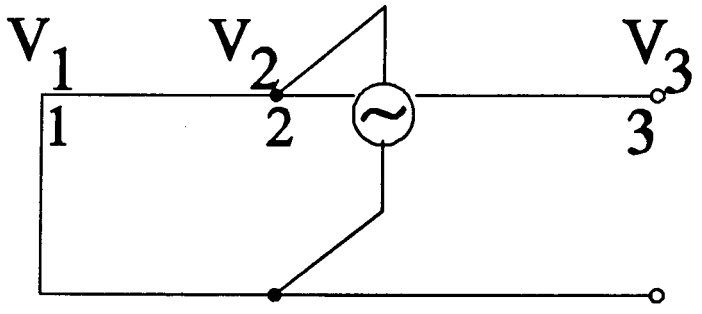

Figure B.1: Direct coupling of power.

The shorting plate is located at the left (position 1), while the gap is located at the right hand side of the figure (position 3). Power is coupled in at position 2. The cavity is represented by 2 transmission line sections, which can be described by two matrices A and B.
Suppose we have a lossless line. The voltage and the current at position 2 are related to the voltage and the current at the shorting plate by the transmission matrix A, which is of the form given in Eq. (3.2). So

$$\begin{pmatrix} V_2 \\ I_2 \end{pmatrix} = \begin{pmatrix} a_{11} & a_{12} \\ a_{21} & a_{22} \end{pmatrix} \begin{pmatrix} V_1 \\ I_1 \end{pmatrix}. \tag{B.1}$$

A similar relation holds for the voltage and current at position 3 related to the voltage and current at position 2 by transmission matrix B

$$\begin{pmatrix} V_3 \\ I_3 \end{pmatrix} = \begin{pmatrix} b_{11} & b_{12} \\ b_{21} & b_{22} \end{pmatrix} \begin{pmatrix} V_2 \\ I_2 \end{pmatrix}. \tag{B.2}$$

For the entire system we get

$$\begin{pmatrix} V_3 \\ I_3 \end{pmatrix} = (B)(A) \begin{pmatrix} V_1 \\ I_1 \end{pmatrix}. \tag{B.3}$$

Because of the short circuit (V_1=0) and due to the open circuit (I_3=0), this leads to the requirement that the right under element of matrix (B)(A) from Eq. (B.3) is zero. The resonance condition is then

$$b_{21}a_{12}+b_{22}a_{22}=0 \ . \tag{B.4}$$

The impedance Z at position 2 can be seen as a parallel circuit of the impedances Z_1 and Z_2, drawn in Fig. B.2. Z_1 is the impedance seen when looking toward the shorting plate, while Z_2 is the impedance seen when looking to the open end.

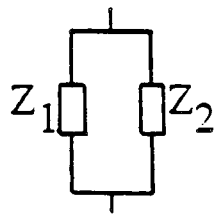

Figure B.2: Impedances seen by the generator for a lossless line.

For the impedances we find

$$Z_1=\frac{V_2}{I_2}=\frac{a_{12}I_1}{a_{22}I_1}=\frac{a_{12}}{a_{22}} \ , \tag{B.5}$$

$$Z_2=-\frac{V_2}{I_2}=-\frac{B_{11}^{-1}V_3}{B_{21}^{-1}V_3}=\frac{b_{22}}{b_{21}} \ , \tag{B.6}$$

because Det(B)=1. The minus sign takes into account the direction of the current. Seen from position 2 the current left from position 2 flows toward the generator, while at the right it flows away from the generator to the open end of the circuit. The total impedance seen by the generator is

$$\frac{1}{Z}=\frac{1}{Z_1}+\frac{1}{Z_2}=0 \ , \tag{B.7}$$

when we use the resonance condition. This means that the impedance seen by the generator is infinite, and no power can be coupled into the resonator.

We now assume that there is a lossy line, but that the losses are that small that the voltage and current distributions along the line remain the same as in the lossless case. These losses are depicted as extra parallel ohmic resistors in Fig. B.3, where the total impedance seen by the generator is drawn.

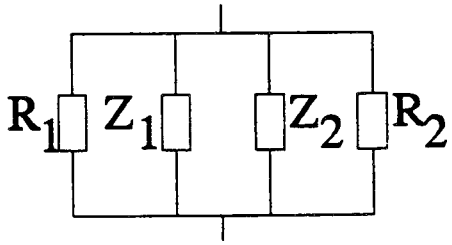

Figure B.3: Impedance seen by the generator for a lossy line.

The relation $1/Z_1+1/Z_2=0$ is still valid because we assumed that the voltage and current profiles remained the same. The total impedance is therefore

$$\frac{1}{Z}=\frac{1}{R_1}+\frac{1}{R_2}=\frac{1}{R} \quad . \tag{B.8}$$

The dissipated powers left and right of the coupling position are

$$P_1=\frac{V_1^2}{2R_1} \quad , \quad P_2=\frac{V_2^2}{2R_2} \quad , \tag{B.9}$$

where V_2 is the voltage at the coupling position. The resistance is then

$$\frac{1}{R}=\frac{2}{V_2^2}(P_1+P_2) \quad , \tag{B.10}$$

and is with the total dissipated power of the cavity

$$P=P_1+P_2=\frac{V_3^2}{R_{sh}}=\frac{V_3^2}{2R_{sh}^*} \quad , \tag{B.11}$$

equal to

$$\frac{1}{R}=\frac{V_3^2}{V_2^2}\frac{1}{R_{sh}^*} \quad . \tag{B.12}$$

To obtain perfect matching the resistance seen by the generator must be equal to the characteristic impedance R_0 of the coupling line, $R=R_0$. Thus the relation for matched coupling becomes, with $V_2=V_c$ the voltage at the coupling position and $V_3=V_{max}$ the maximum voltage at the gap

$$\frac{V_c}{V_{max}}=\left(\frac{R_0}{R_{sh}^*}\right)^{1/2} \quad . \tag{B.13}$$

Suppose the cavity can be approximated by ideal ¼λ-system. Then $V_{max}=Z_0 I_1$, with Z_0 the characteristic impedance, and $V_c=V_{max}\sin kx$, where x is the distance from the gap to the position where power is coupled into the system. Filling these expressions into Eq. (B.13) we get

$$x=\frac{c}{2\pi f_0}\arccos\left(\frac{R_0}{R_{sh}^*}\right)^{1/2} \quad , \quad k=\frac{2\pi f_0}{c} \quad , \tag{B.14}$$

where c is the speed of light. Using the data for the model cavity, $R_{sh}^*=R_{sh}/2=286.7\ k\Omega$,

R_0=50 Ω, and f_0=43.974 Mhz we get for the distance from the gap to the coupling position x=1.69 m. A ¼λ is 1.71 m. So the power must be coupled into the resonator at 2 cm from the shorting plate.

Appendix C: RELAX3D calculations of the capacitance of a return section.

The capacitance of a system consisting of two conductors is defined by the ratio of the magnitude of the electric charge on one of the conductors and the magnitude of the potential difference between the conductors,

$$C \triangleq \frac{|Q|}{|V_{ab}|} \quad (F) \; . \tag{C.1}$$

Written in terms of surface charge density ρ_s and the electric field $\vec{E}$ the equation becomes

$$C = \frac{\left| \int_S \rho_s dS \right|}{\left| -\int_a^b \vec{E} \cdot d\vec{l} \right|} \; . \tag{C.2}$$

It is difficult to find an analytical description for the electric field of the return section, because the two dimensional Poisson equation for the potential

$$\frac{\partial^2 V}{\partial r^2} + \frac{\partial^2 V}{\partial z^2} = -\frac{1}{r}\frac{\partial V}{\partial r} \tag{C.3}$$

is difficult to solve for this section.

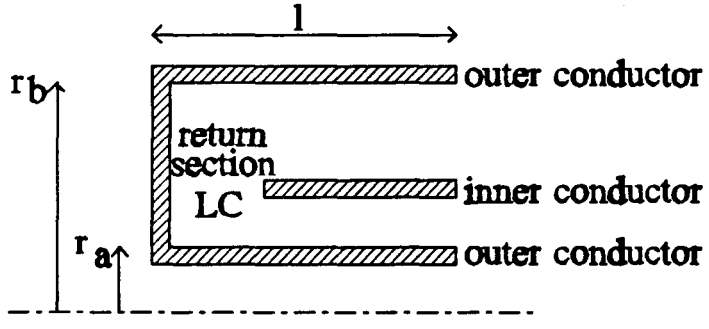

Figure C.1: The return section.

The computer code RELAX3D is an interactive FORTRAN-program [REL 88], that is able to solve numerically general three dimensional Laplace and Poisson problems. The return section geometry must be fitted on a three dimensional grid, determined by the variables IMAX, JMAX and KMAX. The product of these variables should not exceed 500.000. The geometry can be defined by three boundary conditions: the Neumann-condition, the Dirichlet-condition, and a dielectric transition between two media having a different permittivity. The latter one will not be used in our problem. The Neumann-condition implies that the gradients of the charge-density, permittivity and the potential perpendicular to the boundary are zero. The Dirichlet-condition implies that the points that satisfy the former condition, have a fixed value for the potential.

The solution of a potential problem is found by solving finite differential equations in these points by using point-iteration, with regard of the conditions. Before starting an iteration, a FORTRAN subroutine must have been written and compiled in which the geometry and starting conditions are defined. The name of this subroutine must start with the letters 'BND'. In this subroutine a starting value of the potential and when needed the condition of the points are given. A Dirichlet boundary is defined by a negative value of the potential. The magnitude of this negative value is the value of the potential held constant. Every point that is on a boundary for which the potential isn't defined by a Dirichlet-condition, satisfies automatically the Neumann-condition. An example of an input file for RELAX3D is given below.

```
      SUBROUTINE BND2CEL1(I,J,K,V,F,LL)
C=====================================================================C
C
C   RELAX3D PROEF1.OBJ
C   LAPLACE IN CYLINDERCOORDINATEN
C   ONDERZOEK NAAR DE CAPACITEIT VAN HET OMKEERPUNT
C   VAN EEN TESTCAVITY BESTAANDE UIT TWEE CELLEN
C   R1= 2.5 CM     Z1= 3.0 CM
C   R2= 5.5 CM     Z2=15.0 CM
C   R3= 6.0 CM
C   R4=13.2 CM
C   IMAX=31 JMAX=133 KMAX=1 OPT=2 HX=0.5 HY=0.1
C
C=====================================================================C
C
C STARTING VALUE FOR NON-BOUNDARY POINTS
C
      V=0.5
C
C DIRICHLET BOUNDARY
C
      IF (I.EQ.1)V=-1.
      IF (J.EQ.133)V=-1.
      IF (J.LE.26)V=-1.
      IF (I.GE.7.AND.J.GE.56.AND.J.LE.61)V=-1.E-20
C
C NEUMANN BOUNDARY
C
      IF (I.EQ.31.AND.J.GT.61.AND.J.LT.133)V=0.5
      IF (I.EQ.31.AND.J.GT.26.AND.J.LT.56)V=0.5
      RETURN
      END
```

In order to calculate the capacitance of the return section we use a potential difference between the inner and outer condition of 1 volt. This simplifies Eq. (C.2), using Gauss's law, to

$$C=|Q|=|\int_S \rho_s dS|=\varepsilon_0|\int_S (\vec{E}\cdot\vec{n})dS|=\sigma \ . \qquad \text{(C.4)}$$

So the capacitance of the return section is numerically equal to the charge on one of the conductors.

One conductor of the return section consists of the outer cylinder, the return section plate and the inner cylinder. For these three sections we can write down expressions for the charges as a function of the potential calculated by RELAX3D.

For the outer cylinder we have

$$\begin{aligned}\sigma_1 &= \varepsilon_0 \left| \int\int \vec{E}\cdot\hat{r}\, dz\, r\, d\phi \right| = 2\pi\varepsilon_0 r \left| \int \vec{E}\cdot\hat{r}\, dz \right| \\ &= 2\pi\varepsilon_0 r \left| \int \left(\frac{\partial V}{\partial r}\hat{r} + \frac{\partial V}{\partial z}\hat{z} + \frac{1}{r}\frac{\partial V}{\partial \phi}\hat{\phi} \right) \cdot \hat{r}\, dz \right| \\ &= 2\pi\varepsilon_0 r \left| \int_0^l \frac{\partial V}{\partial r} dz \right| .\end{aligned} \tag{C.5}$$

For the return section plate we have

$$\sigma_2 = 2\pi\varepsilon_0 \left| \int \vec{E}\cdot\hat{z}\, r\, dr \right| = 2\pi\varepsilon_0 \left| \int_{r_a}^{r_b} \frac{\partial V}{\partial z} r\, dr \right| . \tag{C.6}$$

And for the inner cylinder we have

$$\sigma_3 = 2\pi\varepsilon_0 r \left| \int \vec{E}\cdot\hat{r}\, dz \right| = 2\pi\varepsilon_0 r \left| \int_0^l \frac{\partial V}{\partial r} dz \right| . \tag{C.7}$$

The capacitance of the return section with length l is thus

$$C_a = \sigma_1 + \sigma_2 + \sigma_3 . \tag{C.8}$$

The capacitance can also be calculated from the charge on the inner conductor, consisting of the middle cylinder. The resulting value of the capacitance would be the same. The length *l*, defined in Fig. C.1 should be chosen long enough, so that the equipotential lines are situated parallel to each other at the right hand side of the figure. This is necessary in order to take the effect of the fringing fields near the inner conductor entirely into account.
Command files have been written for the Vax software package PLOTDATA, calculating the charge of a conductor from the potential given in every grid-point by RELAX3D. In Fig. C.2 the results of a RELAX3D calculation are shown.

The capacitance C_a calculated in Eq. (C.8) is not the capacitance used in the equations in chapter 4. It must be reduced with the capacitance of the two coaxial parts of the inner and outer layer. The equation for the capacitance of a coaxial structure is given by Eq. (3.33) times the length (*l*-*g*), where *g* is the gap. The result is a useful approximation for the return section capacitance which can be used in the equations derived in chapter 3.

Using the dimensions of the model cavity to calculate the capacitance C of the return section, the results are

Method	C_a (pF)	C (pF)
RELAX3D	15.8	3.7
Fringing field capacitance equations (Appendix A.1)	16.4	4.4
Equations derived by conformal mapping (Appendix D)	15.3	3.2

Table C.1: Comparison of capacities C calculated in three different ways for the return section of the model cavity.

The third method in the table using conformal mapping equations is discussed in appendix D. As we will see it is a very useful tool to calculate the return section capacitance because it has better results than the method using the fringing field capacitance equations.

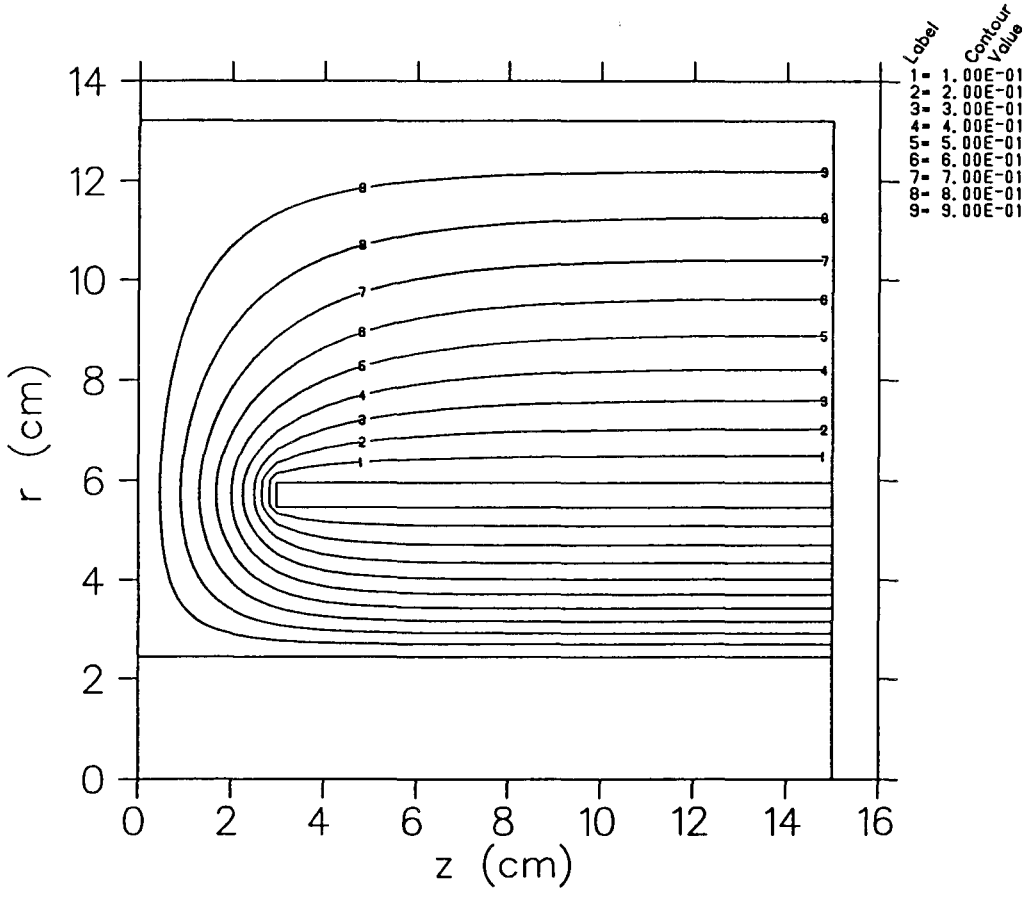

Figure C.2: Results of RELAX3D calculations on the return section of the model cavity.

Note that the length *l* is chosen long enough, because the equipotential lines are parallel to each other in the right hand side of the figure.

Appendix D: Conformal mapping, calculation of the capacitance of a return section.

A schematic layout in the z-plane of a cross section of the return section of the cylinder symmetrical EUTERPE cavity employing longitudinal transmission line folding is given in Fig. D.1. The longitudinal z-component is replaced by the x component while the radial component is replaced by the y component. Because of cylinder symmetry, there is no angular ϕ component. In order to calculate the capacitance of the return section, the potential distribution in a 2D cross section is calculated using the analytical tool of conformal mapping. The middle cylinder is for convenience approximated by a infinitely thin cylinder.

The outer boundary is set at a potential of 0 while the inner plate is at a potential of V_0. This plate is situated at a vertical distance P from the lower boundary y=0, a vertical distance Q from the upper boundary y=P+Q, and a horizontal distance G from the return section plate. In order to solve the potential distribution in this polygon, the problem can be simplified by transforming it to the so called t-plane. The points on the corners of the polygon in the z-plane are transformed to points on the real t-axis of the t-plane. Here t=-a corresponds to z=0 while t=-b is given by z=j(P+Q).
To describe the transformation of the z-plane into the t-plane the Schwarz-Christoffel transformation is used,

$$\frac{dz}{dt}=K\prod_{n=1}^{N}(t-a_n)^{\frac{\beta_n}{\pi}-1} . \tag{D.1}$$

Here β_n is the angle at a point A_n in the z-plane which is transformed to the point a_n in the t-plane. K is a complex constant and N is the number of angles in the polygon. Using the nomenclature in Fig. D.1 we get for the Schwarz-Christoffel transformation

$$\frac{dz}{dt}=K\frac{t-1}{t\sqrt{t+a}\sqrt{t+b}} . \tag{D.2}$$

K is found by integration near t=0 where z varies from Im(z)=0 to Im(z)=P [WEB 92]:

$$jP=\int_{t=-\epsilon}^{t=\epsilon}\frac{dz}{dt}dt=\int_{\pi}^{0}\frac{-jK}{\sqrt{ab}}d\theta \quad \Rightarrow \quad K=\frac{P}{\pi}\sqrt{ab} , \tag{D.3}$$

using $t=Re^{j\theta}$, where $0\le\theta\le\pi$ is an angle in the t-plane, and R a small radius.
Integrating Eq. (D.2), using z(-a)=0 to determine the constant of integration, gives

$$z(t)=K\left[\ln\left(\frac{2\sqrt{t+a}\sqrt{t+b}+2t+(a+b)}{b-a}\right)+\frac{1}{\sqrt{ab}}\ln\left(\frac{2ab+(a+b)t+2\sqrt{ab}\sqrt{t+a}\sqrt{t+b}}{t(a-b)}\right)\right] . \tag{D.4}$$

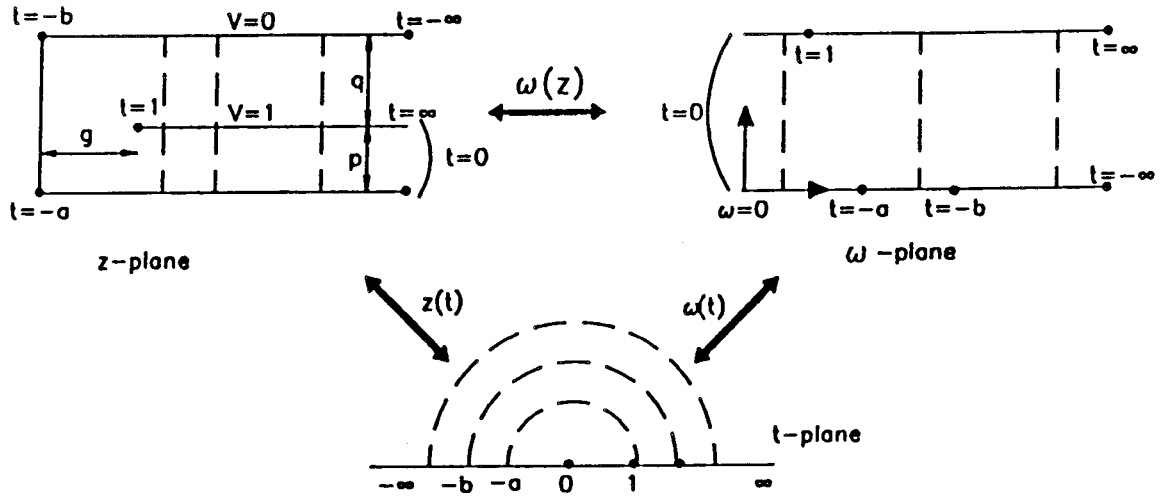

Figure D.1: Schematic layout of a cross section of the return section in three planes.

Transforming the t-plane into the ω-plane, the potential distribution describes a homogeneous field. This ω(t) transformation is given by:

$$\frac{d\omega}{dt}=\frac{A}{t} \quad \Rightarrow \quad \omega(t)=A\ln(t)+C \ . \tag{D.5}$$

The constant C is determined by the choice of the origin in the ω- plane.
The complex constant A is found by integration near t=0 where ω varies from Im(ω)=0 to Im(ω)=1,

$$j=\int_{t=-\epsilon}^{t=\epsilon}\frac{d\omega}{dt}dt=\int_{\pi}^{0}jAd\theta=-j\pi A \quad \Rightarrow \quad A=-\frac{1}{\pi} \ , \tag{D.6}$$

using again $t=Re^{j\theta}$.

The electrical field $\vec{E}$ is given by $\vec{E}=\nabla V$, with V the potential distribution. The non-zero component E is given by

$$E=\frac{d\omega}{dz} \ . \tag{D.7}$$

The capacitance between two conducting planes with a potential difference V_{ab} is given by Eq. (C.1). The total amount of charge on a conducting plate can be expressed in terms of electrical field at some enclosed area, using Gauss's law

$$Q=\varepsilon_0 \oint (E\cdot\vec{n})\,dS\ , \tag{D.8}$$

where $\vec{n}$ the normal vector on the surface, shown in Fig. D.2. Considering the real situation of the return section, it is seen that it is displaced at a distance R_0 with respect to the cavity axis. So the radial position is given by $r=R_0+y$.

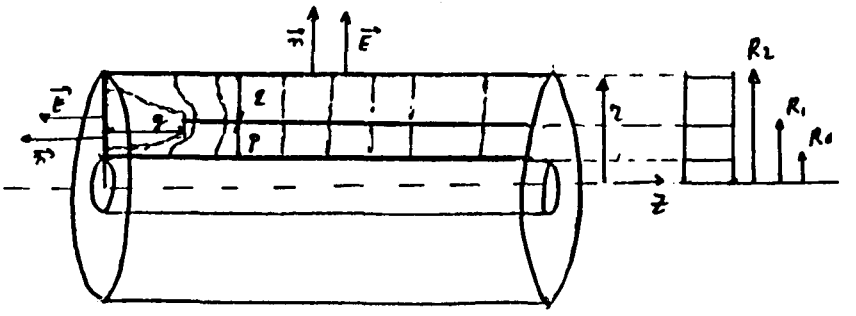

Figure D.2: Schematic layout of the return section.

The capacitance C_1 of the outer cylinder at a distance $r=R_2=R_0+(P+Q)$, is equal to the total charge on the outer cylinder when the potential difference is 1 V between the two conductors, which is

$$C_1=2\pi R_2\left|\int_0^l E(x)dx\right|=2\pi R_2\left|\int_0^l\left(\frac{d\omega}{dx}\right)dx\right|=2\pi R_2\left|\omega(t)\right|\Big|_{t=-b}^{t(x=l)}\ . \tag{D.9}$$

The contribution of the charge at the return section plate to the total capacitance is

$$C_2=2\pi\left|\int_{R_0}^{R_2} E(r)rdr\right|=2\pi\left|\int_{-a}^{-b}\left(\frac{d\omega}{dt}\right)r(t)dt\right|\ . \tag{D.10}$$

This integral must be evaluated numerically, using a second order integration routine, because the first order integration method, having a convergence factor of ≈1 doesn't converge well. The second order integration method has a convergence factor of ≈2.

The contribution of the charge at the lower boundary to the capacitance is

$$C_3=2\pi R_0\left|\int_0^l E(x)dx\right|=2\pi R_0\left|\int_0^l\left(\frac{d\omega}{dx}\right)dx\right|=2\pi R_0\omega(t)\Big|_{t=-a}^{t(x=l)}. \qquad (D.11)$$

The total capacitance of the return section with a length l is

$$C_a=C_1+C_2+C_3\ . \qquad (D.12)$$

The capacitance C of the return section that is used in chapter 3 is C_a minus the capacitance contribution of the coaxial parts with a length l-G.

The length l is chosen large enough so that the electrical field has only a radial component at the right hand side of Fig. D.2.
For a general EUTERPE cavity R_0 is fixed at 25 mm, with a plate thickness of the middle cylinder of 5 mm. To describe the integration path along the outer cylinder, Q must be increased by 5 mm, because the model we used for conformal mapping can only handle an infinitely thin middle cylinder. This implies that the electrical field far away from the symmetry axis is systematically too small by the amount (Q-5 mm)/Q. To compensate for this, the electrical fields at the outer cylinder and at the return section plate are multiplied by the fraction Q/(Q-5 mm). This results in an electrical field near $r=R_0$ that is too high. But due to the radius dependence of the integral in C_2, this effect can be neglected. In Fig. D.3 the capacitances (in pF) are plotted as a function of P and Q (in mm) with different gaps, G=20, 30 and 40 mm. A special case occurs if the characteristic impedances of the two layers are equal. Q and P are then related by $(P+Q+R_0)/(P+R_0)=(P+R_0)/R_0$. This relation is plotted by the dashed curve. We see an increase of area with low capacitance, when G is increased. This occurs because the electrical field at the return section plate is decreased, and therefore the capacitance. Furthermore we see that the capacitance along the dashed line doesn't decrease monotonically.
To verify the shape of the curves in Fig. D.3, the same calculations have been done using the model of fringing field capacitances described in appendix A.1. The results are shown in Fig. D.4. Comparing Fig. D.4 with Fig. D.3 we see that the general shape is the same, but that the values of the capacitances calculated using the fringing fields capacitance model are higher, especially for larger Q.
This is probably caused by the fact that the fringing fields capacitance equations only hold when the fringing fields at the different corners do not interact with the other corners. When increasing Q these interactions become larger. For small Q values the two methods agree well.

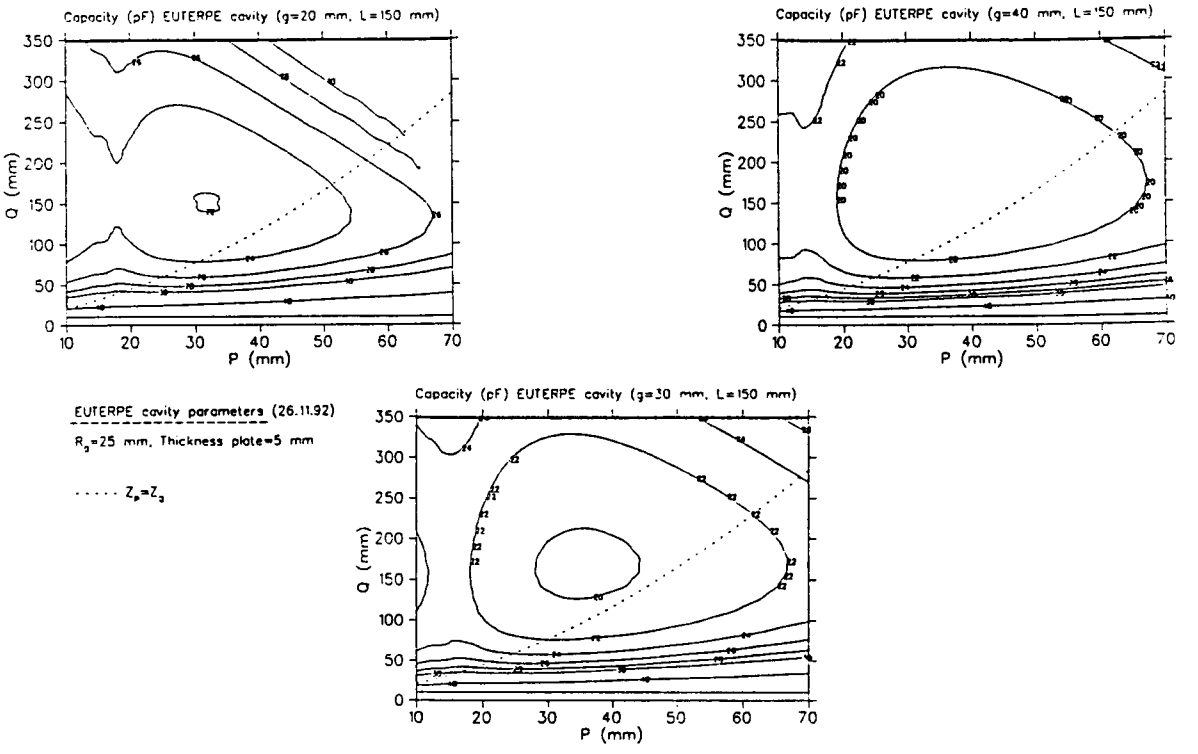

Figure D.3: Equi-capacitance contours versus P and Q with l=150 mm and a: G=20 mm, b: G=30 mm and c: G=40 mm, using conformal mapping.

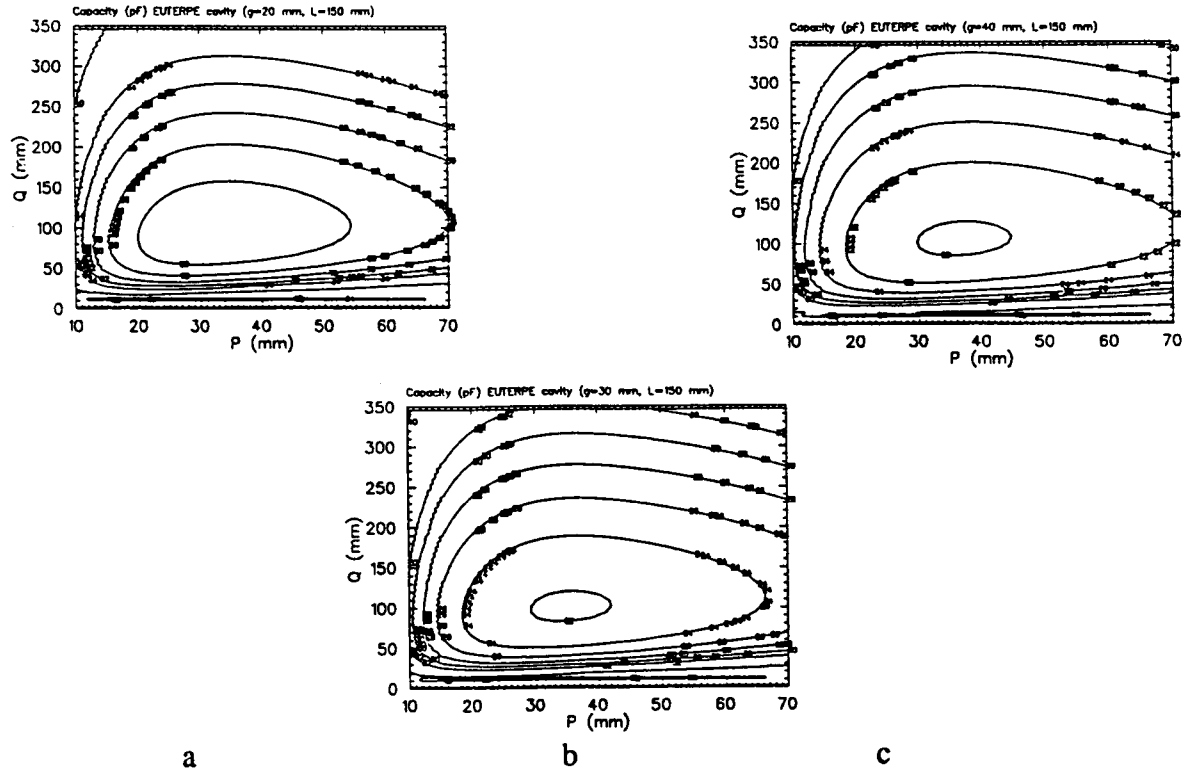

Figure D.4: Equi-capacitance contours calculated by using the fringing fields capacitance model in appendix A.1, with the same data as in Fig. D.3

Keeping P=30 mm and G=30 mm constant and letting Q increase we see in Fig. D.3 that for one value of P there are two equal values for C with different Q. To verify this we used the numerical program RELAX3D. Also, for the same geometries, we calculated the capacitances using the fringing fields capacitance equations. The results are shown in table D.1.

Method	Q=72 mm	Q=320 mm
RELAX3D	21.7 pF	20.3 pF
Conformal mapping	≈22 pF	≈22 pF
Fringing field equations	22.4 pF	30.6 pF

Table D.1: Capacitances calculated using three different methods.

The results is that calculating the capacitance of a return section with the conformal mapping method is superior to the method using fringing fields capacitance equations, especially when Q becomes large.

Appendix E: The resonance condition.

Suppose a two cell cavity can be described by two lossless transmission line sections. For simplicity we, for the moment, consider a 2-layer cavity and ignore the effect of the return section as well as the losses. This is the simplest model to describe the cavity. This is shown schematically in Fig. E.1.

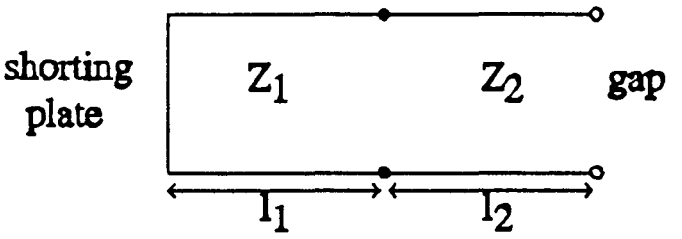

Figure E.1: Simplified representation of a 2-layer cavity by two transmission line sections.

In order to find the resonance condition the problem is split into two sections. Each section can be represented by a lossless transmission line terminated in a load impedance Z_L. Z_L=0 for section 1 (short circuit) and Z_L=∞ for section 2 (open end). See Fig. E.2.

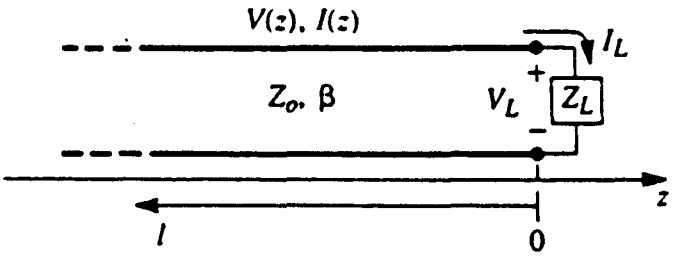

Figure E.2: A transmission line terminated in a load impedance Z_L.

The total voltage on the line can then be written as a sum of incident and reflected waves:

$$V(z)=V_0^+ e^{-j\beta z}+V_0^- e^{j\beta z} \quad . \tag{E.1}$$

Similar, the total current on the line is described by:

$$I(z)=\frac{V_0^+}{Z_0}e^{-j\beta z}-\frac{V_0^-}{Z_0}e^{j\beta z} \quad . \tag{E.2}$$

At z=0 we have

$$Z_L=\frac{V(0)}{I(0)}=\frac{V_0^+ + V_0^-}{V_0^+ - V_0^-}Z_0 \quad , \tag{E.3}$$

and when solving for V_0^-

$$V_0^- = \frac{Z_L - Z_0}{Z_L + Z_0} V_0^+ \ . \tag{E.4}$$

So the voltage reflection coefficient, Γ, is

$$\Gamma = \frac{V_0^-}{V_0^+} = \frac{Z_L - Z_0}{Z_L + Z_0} \ . \tag{E.5}$$

The total voltage and current waves on the line can then be written as

$$V(z) = V_0^+ [e^{-j\beta z} + \Gamma e^{j\beta z}] \ , \tag{E.6}$$

$$I(z) = \frac{V_0^+}{Z_0} [e^{-j\beta z} - \Gamma e^{j\beta z}] \ . \tag{E.7}$$

Thus the voltage and the current on the line consist of a superposition of an incident and a reflected wave. When $Z_L = Z_0$ then $\Gamma = 0$ and there is no reflected wave. Such a load is then said to be matched to the line.
Now the two sections are considered. First we look at the line that is terminated in a short circuit, $Z_L = 0$, and $Z_0 = Z_1$. From Eq.(E.5) it is seen that the reflection coefficient is $\Gamma = -1$. From Eqs.(E.6) and (E.7) the voltage and the current on the line are

$$V(z) = V_0^+ [e^{-j\beta z} - e^{j\beta z}] = -2jV_0^+ \sin\beta z \ , \tag{E.8}$$

$$I(z) = \frac{V_0^+}{Z_1} [e^{-j\beta z} + e^{j\beta z}] = \frac{2V_0^+}{Z_1} \cos\beta z \ . \tag{E.9}$$

These formulas show that for a short circuit V=0 and the current is at a maximum. With $l = -l_1$, the transformed impedance as seen from the transition point is:

$$Z_{trans} = \frac{V(-l_1)}{I(-l_1)} = jZ_1 \tan\beta l_1 \ . \tag{E.10}$$

Next we consider the line terminated by the open circuit where $Z_L = \infty$. Then the reflection coefficient becomes

$$\Gamma = \lim_{Z_L \to \infty} \frac{Z_L - Z_2}{Z_L + Z_2} = 1 \ . \tag{E.11}$$

The voltage and the current on this line are

$$V(z)=V_0^+[e^{-j\beta z}+e^{j\beta z}]=2V_0^+\cos\beta z \ , \tag{E.12}$$

$$I(z)=\frac{V_0^+}{Z_2}[e^{-j\beta z}-e^{j\beta z}]=\frac{-2jV_0^+}{Z_2}\sin\beta z \ . \tag{E.13}$$

These formulas show that for an open circuit I=0 and the voltage is at a maximum. With $l=-l_2$, the transformed impedance as seen from the transition point is:

$$Z_{trans}=\frac{V(-l_2)}{I(-l_2)}=jZ_2\cot\beta l_2=jZ_2\frac{1}{\tan\beta l_2} \ . \tag{E.14}$$

Since the impedances transformed from the short circuit and the open end to the transition point must be equal, the resonance condition can immediately be written as:

$$\tan\beta l_1\tan\beta l_2=\frac{Z_2}{Z_1} \ . \tag{E.15}$$

The cavity length should be as small as possible, so l_1+l_2 should be minimal. Suppose $l_1=l_2=l$, then we get a condition for the characteristic impedances

$$l=\frac{1}{\beta}\arctan\sqrt{\frac{Z_2}{Z_1}} \ . \tag{E.16}$$

This means that the cavity length decreases when Z_1/Z_2 increases, as we have also seen with the numerical calculations in paragraph 3.3.

Appendix F: Tetrode current characteristics.

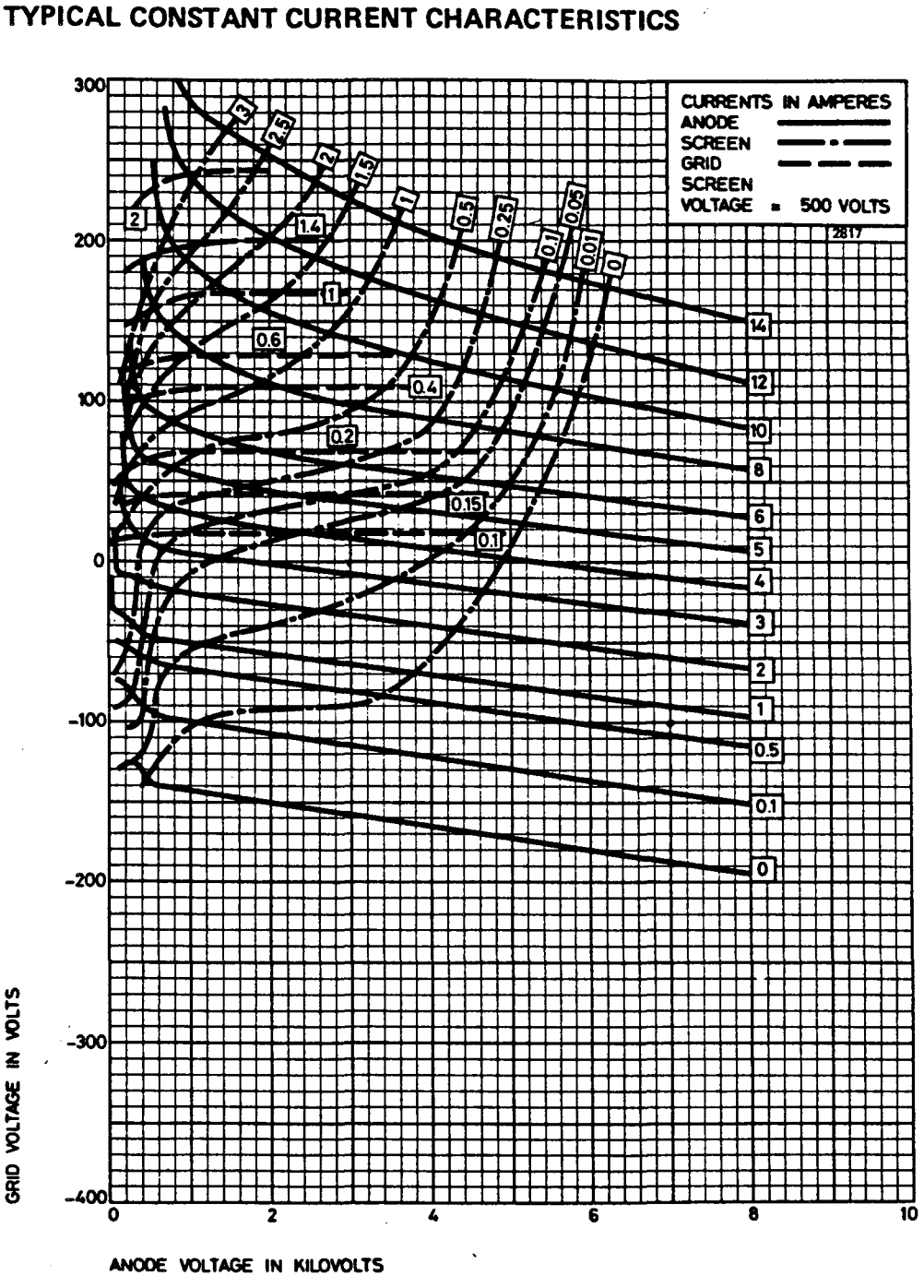

4CW10,000A

TYPICAL CONSTANT CURRENT CHARACTERISTICS

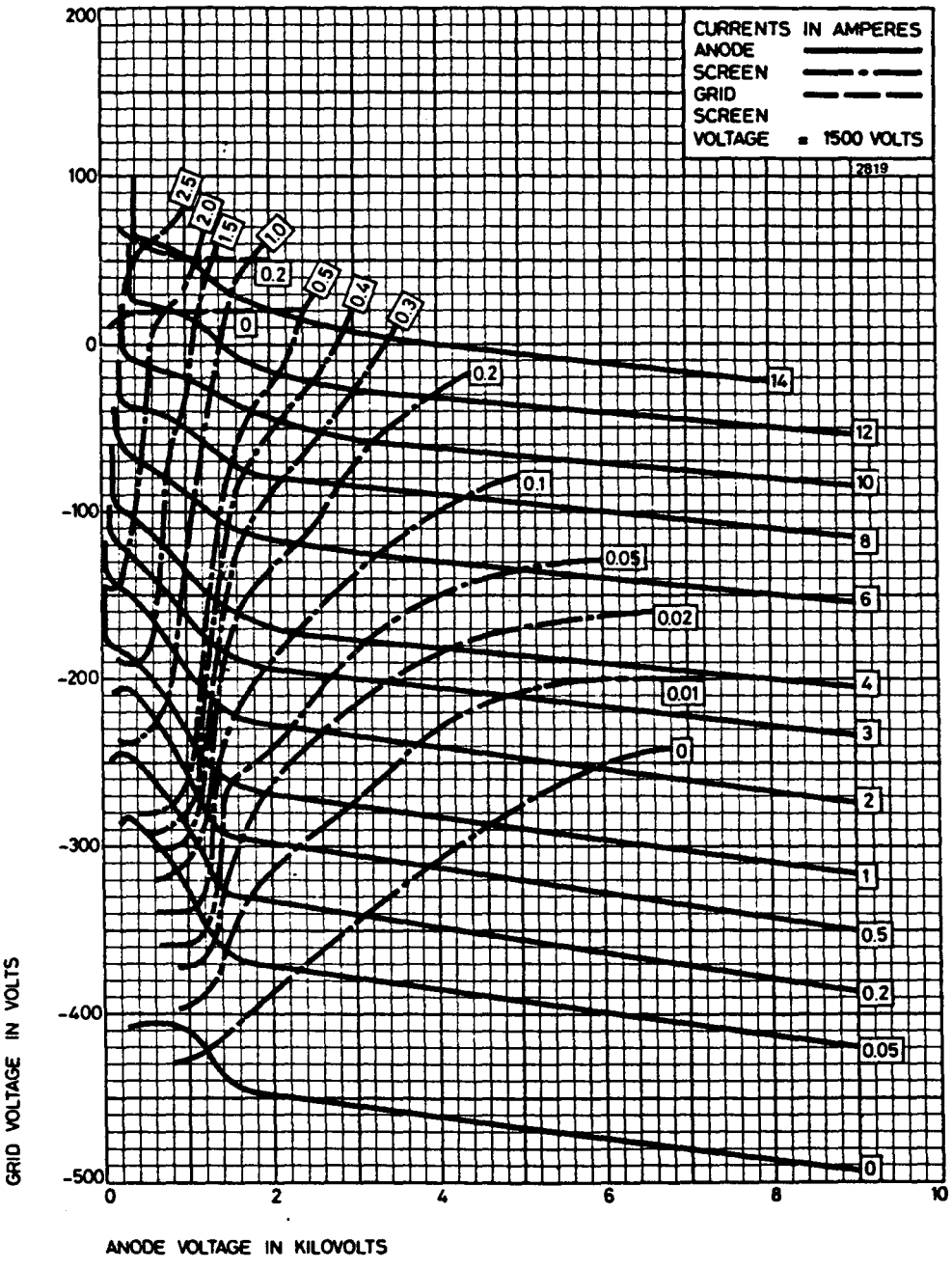

4CW10,000A

Appendix G: Input files for the computercodes URMEL-T and SUPERFISH.

```
 $FILE ITEST=0, LPLO=.T. $END
EUTERPE 43,5 MHz CAVITY 2 PRODUCTIEONTWERP
 $BOUN $END
 $MESH NPMAX=7000 $END
 #MATDIS
1 1
0.0000  0.9340
0.0000  0.0000
0.1250  0.0000
0.1250  0.9340
0.0000  0.9340
8888 8888
0 0
0.0000  0.0000
0.0230  0.0000
0.0230  0.8455
0.0250  0.8455
0.0250  0.0100
0.1220  0.0100
0.1220  0.8730
0.0555  0.8730
0.0555  0.0765
0.0525  0.0765
0.0525  0.8730
0.0230  0.8730
0.0230  0.9340
0.0000  0.9340
0.0000  0.0000
8888    8888
9999    9999
 $MODE MROT=0, NMODE=10, FUP=838, DVLIM=2, PFAC0=0.001, PFAC2=1 $END
 $PLOT MODPL=1 $END
 $PRIN MODPR=1, LER=.T., LEZ=.T., LHFI=.T., LMATPR=.F. $END
```

```
ssuperfish productie cavity 43 MHz
 $reg nreg=2, dx=0.467, dy=0.203, xmax=93.400, ymax=12.200,
  ndrive=1, npoint=15 $
 $po x= 0.0     y= 0.0    $
 $po x= 0.0     y= 2.3    $
 $po x=84.550   y= 2.3    $
 $po x=84.550   y= 2.5    $
 $po x= 1.0     y= 2.5    $
 $po x= 1.0     y=12.2    $
 $po x=87.300   y=12.2    $
 $po x=87.300   y= 5.55   $
 $po x= 7.65    y= 5.55   $
 $po x= 7.65    y= 5.25   $
 $po x=87.300   y= 5.25   $
 $po x=87.300   y= 2.3    $
 $po x=93.400   y= 2.3    $
 $po x=93.400   y= 0.0    $
 $po x= 0.0     y= 0.0    $
 $reg cur=1, ibound=-1, npoint=1 $
 $po x=87.300   y= 5.55   $
```

Acknowledgement

I would like to thank the people who helped me last year completing my study.

Piet Magendans, who made all the drawings of the model cavity. I thank him for his knowledge and experience. The cavity he drew was made by the people from the technical workshop. I thank Marius Bogers, Frank van Hoof and their team, who worked on the project, for their hospitality. I was always welcome to have a look.

Wim Verseijden, who always found the time to help me adjusting programs. I thank him for his useful suggestions and patience.

Godfried Webers, for his experience on the field of conformal mapping. He made me see what a beautiful tool this theory can be.

Willy Koppens, my predecessor, who helped me starting my graduate study by sharing his knowledge.

I thank my roommates, André, Boling, Carlo, Dolf, Godfried and Johannes for their advice and companionship.

I also thank all the friendly people in the cyclotron building who were always in for a nice chat. Together they created a fantastic environment to work in.

Herman, Susanne and Jan-Eric thanks for standing by me and helping me.

Last, but not least, I thank my parents. They made it possible that I could study, and supported me all the way. Pap, Mam, I couldn't have made it without you. I dedicate this report to you both.

Geldrop, June 11th 1993